2014

Silver Nanoparticle Oligonucleotide Conjugate For Targeted Gene Silencing

Alyson Nanette Moll
Louisiana State University and Agricultural and Mechanical College

SILVER NANOPARTICLE-OLIGONUCLEOTIDE CONJUGATE FOR TARGETED GENE SILENCING

A Thesis

Submitted to the Graduate Faculty of the
Louisiana State University and
Agricultural and Mechanical College
in partial fulfillment of the
requirements for the degree of
Masters of Science in Engineering Science

in

The Department of Engineering Science

by
Alyson N. Moll
B.S., Louisiana State University, 2007
December 2014

I would like to dedicate this thesis to my family in Metairie and new family members in Baton Rouge and Shreveport for their unfailing kindness and love entrusted to me during an opportune time of growth.

ACKNOWLEDGEMENTS

I would like to gratefully acknowledge the following people: Dr. Todd Monroe, Dr. Daniel Hayes, Dr. Cristina Sabliov, and Dr. Zhijun Liu for serving on my committee and for guiding me throughout my research experience; Paige Brown, Junzi Dong, Dana Trahan, Hannah Russin, Craig Richard, and all additional Monroe/Hayes crew members for their benevolence, guidance, and enthusiasm; Angela Singleton, Donna Elisar, and Ronda Shepard for assistance in scheduling classes and accomplishing graduate school requirements; Marilyn Dietrich for her assistance with flow cytometry; Karen McDonough for sharing her cell culture expertise; Dr. Cueto, Mark Hoppens, Nick Totaro, and Leah Garber for their assistance with DLS and zeta potential; Dr. Robert Gambrell and Dr. Blanchard for their assistance with ICP-OES; Dr. Ammar Qureshi and Dr. Sokolova Yuliya for their assistance in TEM imaging, and Dr. Ted Gauthier and Tamara Chouljenko for assistance in gel imaging.

TABLE OF CONTENTS

LIST OF ABBREVIATIONS

SNP-DNAzyme	Silver Nanoparticle-10-23 Deoxyribozyme
SNPs	Silver Nanoparticles (aka SmartSilver^{TM} AS)
Citrate SNP	Cittrate Silver Nanoparticles
HPC SNP	Hydroxypropyl Cellulose Silver Nanoparticle
KRAS	Kirsten rat sarcoma viral oncogene homolog
DNAzyme	Deoxyribozymes
miRNA	microRNA
RNAi	RNA interference
LSPR	Localized surface plasmon resonance
DMNPE	1-(4,5-dimethoxy-2-nitrophenyl) ethyl ester
SDS	Sodium dodecyl sulfate
UV-vis spectroscopy	Ultraviolet-Visible spectroscopy
TEM	Transmission Electron Microscopy
DLS	Dynamic Light Scattering
ICP-OES	Inductively Coupled Plasma Optical Emission Spectrometry
DTT	DL-Dithiothreitol
KRAS DZ	KRAS DNAzyme
Thiol DZ	Thiol DNAzyme
PC DZ	Photocleavable linker DNAzyme
TAMRA DZ	TAMRA fluorophore conjugation DNAzyme
DMEM	Dulbecco's Modified Eagle's Medium

DPBS	Dulbecco’s Phosphate-Buffered Saline
FBS	Fetal Bovine Serum
Na Pyr	Sodium pyruvate
NEAA	Non-Essential Amino Acids
ITS	Supplement of Insulin, Transferrin and Selenium
DMEMHG	Dulbecco’s Modified Eagle’s Medium-High glucose
MEM	Minimum Essential Medium
DMEM-RS	Dulbecco’s Modified Eagle’s medium-reduced serum
UV	Ultraviolet
DOX	Doxorubicin-HCl
MTS	(3-(4,5-dimethylthiazol-2-yl)-5-(3-carboxymethoxyphenyl)-2-(4-sulfophenyl)-2H-tetrazolium),

ABSTRACT

This project explored a gene-regulated chemotherapy using a silver nanoparticle (SNP) conjugated with deoxyribozyme (DNAzyme) oligonucleotides which target a mutated gene in select cancer cells, sensitize them to doxorubicin treatment. Light exposure to the SNP-DNAzyme conjugates disengages the oligonucleotides and permits specific cleavage of the Kirsten Rat Sarcomal Oncogene Homolog (K-RAS) mRNA. These conjugates could provide spatiotemporal specificity in killing only those photoexposed cells with the mutant gene. Synthesis, functionalization and characterization of citrate and hydroxypropyl cellulose SNP conjugates confirmed attachment and photolytic release of the thiol-modified 10-23 DNAzyme. Gel electrophoresis was used to demonstrate DNAzyme photoactivation, showing greater K-RAS RNA degradation when disengaged compared to the SNP-tethered form. DNAzyme in the tethered form was also protected from DNAse degradation compared to photolyzed DNAzyme. Characterization of the toxicity and localization of the nanoparticle drug delivery system constructed for the release of a photolabile DNA oligonucleotide was checked within several sets of cells to check for temporal and spatial control efficiency. MTS, alamar blue, and flow cytometry assays were performed to assess cell viability in several sets of cell cultures, including HEK293 and MCF-7 (wildtype K-RAS), SW480 and MDA-MB-231 (mutant K-RAS), and 3T3 (negative control) lines. Following the 5-day experimental protocol involving staggered treatment with SNP-DNAzyme, UV light, and doxorubicin, no cell group showed the intended pattern of necrosis in mutant K-RAS cells without morbidity in controls or partial treatments. Thus further evaluation of K-RAS+/- cells which respond consistently in

viability assays is necessary before this strategy can be deemed of potential as a targeted therapeutic.

CHAPTER 1. SIGNIFICANCE AND BACKGROUND

1.1 OBJECTIVES

This project has proposes a nanoscale oligonucleotide delivery system that is designed to overcome some known hurdles in chemotherapeutic applications. Because some reports have shown that K-RAS mutations in colon and breast cancer cells increase their survival, this approach seeks to disrupt the mutant gene in targeted cells and sensitize them to doxorubicin, a standard chemotherapeutic. K-RAS mRNA is cleaved by a specific deoxyribozyme (DNAzyme) oligonucleotide tethered with a photolabile linker to a silver nanoparticle (SNP) which facilitates protection from nucleases as well as cellular delivery.

Nanoparticle conjugate synthesis, functionalization, and characterization were performed on the SNP-DNAzyme constructs along with their evaluation in cell cultures as models for targeted killing of cancer cells, as shown in Figure 1.1. SNP-DNAzyme conjugates were constructed using a citrate-based SNP synthesis approach as well as with hydroxypropylcellulose (HPC SNPs) as starting materials. Kirsten rat sarcoma viral oncogene homolog (KRAS) genes were evaluated for cleavage by KRAS DNAzymes in standard deoxyribonucleotide and modified oligonucleotide forms. Staggered delivery of SNP-DNAzyme and Doxorubicin in SW620 KRAS mutant colon cancer cell lines was evaluated. Staggered delivery of SNP-DNAzyme and Doxorubicin within SW480 KRAS mutant colon cancer cell lines and MDA-MB-231 KRAS mutant breast cancer cells were also are characterized as an alternative method.

1.2 SIGNIFICANCE: THE CLINICAL NEED

In addition to traditional pharmacological agents, some treatments utilize internal machinery already present in cells to produce the desired therapeutic effect. At present, a number of methods are well characterized for acting on the mRNA level by preventing protein

expression. Specifically, these methods can be used to inhibit production of diseases in which gene silencing is critical (reviewed by (Bianco and Robey 2001)). These therapeutic techniques make use of deoxyribozymes (DNAzyme), microRNAs (miRNA), and antisense oligonucleotides (reviewed by (Kurreck 2003)). DNAzymes are RNA-cleaving DNA oligonucleotides with enzyme characteristics (Santoro and Joyce 1998). miRNAs are endogenous single-stranded RNAs approximately 22 nucleotides long that utilize the RNA interference (RNAi) pathway's machinery, which cleaves the miRNA's complementary target (reviewed by (Lingel and Sattler 2005)). Antisense oligonucleotides are strands of 15 to 20 nucleotides long that hybridize to their intended target mRNA and block translation (reviewed by (Dias and Stein 2002)). The basic premise of this project is to design and test a DNAzyme-functionalized nanoparticle whose attachment site is photocleavable to achieve temporal and spatial control of the oligonucleotide drug release. Temporal and spatial control addresses one of the main problems for reduction of incorrect targeting, thus reducing secondary symptomatic problems.

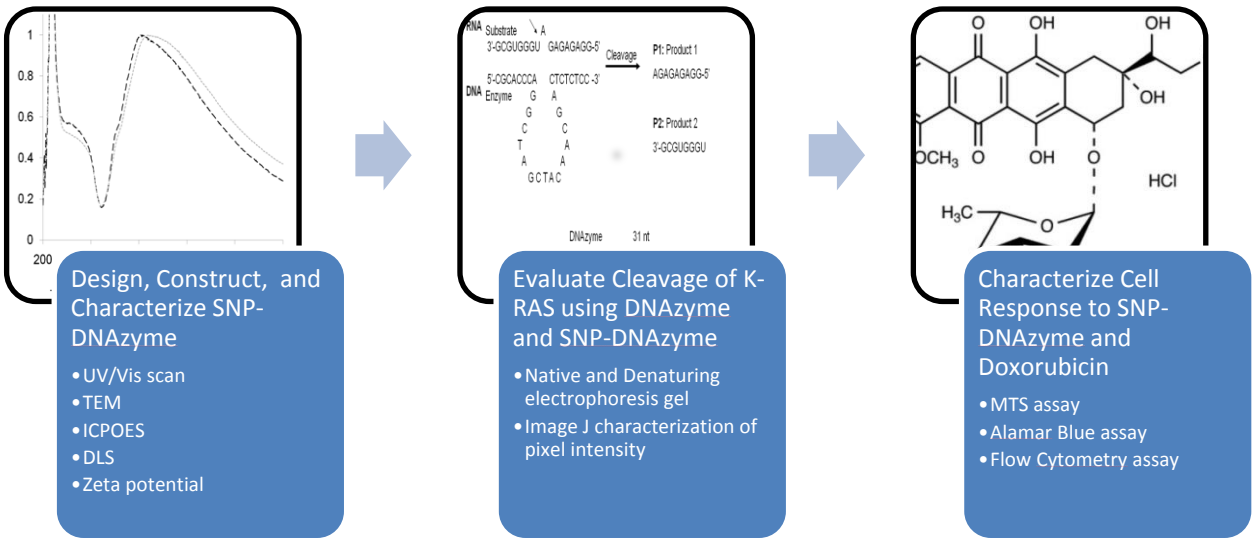

Figure 1.1. Objectives for the project.

Some oligonucleotide drugs are used in clinical trials while others are in the earliest stage of development (reviewed by (Akkina, Banerjea et al.)). The use of DNAzymes, antisense oligonucleotides, and the RNA interference pathway are the most explored techniques at present. Figure 1.2 illustrates the mechanism of action for all three of these techniques. Although their end results all include the prevention of protein expression, their pathways utilize separate machinery (reviewed by (Kurreck 2003)). Antisense oligonucleotides stop translation of their intended target by blocking the complementary sequence or by cleaving the complement using RNAse H. DNAzymes cleave their targeted complementary sequence.

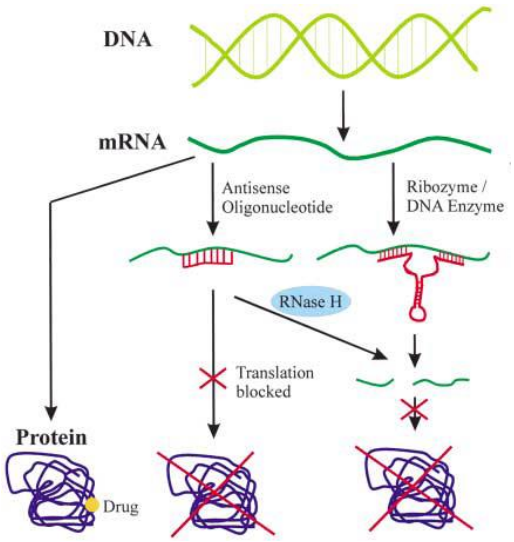

Figure 1.2. Antisense oligonucleotide and DNAzyme pathways(Kurreck 2003).

Antisense oligonucleotides and DNAzymes use distinct internal machinery, thus specific cleavage of mRNA is performed. However, common problems persist for the therapeutic applications using these systems. The problems to improve include protecting the gene silencing oligonucleotides from degradation by enzymes and achieving cellular uptake (reviewed by (Kurreck 2003)). The carriers utilized in this project, silver nanoparticles (SNPs), are used to address the protection of the gene silencing oligonucleotides by blocking the attachment of

endonucleases. SNPs have also shown promise in delivering oligonucleotides intracellularly(Brown, Qureshi et al. 2013). The SNPs will be functionalized with a 10-23 DNAzyme that has demonstrated cleavage of RNA. In addition to the SNP and DNAzyme being joined by a thiol bond, the DNA construct includes a photocleavable nitrobenzyl linker to control oligonucleotide release from the SNP. The SNP-DNAzyme construct is designed to work in a system requiring targeted gene silencing.

KRAS DNAzymes actively cut the corresponding KRAS mRNA. miRNA125b DNAzymes were originally used for a breast cancer treatment. Cleavage of the miRNA 125b's complement was unsuccessful, thus the project changed to cells with the KRAS mutation. Some populations of colon cancer and breast cancer cells benefit from the mutation of the KRAS gene. KRAS translationally produces a mutated GTPase protein causing abnormal tissue signaling, accordingly increasing the formation of tumors. SW620 and SW480 colon cancer cell lines have the KRAS mutation in codon 12 from the nucleotide exchange from a glycine to a valine codon(Yu, Wang et al. 2009). MDA-MB-231 breast cancer cell lines have the KRAS mutation in codon 13 from the nucleotide exchange from a glycine to an aspartic acid codon(Hollestelle, Elstrodt et al. 2007). Figure 1.3 displays the overall goal of this project; the focal point is on a gene-regulated chemotherapy system using the staggered delivery of SNP-DNAzyme and doxorubicin to improve targeted killing of colon and breast cancer cells.

In summary, this project has significance because it proposes a drug delivery system that is designed to overcome some known hurdles in therapeutic applications. More specifically, the project addresses the method in which colon and breast cancer cells survive by taking advantage of a mutated gene important in normal cell signaling; the mutated mRNA is cleaved using a functionalized nanoparticle with a photocleavable oligonucleotide, and a well-known

chemotherapeutic agent, doxorubicin. This system is novel because it allows for temporal and spatial control of the oligonucleotide release and may lead to a reduction of the dosage of doxorubicin drug needed due to the actions of the DNAzyme.

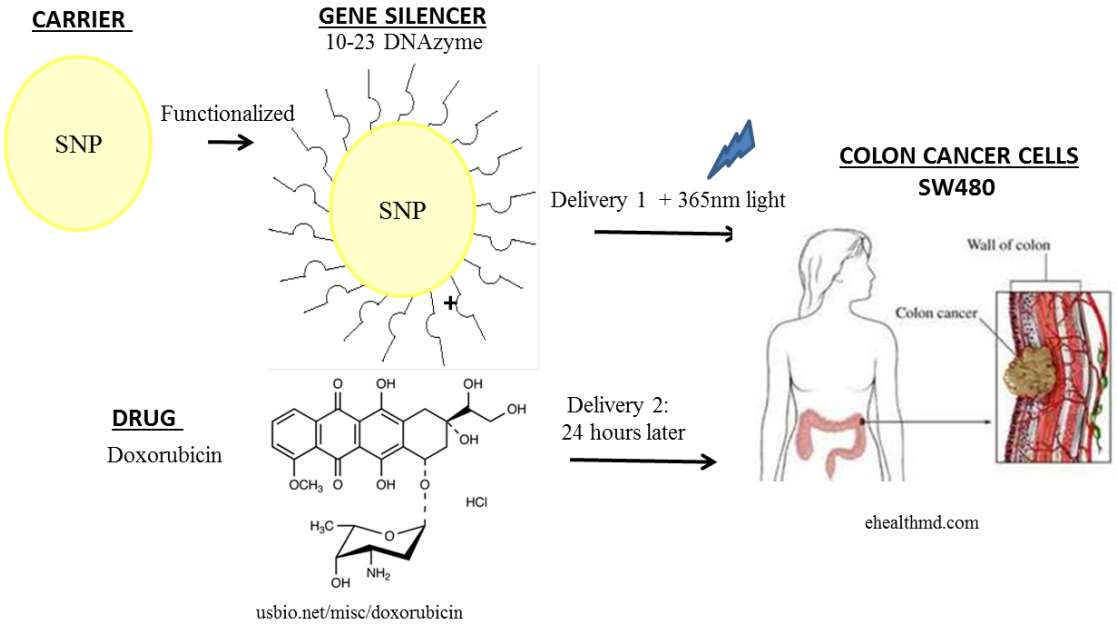

Figure 1.3. Aims of project include gene regulated chemotherapy using nanoscale DNA conjugates.

1.3 10-23 DNAZYME FOR GENE SILENCING

In 1980, Cech *et al.* found that certain RNA molecules, now termed ribozymes, catalyze reactions without any help from proteins (Cech, Zaug et al. 1981). Subsequently, several catalytically active nucleic acids have been found to cleave RNA. Ribozymes and DNAzymes are nucleic acid oligonucleotides that catalytically cleave RNAs with great specificity (reviewed by (Vaish, Kore et al. 1998)). The mechanisms and detailed cleavage sites have been determined for several of these enzymatic oligonucleotides as shown in Figure 1.4 (reviewed by (Schubert and Kurreck 2004)). Ribozymes have been proposed for several therapeutic applications, including targeting cancer(Warashina, Kuwabara et al. 1999), viral(Michienzi, Castanotto et al. 2003), rheumatoid arthritis(Rutkauskaite, Zacharias et al. 2004), and cardiovascular diseases

(Yamamoto, Morishita et al. 2000). Since ribozymes and deoxyribozymes are nucleic acids, they are easily degraded in the cells. Therefore, modifications to the backbone and sugars are made to facilitate their survival so that they may carry out their intended purpose. However, modifications can cause conformational changes that possibly stop catalytic activity of the ribozymes, thus the modifications must be chosen wisely (reviewed by (Schubert and Kurreck 2004)).

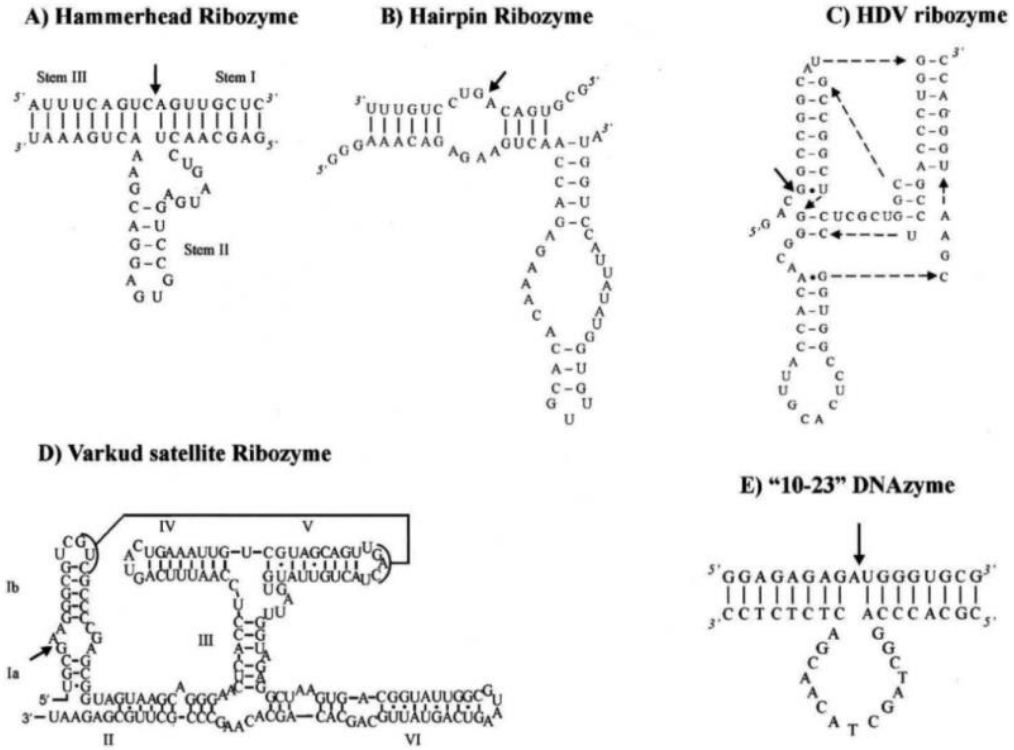

Figure 1.4. Structures for Ribozymes and DNAzymes(Schubert and Kurreck 2004).

1.3.1 Classes of Ribozymes/Deoxyribozyme and Production of Cleavage

The size of the ribozyme and the products made during cleavage determine the class of the ribozyme. Large ribozymes are comprised of hundreds of nucleotides with the largest being 3000 nucleotides (reviewed by (Schubert and Kurreck 2004)). The hydrolyzed products contain a hydroxyl group on the 3' end and a phosphate group on the 5' end. The large ribozymes include self-splicing group I and group II introns and the RNA component of RNase P (reviewed

by (Tanner 1999)). Self splicing group I introns perform splicing in two steps using a transesterification reaction. Although the exact mechanism for group II introns is not known, the intron uses a nucleophilic attack on the splice site ultimately forming a lariat-type structure. RNase P cleaves a strand after an external guide sequence binds to the sequence of choice (reviewed by (Schubert and Kurreck 2004)). Small ribozymes are comprised of 30 to 150 nucleotides. The small ribozymes have distinct structures, but they all contain specific cleavage sites shown in Figure 1.4 (reviewed by (Schubert and Kurreck 2004)). These molecules produce products that contain 2'-3'-cyclic phosphate and a 5' hydroxyl group. The small ribozymes include hammerhead ribozymes(Haseloff and Gerlach 1988), hairpin ribozymes(Hegg and Fedor 1995), hepatitis delta virus ribozymes(Wadkins and Been 2002), and varkud satellite ribozymes(Saville and Collins 1990).

Santoro *et al.* found the most robust deoxyribozyme known to date, named 10-23 DNAzyme. As shown in Figure 1.4, it has 15 nucleotides making up the loop and catalytic core flanked by two extended substrate recognition arms with 6-12 nucleotides on either side of the core to ensure complementary pairing to its intended target (reviewed by (Kurreck 2003)). Specifically, the 10-23 DNAzyme cuts between a pyrimidine and a purine (Joyce 2001). An unmodified DNAzyme lasted 2 hours in serum while an added inverted nucleotide at the 3' end increased the lifespan to 20 hours(Sun, Cairns et al. 1999). The biggest advantage of using deoxyribozymes is the ease of synthesis and handling over ribozymes (reviewed by (Schubert and Kurreck 2004)). The 10-23 DNAzyme specifically cuts single-stranded RNA that is complementary to its two extended substrate recognition arms. In this project, the 10-23 DNAzyme's complementary target is a KRAS mutant mRNA product.

1.4 SNP-CONJUGATE TARGET

This project is focused on designing a nanoparticle drug delivery system based on the gene silencing effects of a 10-23 deoxyribozyme(Santoro and Joyce 1998). The drug delivery vehicle, SNP, is functionalized with a thiol-modified deoxyribozyme with internal photocleavable linkers(Brown, Qureshi et al. 2013). The internal photocleavable linkers are essential to the spatiotemporal control of the release of the gene silencing deoxyribozymes(reviewed by(Pelliccioli and Wirz 2002)).

The original proposed plan shown in Figure 1.5 targeted miRNA 125b(Zhou, Liu et al. 2010). It was hypothesized that the blockage of miRNA 125b via DNAzyme cleavage and the addition of naturally-formulated rubusoside-Paclitaxel would offer a means to sensitize targeted cancer cells. Thus, new chemotherapeutic treatments could be explored. miRNA 125b is an important component in breast cancer cell lines that cleaves the Bak1 mRNA, responsible for apoptosis(Zhou, Liu et al. 2010). Three DNAzymes were synthesized to cut miRNA 125b:1) same core as the 10-23 DNAzyme and the recognition arms with complimentary bases, 2) modified core to the DNAzyme with wobble base pairs and shorter complementary recognition arms, 3) modified core to the DNAzyme with wobble base pairs and longer complementary recognition arms. None of the DNAzymes were successful in cutting the mRNA even though buffer conditions, time conditions, and concentration conditions were varied. Breast cancer cell lines, MDA-MB-231 and MDA-MB-435, were proposed to be treated with increasing doses of naturally-formulated rubusoside-Paclitaxel to form sensitive and resistant cell lines. The cell lines used started at high passage numbers and did not survive after two weeks of splitting.

The alternate approach is targeting the mutant K-Ras gene as shown in Figure 1.3, a critical component that encodes signal transduction pathway proteins causing pancreatic,

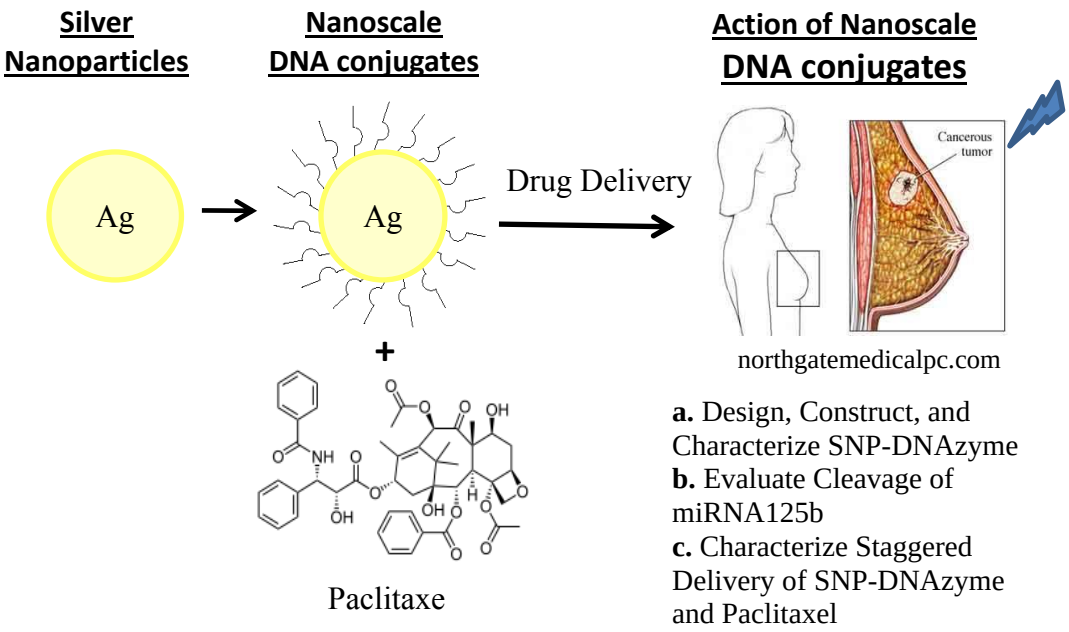

Figure 1.5**.** Aims of original project included gene regulated chemotherapy using nanoscale DNA conjugates focused on SNP-Conjugate target miRNA125b.

colorectal, endometrial, biliary tract, lung, and cervical cancers(Yu, Wang et al. 2009). This project is hypothesized to work since the pyrimidine-purine pair to be cut by the K-Ras 10-23 DNAzyme is a 'G-U' pair, unlike the 'A-C' pair to be cut by the miRNA 125b DNAzyme (Yu, Wang et al. 2009, Zhou, Liu et al. 2010). In comparison to the original Ras gene, the mutant K-Ras gene has a point mutation with a uracil nucleotide substituted for a guanine nucleotide. Due to that specific change, a 10-23 deoxyribozyme can hybridize to the pyrimidine-purine site and cleave the mutant K-Ras mRNA (Yu, Wang et al. 2009). "AU = GU > GC >> AC" is the pairs decreasing the effectiveness of a deoxyribozyme cutting suggested by Cairns et al(Cairns, King et al. 2003). The K-Ras 10-23 DNAzyme will be used to prime mutant K-RAS colon and breast cancer cells to be more impacted by the addition of doxorubicin.

The addition of UV light will increase uncaging the DNAzyme from silver nanoparticles, thus allowing for an effective therapy treatment. The addition of 11-Mercaptoundecanoic acid backfilling will decrease aggregation of particles and increase DNAzyme packing. Johnson *et*

al. used 11-mercaptoundecanoic acid to increase homogeneous dispersion of silver nanoparticles in their study(Johnson Jr, Kang et al. 2008). Paclitaxel will not be an appropriate option for treatment since taxol works through the microtubule network and so does the expression of the K-Ras proteins(Thissen, Gross et al. 1997, Chen, Otto et al. 2000). The colon cancer cell lines system include control lines, HT29 and HEK293, and treated lines, SW480 and SW620. HT29 and HEK293 do not have positive expression of the K-Ras mutant gene. SW620 and SW480 cell lines express the KRAS mutant ras protein in codon 12. The breast cancer cell lines system includes a control line, MCF-7, and treated line, MDA-MB-231. MCF-7 does not have positive expression of the K-Ras mutant gene. MDA-MB-231 cell line express the KRAS mutant ras protein in codon 13.

1.4.1 miRNA

miRNA containing a sequence on average of 22 nucleotides long has been found to use the RNAi pathway in mammalian systems(Elbashir, Harborth et al. 2001). miRNAs are endogenous regulators of gene expression. miRNA molecules are derived from primary miRNA and cleaved by Drosha, an RNase III enzyme, into precursor miRNA in the nucleus(Lee, Ahn et al. 2003). The structure forms into a hairpin, which is then exported into the cytoplasm. Dicer cleaves the precursor miRNA into the double stranded miRNA that takes part in the RNAi pathway (reviewed by (Lingel and Sattler 2005)). It includes in its structure overhanging parts at the ends of the sequences. The 3' ends have hydroxyl groups and the 5' ends have phosphate groups. miRNAs act in two different ways (reviewed by (He and Hannon 2004)). If their sequences are not perfectly complementary to their intended target, they stop translation of a protein by blocking the ribosome. However, if their sequence is completely complementary to the target, the miRNA can induce mRNA degradation using the RNA-inducing silencing

complex(Hammond 2005, Lingel and Sattler 2005). The RISC complex is comprised of several proteins including Argonaute 2, which aids in the cleavage of mRNA (Hammond 2005). Classically, it was thought that mRNA was broken down in the cytoplasm following translation; however recent studies demonstrate that mRNA degradation occurs in processing bodies (Marx 2005).

RNAi Pathway

RNA interference (RNAi) performs its regulation post-transcriptionally (Hammond 2005). In 1991, Fire *et al.* first demonstrated the RNAi phenomenon by blocking the expression of two genes for myofilament proteins present in *C. elegans* body wall muscles (Fire, Albertson et al. 1991). Two key disadvantages to the RNAi pathway are more commonly proper delivery but also evading off-target effects (reviewed by (Hannon and Rossi 2004)). The myriad targets currently explored using gene silencing by the RNAi pathway include HIV(Jacque, Triques et al. 2002), viral hepatitis(McCaffrey, Nakai et al. 2003), cancer(Ngo, Davis et al. 2006), and genetic diseases(Miller, Gouvion et al. 2004).

1.4.2 KRAS mRNA

K-RAS gene encodes the eventual translation of the KRAS protein, an oncogene important for regulating cell division (Reviewed by(Dahabreh, Terasawa et al. 2011)). Oncologists report most KRAS mutations on codons 12 and 13, and more rare KRAS mutations on codons 61 and 146 (Reviewed by (Allegra, Jessup et al. 2009)). The KRAS protein is a part of the RAS/MAPK pathway. Through this pathway, signals are sent causing growth or division and eventually differentiation. Specifically, KRAS protein is a GTPase that acts as a switch when combined to either GTP or GDP. Wild type cell lines have normal conversions on and off in normal KRAS genes. On the other hand, mutant cell lines are continuously dividing due to

the inactivation of this essential cellular division toggle switch. These mutant signal transduction pathway proteins are major causes for pancreatic, colorectal, endometrial, biliary tract, lung, and cervical cancers (Reviewed by (Yu, Wang et al. 2009)). Certain therapies are not recommended due to the KRAS mutation, thus other therapies are required. Specifically, Allegra *et al.* did not recommend the use of anti-EGFR monoclonal antibody therapy (Reviewed by (Allegra, Jessup et al. 2009, Dahabreh, Terasawa et al. 2011)). Yu *et al.* suggest a treatment of DNAzyme and doxorubicin as alternative method of treatment(Yu, Wang et al. 2009). Our project suggests a step further with the addition of a silver nanoparticle carrier for ease of entrance into cancerous cells and spatial and temporal control.

1.5 DRUG FOR STAGGERED GENE-MEDIATED CHEMOTHERAPY

1.5.1 Paclitaxel

Paclitaxel is a chemotherapeutic agent currently used for breast cancer therapy whose action is an inhibition of microtubule formation and disassembly thus inducing apoptosis(Rowinsky, Cazenave et al. 1990, Perez 1998). Paclitaxel is isolated from the bark of the yew, *Taxus brevifolia* (Wani, Taylor et al. 1971). The scarce amount of Paclitaxel available to early studies led to restricted clinical trials. However, the drug is now semi-synthesized from baccatin III, a precursor to Paclitaxel(Holton, Biediger et al. 1995). Paclitaxel is used in the treatment of a variety of cancers, including carcinomas of the ovary, breast, lung, head and neck, bladder and cervix, melanomas, and AIDS-related Karposi's sarcoma (reviewed by (Jennewein and Croteau 2001)). Liu *et al.* have had success with Paclitaxel by formulating it with a naturally-derived solubilizing agent, rubusoside, to facilitate intracellular delivery (LIU 2009). Rubusoside is a sweetener extracted from the leaves of the *Rubus Suavissimus S. Lee* plant(Sugimoto, Sato et al. 2002). Rubusoside has shown promise for being less toxic than

existing solubulizers such as ethanol (reviewed by (Singla, Garg et al. 2002)). In our originally proposed study, SNP-DNAzyme and rubusoside-Paclitaxel will be delivered in staggered mode, allowing the DNAZyme to degrade miRNA 125b and sensitizing the cell to Paclitaxel before the drug's application. SNP-DNAzyme will be delivered and photoactivated in the breast cancer cell cultures 24 to 48 hours before the dose of rubusoside-Paclitaxel is applied. The effectiveness of photoreleasing the DNAzyme from the SNP and initiating gene-regulation of miRNA 125b will enhance the sensitivity of breast cancer cells to Paclitaxel, and demonstrate potential for targeting this therapy.

miRNA125b

The mechanism underlying cancer cells resistance to Taxol is not fully understood. Zhou et al. demonstrated that miRNAs have an effect on the role of breast cancer resistance(Zhou, Liu et al. 2010). miRNA 125b is upregulated in Taxol-resistant cancer cells, leading to paclitaxel drug resistance. miRNA 125b inhibits Taxol-induced cytotoxicity and apoptosis. Specifically, it targets pro-apoptotic Bcl-2 antagonist killer 1 (Bak1). Downregulation of Bak1 suppresses taxol-induced apoptosis and increases resistance to taxol. By cleaving miRNA125b, Bak1 is restored; thereby, paclitaxel sensitivity increases and the apoptosis of breast cancer cells increases .

1.5.2 Doxorubicin

Paclitaxel will not be an appropriate option for treatment since taxol works through the microtubule network and so does the expression of the K-Ras proteins(Thissen, Gross et al. 1997, Chen, Otto et al. 2000). Doxorubicin is an excellent alternative chemotherapeutic agent since it functions by intercalating DNA. Doxorubicin is an anthracycline antibiotic, administered intravenously (Reviewed by (Aubel-Sadron and Londos-Gagliardi 1984)). Doxorubicin can be

delivered liposome-encapsulated or as a hydrochloride salt (Reviewed by(Gabizon, Shmeeda et al. 2003)). Doxorubicin is derived from a bacterial species *Streptomyces* using a chemical semisynthesis(Guilfoile and Hutchinson 1991). The drug is used in the treatment of several cancers including breast and colon cancer (Reviewed by (Travis, Curtis et al. 1991, Khasraw, Bell et al. 2012)). In the final study, SNP-DNAzyme and Doxorubicin-HCl were delivered in staggered mode, allowing the DNAzyme to degrade KRAS mRNA and sensitizing the cell to doxorubicin before the drug's application. SNP-DNAzyme will be delivered and photoactivated in the corresponding colon and breast cancer cell lines 24 hours before the dose of doxorubicin is applied. The effectiveness of photoreleasing the DNAzyme from the SNP and initiating gene-regulation of KRAS mRNA will enhance the sensitivity of the colon and breast cancer cells to doxorubicin, and demonstrate potential for targeting this therapy.

1.6 SNP ASSISTED TRANSPORT BACKGROUND

In this application, silver nanoparticles(SNPs) serve as carriers for the oligonucleotides to facilitate their cellular delivery. If the SNPs are formed within the range of 1-100 nm in diameter, they have excellent cellular delivery capabilities because particles of that size are not generally removed by the reticuloendothelial system (reviewed by (Bawarski, Chidlowsky et al. 2008)). In general, the number of applications utilizing nanoparticles has increased greatly due to improvements in ease of their synthesis and bioconjugation (reviewed by (Biju, Itoh et al. 2008)). A noble metal nanoparticle has distinctive electronic and photonic properties (reviewed by (Hutter and Fendler 2004)). Assays can be made using these distinctive properties of SNPs in order to evaluate the DNA-functionalized SNPs.

1.6.1 Properties of Silver Nanoparticles

The advantageous photoelectric properties of a SNP include high scattering efficiency, large extinction coefficients and localized surface plasmon resonance (LSPR) by (Yguerabide and Yguerabide 1998, Hutter and Fendler 2004). When these properties are present, as in the case of using colloidal silver nanoparticles, there is an additive effect causing surface enhanced spectroscopy, which enables qualitative or possibly quantitative analysis of low levels of target analytes (Munro, Smith et al. 1995, Munro, Smith et al. 1995) . These properties ultimately assist in driving the reactions for drug delivery since the electric field will cause strain to the bonds of the nanoparticle, allowing for easier release of functionalized oligonucleotides(Chen and Goodman 2004, Eustis and El-Sayed 2006).

High Scattering Efficiency and Large Extinction Coefficient

Gold and silver particles are extremely advantageous to use as tracers because they are light-scattering particles; they act similarly to fluorescent molecules with the addition of being sensitive to concentrations as low as 10^{-16} M (Yguerabide and Yguerabide 1998). Yguerabide *et al.* showed that silver has larger extinction coefficients than gold for particles of similar size as shown in Table 1.1. Yguerabide *et al.* also reported that silver scatters light 10 times stronger than gold. Yguerabide *et al.* reported in Table 1.2 the molar extinction coefficients of the SNPs enlarged with increasing diameter. The surface plasmon resonance of 60 nm SNPs displays a strong absorbance peak at 420 nm wavelength allowing for the use of UV-vis spectroscopy for characterization of the nanoparticles for this study. The strong scattering capability and large extinction coefficient allows for quantitation of silver concentration using the Beer-Lambert law ($A= \varepsilon cl$). Where A is absorbance, ε is the extinction coefficient, c is the concentration of the absorbing molecule, and l is the optical pathlength.

Table 1.1. Differences in Rel C_{sca} (Yguerabide and Yguerabide 1998).

Calculated Light-Scattering and Absorption Properties for Particles of Different Compositions (Rayleigh Scattering)

	C_{sca} (cm^2)	Wave (nm)	Rel C_{sca}	ϵ (M^{-1} cm^{-1})	φ_s
Silver	8×10^{-12}	380	1000	1.68×10^{10}	0.126
Gold	9.02×10^{-13}	530	112.7	5.88×10^{9}	0.04

Note. Values given in the table were calculated with the Rayleigh equation. Particle diameter = 30 nm. Medium refractive index = 1.33. C_{sca} = scattering cross section at specified wavelength; Wave = wavelength; Rel C_{sca} = scattering cross section divided by scattering cross section of silver at 380 nm and multiplied by 1000. ϵ = Molar decadic extinction coefficient = 2.63×10^{20} C_{ext}. φ_s = Light scattering yield = $C_{sca}/(C_{sca} + C_{abs})$.

[a] This particle does not have a prominent light-scattering or absorption peak in the visible region of the spectrum. The cross sections decrease continuously with increasing wavelength. Data are arbitrarily tabulated at the wavelengths shown in the table.

Table 1.2. Differences in C_{sca} for increasing sizes of SNPs (Yguerabide and Yguerabide 1998).

Calculated Light Absorption and Scattering Properties for Silver Particles of Different Sizes

Dia (nm)	λ_{max} (nm)[a]	C_{sca} (cm^2)	$I_U(0)$	$I_U(90)$	ϵ (M^{-1} cm^{-1})	φ_s	Q_{sca}
20	390	6.42×10^{-13}	13.6	6.77	4.16×10^{9}	0.041	0.204
40	400	2.78×10^{-11}	593	294	2.87×10^{10}	0.255	2.214
60	420	1.41×10^{-10}	3.03×10^{3}	1.49×10^{3}	6.75×10^{10}	0.55	5
80	445	2.92×10^{-10}	6.32×10^{3}	3.1×10^{3}	1.04×10^{10}	0.741	5.8
100	485[b]	4.28×10^{-10}	9.23×10^{3}	4.55×10^{3}	1.35×10^{11}	0.835	5.45

[a] Wavelength of the maximum peak of the scattering cross section vs wavelength graph in the wavelength range 380–700 nm. Entries in all columns of the same row are for the maximum peak wavelength.

[b] For diameters greater than 100 nm, two peaks appear in the light-scattering spectrum. See Fig. 8b. Data are tabulated at the wavelength of the most intense peak.

Note. C_{sca}, Light-scattering cross section. $I_U(0)$ and $I_U(90)$, Scattered light intensities measured at 0 (forward) and 90° with respect to the direction of an unpolarized incident light beam. ϵ(M^{-1} cm^{-1}), Molar decadic extinction coefficient. φ_s, Light-scattering yield defined by Eq. [17]. Q_{sca}, Scattering efficiency defined by Eq. [14]. Medium refractive index = 1.33.

Localized Surface Plasmon Resonance

Localized surface plasmons are charge density oscillations present only on metallic nanoparticles and metallic nanostructures (reviewed by (Hutter and Fendler 2004)). As shown in Figure 1.6, a colloidal silver nanoparticle is excited by an electric field at a particular wavelength causing an oscillation of the outermost electrons of the metal (Kelly, Coronado et al. 2003). Strong light scattering occurs due to resonance causing intense surface absorption bands to appear; the overall effect is surface enhanced spectroscopy (reviewed by (Willets and Van Duyne 2007)). In general, the material, size, and shape of the nanoparticle are distinctly characterized by certain absorption maxima and color due to these surface plasmon absorption bands (reviewed by (Hutter and Fendler 2004)).

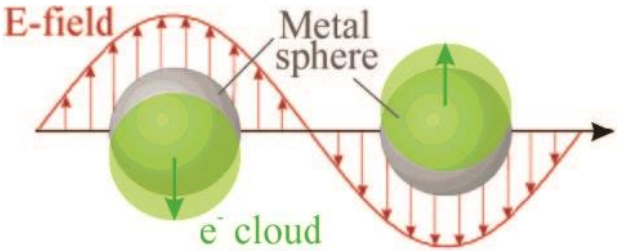

Figure 1.6. Surface plasmon oscillation of metal sphere (Kelly, Coronado et al. 2003).

1.7 THIOL LINKAGE BACKGROUND

Functionalization of nanoparticles with specific biomolecules can be accomplished through various methods employing varying strengths of bonds in an aqueous environment (Goldys 2009). Electrostatic attraction and adsorption methods are the simplest, but the most stable method is a covalent linkage between the intended biomolecule and its compatible nanoparticle surface groups (reviewed by (Bawarski, Chidlowsky et al. 2008). Brown *et al.* use the binding of thiols to the metal nanoparticle surface through a covalent bond as their method used to connect the oligonucleotide to the silver nanoparticle(Herne and Tarlov 1997). The covalent bond between the thiol and SNP can be detected by the changes induced in the electron density on the SNP surface, resulting in a shift in the surface plasmon absorption maximum (reviewed by (Eustis and El-Sayed 2006)).

1.8 PHOTOACTIVATED CONTROL LINKERS BACKGROUND

Many biomolecules and second messengers can be chemically modified in order to block their activity. This can be performed by adding blocking groups or photocleavable groups to the compound which alter its structure and thus biochemical activity. Photocleavable groups have advantages over the blocking groups since they can work on highly sensitive molecules that are normally incompatible with acids or bases (Dmochowski and Tang 2007). Caged compounds are molecules with inactive function rendered by attachment of photocleavable groups (reviewed by (Ellis-Davies 2007)). Ghosn *et al.* used 1-(4,5-dimethoxy-2-nitrophenyl) ethyl ester

(DMNPE) to block transcription of DNA plasmids; DMNPE was released using light. A fluorescence based assay was used to detect hybridization of the unblocked oligonucleotide. Activity of ribozymes have been modulated with a caged adenosine that blocked enzymatic activity until photoactivation (Chaulk and MacMillan 1998). Dmochowski and coworkers have worked on photoactivating caged fluorescent oligodeoxynucleotides, caged peptide nucleic acid oligonucleotides, and more currently caged 10-23 DNAzymes (Tang and Dmochowski 2005, Tang and Dmochowski 2007, Richards, Seward et al. 2010). More specifically, the caged 10-23 DNAzyme has a light-induced strand break that causes activation of the DNAzyme when it is photocleaved(Richards, Seward et al. 2010).

Caged compounds can also act as linkers and be termed tethered blockage. When Pelliccioli and Wirz reviewed photoremovable protecting groups, they suggested good photoactivating groups needed several factors. The photoactivation should occur with high quantum yield, the chromophore's absorption coefficients should be appropriate to the depth of penetration needed for the sample, photoactivated byproducts should be biocompatible and biologically inert, the release rate for the active compound must be within the timeframe being evaluated, and caged compounds should be soluble in water and pass through appropriate cell membranes (reviewed by (Pelliccioli and Wirz 2002)). In this project, the photocleavable linkers are between the nanoparticle and DNAzyme oligonucleotides. Once the constructed compound is photoactivated with UV light, the 1-(2-nitrophenyl)ethyl (NPE)-based photocleavable linker undergoes photolysis as shown in Figure 1.7 (reviewed by (Pelliccioli and Wirz 2002)); thereby, the DNAzyme oligonucleotide is released from the nanoparticle.

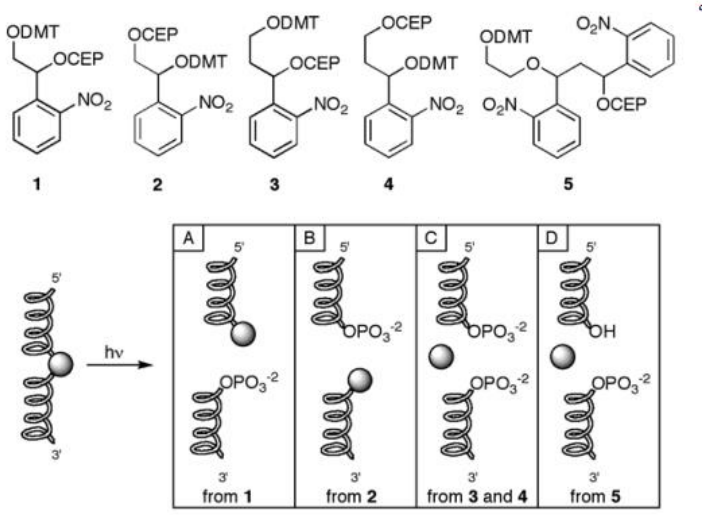

Figure 1.7. Mechanism of 1-(2-nitrophenyl)ethyl (NPE)-based photocleavable linker (Berry & Associates Manual, 2008) .

1.9 GENE-SILENCING OLIGONUCLEOTIDE

In this project, characterization of the stability and activity of citrate and HPC silver nanoparticle drug delivery systems constructed for the release of a photolabile DNA oligonucleotide were tested to show the improvement of temporal and spatial control efficiency of the designed construct. The drug delivery vehicle, silver nanoparticle, is functionalized with a thiol-modified 10-23 DNAzyme oligonucleotide with internal photocleavable linkers. The intended target for hybridization and gene silencing control is K-RAS mRNA. The internal photocleavable linkers permit spatiotemporal control release of the gene silencing K-RAS 10-23 DNAzyme oligonucleotides. HPC SNPs are more reliable as an oligonucleotide carrier than the citrate SNPs. To increase more protection to the DNAzyme, the SNPs were backfilled with 11-mercaptoundecanoic acid. Our results suggest the photoactivatable HPC SNP-10-23 DNAzyme oligonucleotide may enable a light-targeted gene silencing therapy if a robust cell line system can be identified for its validation.

1.10 REFERENCES

Akkina, R., A. Banerjea, J. Bai, J. Anderson, M. Li and J. Rossi "siRNAs, ribozymes and RNA decoys in modeling stem cell-based gene therapy for HIV/AIDS." Anticancer research **23**(3A): 1997.

Allegra, C. J., J. M. Jessup, M. R. Somerfield, S. R. Hamilton, E. H. Hammond, D. F. Hayes, P. K. McAllister, R. F. Morton and R. L. Schilsky (2009). "American Society of Clinical Oncology provisional clinical opinion: testing for KRAS gene mutations in patients with metastatic colorectal carcinoma to predict response to anti–epidermal growth factor receptor monoclonal antibody therapy." Journal of Clinical Oncology **27**(12): 2091-2096.

Aubel-Sadron, G. and D. Londos-Gagliardi (1984). "Daunorubicin and doxorubicin, anthracycline antibiotics, a physicochemical and biological review." Biochimie **66**(5): 333-352.

Bawarski, W., E. Chidlowsky, D. Bharali and S. Mousa (2008). "Emerging nanopharmaceuticals." Nanomedicine: Nanotechnology, Biology and Medicine **4**(4): 273-282.

Bianco, P. and P. Robey (2001). "Stem cells in tissue engineering." NATURE-LONDON-: 118-121.

Biju, V., T. Itoh, A. Anas, A. Sujith and M. Ishikawa (2008). "Semiconductor quantum dots and metal nanoparticles: syntheses, optical properties, and biological applications." Analytical and Bioanalytical Chemistry **391**(7): 2469-2495.

Brown, P. K., A. T. Qureshi, A. N. Moll, D. J. Hayes and W. T. Monroe (2013). "Silver Nanoscale Antisense Drug Delivery System for Photoactivated Gene Silencing." ACS nano.

Cairns, M. J., A. King and L. Q. Sun (2003). "Optimisation of the 10–23 DNAzyme–substrate pairing interactions enhanced RNA cleavage activity at purine–cytosine target sites." Nucleic acids research **31**(11): 2883.

Cech, T., A. Zaug and P. Grabowski (1981). "In vitro splicing of the ribosomal RNA precursor of Tetrahymena: involvement of a guanosine nucleotide in the excision of the intervening sequence." Cell **27**(3): 487-496.

Chaulk, S. and A. MacMillan (1998). "Caged RNA: photo-control of a ribozyme reaction." Nucleic Acids Research **26**(13): 3173.

Chen, M. and D. Goodman (2004). "The structure of catalytically active gold on titania." Science **306**(5694): 252-255.

Chen, Z., J. C. Otto, M. O. Bergo, S. G. Young and P. J. Casey (2000). "The C-terminal polylysine region and methylation of K-Ras are critical for the interaction between K-Ras and microtubules." Journal of Biological Chemistry **275**(52): 41251.

Dahabreh, I. J., T. Terasawa, P. J. Castaldi and T. A. Trikalinos (2011). "Systematic review: Anti–epidermal growth factor receptor treatment effect modification by KRAS mutations in advanced colorectal cancer." Annals of internal medicine **154**(1): 37-49.

Dias, N. and C. Stein (2002). "Antisense oligonucleotides: basic concepts and mechanisms." Molecular cancer therapeutics **1**(5): 347.

Dmochowski, I. and X. Tang (2007). "Taking control of gene expression with light-activated oligonucleotides." BioTechniques **43**(2): 161-171.

Elbashir, S., J. Harborth, W. Lendeckel, A. Yalcin, K. Weber and T. Tuschl (2001). "Duplexes of 21-nucleotide RNAs mediate RNA interference in cultured mammalian cells." Nature **411**(6836): 494-498.

Ellis-Davies, G. C. R. (2007). "Caged compounds: photorelease technology for control of cellular chemistry and physiology." Nature Methods **4**(8): 619-628.

Eustis, S. and M. El-Sayed (2006). "Why gold nanoparticles are more precious than pretty gold: Noble metal surface plasmon resonance and its enhancement of the radiative and nonradiative properties of nanocrystals of different shapes." Chemical Society Reviews **35**(3): 209-217.

Fire, A., D. Albertson, S. Harrison and D. Moerman (1991). "Production of antisense RNA leads to effective and specific inhibition of gene expression in C. elegans muscle." Development **113**(2): 503.

Gabizon, A., H. Shmeeda and Y. Barenholz (2003). "Pharmacokinetics of pegylated liposomal doxorubicin." Clinical pharmacokinetics **42**(5): 419-436.

Goldys, E. (2009). Fluorescence applications in biotechnology and life sciences, Blackwell Pub.

Guilfoile, P. G. and C. R. Hutchinson (1991). "A bacterial analog of the mdr gene of mammalian tumor cells is present in Streptomyces peucetius, the producer of daunorubicin and doxorubicin." Proceedings of the National Academy of Sciences **88**(19): 8553-8557.

Hammond, S. (2005). "Dicing and slicing:: The core machinery of the RNA interference pathway." FEBS letters **579**(26): 5822-5829.

Hannon, G. and J. Rossi (2004). "Unlocking the potential of the human genome with RNA interference." Nature **431**(7006): 371-378.

Haseloff, J. and W. Gerlach (1988). "Simple RNA enzymes with new and highly specific endoribonuclease activities." Nature **334**(6183): 585-591.

He, L. and G. Hannon (2004). "MicroRNAs: small RNAs with a big role in gene regulation." Nature Reviews Genetics **5**(7): 522-531.

Hegg, L. and M. Fedor (1995). "Kinetics and thermodynamics of intermolecular catalysis by hairpin ribozymes." Biochemistry **34**(48): 15813-15828.

Herne, T. and M. Tarlov (1997). "Characterization of DNA probes immobilized on gold surfaces." J. Am. Chem. Soc **119**(38): 8916-8920.

Hollestelle, A., F. Elstrodt, J. H. Nagel, W. W. Kallemeijn and M. Schutte (2007). "Phosphatidylinositol-3-OH kinase or RAS pathway mutations in human breast cancer cell lines." Molecular Cancer Research **5**(2): 195-201.

Holton, R., R. Biediger and P. Boatman (1995). "Semisynthesis of taxol and taxotere." Taxol: Science and Application **97**: 97–121.

Hutter, E. and J. Fendler (2004). "Exploitation of localized surface plasmon resonance." Advanced Materials **16**(19): 1685-1706.

Jacque, J., K. Triques and M. Stevenson (2002). "Modulation of HIV-1 replication by RNA interference." Nature **418**(6896): 435-438.

Jennewein, S. and R. Croteau (2001). "Taxol: biosynthesis, molecular genetics, and biotechnological applications." Applied microbiology and biotechnology **57**(1): 13-19.

Johnson Jr, D. D., B. Kang, J. L. Vigorita, A. Amram and E. M. Spain (2008). "Marangoni Flow of Ag Nanoparticles from the Fluid− Fluid Interface†." The Journal of Physical Chemistry A **112**(39): 9318-9323.

Joyce, G. (2001). "RNA cleavage by the 10-23 DNA enzyme." Methods in Enzymology **341**: 503-517.

Kelly, K., E. Coronado, L. Zhao and G. Schatz (2003). "The optical properties of metal nanoparticles: the influence of size, shape, and dielectric environment." J. Phys. Chem. B **107**(3): 668-677.

Khasraw, M., R. Bell and C. Dang (2012). "Epirubicin: Is it like doxorubicin in breast cancer? A clinical review." The Breast **21**(2): 142-149.

Kurreck, J. (2003). "Antisense technologies." Eur. J. Biochem **270**: 1628-1644.

Kurreck, J. (2003). "Antisense technologies." European Journal of Biochemistry **270**(8): 1628-1644.

Lee, Y., C. Ahn, J. Han, H. Choi, J. Kim, J. Yim, J. Lee, P. Provost, O. Rådmark and S. Kim (2003). "The nuclear RNase III Drosha initiates microRNA processing." Nature **425**(6956): 415-419.

Lingel, A. and M. Sattler (2005). "Novel modes of protein-RNA recognition in the RNAi pathway." Current opinion in structural biology **15**(1): 107-115.

LIU, Z. (2009). DITERPENE GLYCOSIDES AS NATURAL SOLUBILIZERS, WO Patent WO/2009/126,950.

Marx, J. (2005). "Molecular biology: P-Bodies mark the spot for controlling protein production." Science **310**(5749): 764.

McCaffrey, A., H. Nakai, K. Pandey, Z. Huang, F. Salazar, H. Xu, S. Wieland, P. Marion and M. Kay (2003). "Inhibition of hepatitis B virus in mice by RNA interference." Nature Biotechnology **21**(6): 639-644.

Michienzi, A., D. Castanotto, N. Lee, S. Li, J. Zaia and J. Rossi (2003). "RNA-mediated inhibition of HIV in a gene therapy setting." Ann NY Acad Sci **1002**: 63-71.

Miller, V., C. Gouvion, B. Davidson and H. Paulson (2004). "Targeting Alzheimer's disease genes with RNA interference: an efficient strategy for silencing mutant alleles." Nucleic Acids Research **32**(2): 661.

Munro, C., W. Smith, D. Armstrong and P. White (1995). "Assignments and mechanism of SERRS of the hydrazone form for the azo dye solvent yellow 14." The Journal of Physical Chemistry **99**(3): 879-885.

Munro, C., W. Smith, M. Garner, J. Clarkson and P. White (1995). "Characterization of the surface of a citrate-reduced colloid optimized for use as a substrate for surface-enhanced resonance Raman scattering." Langmuir **11**(10): 3712-3720.

Ngo, V., R. Davis, L. Lamy, X. Yu, H. Zhao, G. Lenz, L. Lam, S. Dave, L. Yang and J. Powell (2006). "A loss-of-function RNA interference screen for molecular targets in cancer." Nature **441**(7089): 106-110.

Pelliccioli, A. and J. Wirz (2002). "Photoremovable protecting groups: reaction mechanisms and applications." Photochemical & Photobiological Sciences **1**(7): 441-458.

Perez, E. (1998). "Paclitaxel in breast cancer." The Oncologist **3**(6): 373.

Richards, J., G. Seward, Y. Wang and I. Dmochowski (2010). "Turning the 10–23 DNAzyme On and Off with Light." Chembiochem **11**(3): 320-324.

Rowinsky, E., L. Cazenave and R. Donehower (1990). "Taxol: a novel investigational antimicrotubule agent." Journal of the National Cancer Institute **82**(15): 1247.

Rutkauskaite, E., W. Zacharias, J. Schedel, U. Müller Ladner, C. Mawrin, C. Seemayer, D. Alexander, R. Gay, W. Aicher and B. Michel (2004). "Ribozymes that inhibit the production of matrix metalloproteinase 1 reduce the invasiveness of rheumatoid arthritis synovial fibroblasts." Arthritis & Rheumatism **50**(5): 1448-1456.

Santoro, S. and G. Joyce (1998). "Mechanism and Utility of an RNA-Cleaving DNA Enzyme†." Biochemistry **37**(38): 13330-13342.

Saville, B. and R. Collins (1990). "A site-specific self-cleavage reaction performed by a novel RNA in Neurospora mitochondria." Cell **61**(4): 685-696.

Schubert, S. and J. Kurreck (2004). "Ribozyme-and deoxyribozyme-strategies for medical applications." Current drug targets **5**(8): 667-681.

Singla, A., A. Garg and D. Aggarwal (2002). "Paclitaxel and its formulations." International journal of pharmaceutics **235**(1-2): 179-192.

Sugimoto, N., K. Sato, H. Liu, H. Kikuchi, T. Yamazaki and T. Maitani (2002). "Analysis of rubusoside and related compounds in tenryocha extract sweetener." JOURNAL-FOOD HYGIENIC SOCIETY OF JAPAN **43**(4): 250-253.

Sun, L., M. Cairns, W. Gerlach, C. Witherington, L. Wang and A. King (1999). "Suppression of smooth muscle cell proliferation by a c-myc RNA-cleaving deoxyribozyme." Journal of Biological Chemistry **274**(24): 17236.

Tang, X. and I. Dmochowski (2005). "Phototriggering of caged fluorescent oligodeoxynucleotides." Org. Lett **7**(2): 279-282.

Tang, X. and I. Dmochowski (2007). "Regulating gene expression with light-activated oligonucleotides." Molecular BioSystems **3**(2): 100-110.

Tanner, N. (1999). "Ribozymes: the characteristics and properties of catalytic RNAs." FEMS microbiology reviews **23**(3): 257-275.

Thissen, J. A., J. M. Gross, K. Subramanian, T. Meyer and P. J. Casey (1997). "Prenylation-dependent association of Ki-Ras with microtubules." Journal of Biological Chemistry **272**(48): 30362.

Travis, L. B., R. E. Curtis, J. D. Boice, B. F. Hankey and J. F. Fraumeni (1991). "Second cancers following non-Hodgkin's lymphoma." Cancer **67**(7): 2002-2009.

Vaish, N., A. Kore and F. Eckstein (1998). "Recent developments in the hammerhead ribozyme field." Nucleic Acids Research **26**(23): 5237.

Wadkins, T. and M. Been (2002). "Ribozyme activity in the genomic and antigenomic RNA strands of hepatitis delta virus." Cellular and Molecular Life Sciences **59**(1): 112-125.

Wani, M., H. Taylor, M. Wall, P. Coggon and A. McPhail (1971). "Plant antitumor agents. VI. Isolation and structure of taxol, a novel antileukemic and antitumor agent from Taxus brevifolia." Journal of the American Chemical Society **93**(9): 2325-2327.

Warashina, M., T. Kuwabara, Y. Nakamatsu and K. Taira (1999). "Extremely high and specific activity of DNA enzymes in cells with a Philadelphia chromosome." Chemistry & biology **6**(4): 237-250.

Willets, K. and R. Van Duyne (2007). "Localized surface plasmon resonance spectroscopy and sensing." Physical Chemistry **58**(1): 267.

Yamamoto, K., R. Morishita, N. Tomita, T. Shimozato, H. Nakagami, A. Kikuchi, M. Aoki, J. Higaki, Y. Kaneda and T. Ogihara (2000). "Ribozyme Oligonucleotides Against Transforming Growth Factor-{beta} Inhibited Neointimal Formation After Vascular Injury in Rat Model: Potential Application of Ribozyme Strategy to Treat Cardiovascular Disease." Circulation **102**(11): 1308.

Yguerabide, J. and E. Yguerabide (1998). "Light-Scattering Submicroscopic Particles as Highly Fluorescent Analogs and Their Use as Tracer Labels in Clinical and Biological Applications:: I. Theory." Analytical Biochemistry **262**(2): 137-156.

Yu, S. H., T. H. Wang and L. C. Au (2009). "Specific repression of mutant K-RAS by 10-23 DNAzyme: Sensitizing cancer cell to anti-cancer therapies." Biochemical and biophysical research communications **378**(2): 230-234.

Zhou, M., Z. Liu, Y. Zhao, Y. Ding, H. Liu, Y. Xi, W. Xiong, G. Li, J. Lu and O. Fodstad (2010). "MicroRNA-125b confers the resistance of breast cancer cells to paclitaxel through suppression of pro-apoptotic Bcl-2 antagonist killer 1 (Bak1) expression." Journal of Biological Chemistry **285**(28): 21496.

CHAPTER 2. SYNTHESIS AND CHARACTERIZATION OF PHOTOACTIVATABLE SNP-DNAZYME

2.1 INTRODUCTION

Therapeutic approaches which utilize the internal machinery inherently present in cells are being increasingly explored as an alternative to the use of more standard pharmacological agents. Currently, several methods focus comprehensively on the mRNA level by preventing their translation into proteins. These methods are often implemented for the most critical aspects of gene silencing: halting or preventing production of proteins mediating disease(reviewed by (Bianco and Robey 2001)). The molecular species are most often in nucleic acid form, including antisense oligonucleotides, ribozymes, DNAzymes, and several small RNA species that target the RNA interference pathway (reviewed by (Kurreck 2003)). While many of these approaches are still only being evaluated in the laboratory, several have developed to the clinical stages (reviewed by (Akkina, Banerjea et al.)).

Each class of gene silencing candidates is distinct in the cellular machinery it uses and its specific mechanism of mRNA disruption. However, challenges exist for each class such as finding accessible sites on the target RNA for therapeutic oligonucleotide hybridization, protecting oligonucleotides from degradation by enzymes, and achieving cellular uptake and accurate intracellular localization (reviewed by (Kurreck 2003)).

The original proposed plan in this project targeted the disruption of miRNA 125b(Zhou, Liu et al. 2010) as strategy for treatment of cancer. It was hypothesized that the cleavage of miRNA 125b via DNAzyme action, followed by the administration of naturally-formulated rubusoside-Paclitaxel, would offer a means to sensitize targeted cancer cells. miRNA 125b is an important signal pathway regulator, which in breast cancer cells, cleaves Bak1

mRNA, which is responsible for apoptosis(Zhou, Liu et al. 2010). Three DNAzymes were synthesized to cut miRNA 125b:1) one with the same core as the 10-23 DNAzyme and the recognition arms with complimentary bases, 2) a modified core to the DNAzyme with wobble base pairs and shorter complementary recognition arms, 3) a modified core to the DNAzyme with wobble base pairs and longer complementary recognition arms. None of these DNAzymes were successful in cleaving the substrate RNA despite evaluation in varying buffer, time, and concentration conditions.

Thus an alternate approach was explored, a DNAzyme known to target the mutant K-Ras gene, which is a critical signal transduction pathway that when mutated leads to pancreatic, colorectal, endometrial, biliary tract, lung, and cervical cancers(Yu, Wang et al. 2009). The basis of this hypothesis is that the pyrimidine-purine pair to be cut by the K-Ras 10-23 DNAzyme is a 'G-U' pair, unlike the 'A-C' pair to be cut by the miRNA 125b DNAzyme (Yu, Wang et al. 2009, Zhou, Liu et al. 2010). In comparison to the original Ras gene, the mutant K-Ras gene has a point mutation with a U substituted for a G. This mutation allows a 10-23 deoxyribozyme to hybridize to the pyrimidine-purine site and cleave the mutant K-Ras mRNA (Yu, Wang et al. 2009). Modification of these nucleotide pairs has been explored by Cairns et al., demosnstrating that AU = GU > GC >> AC in the effectiveness of cleavage. (Cairns, King et al. 2003). The K-Ras 10-23 DNAzyme will be used in this project to sensitize mutant K-RAS colon and breast cancer cells to the chemotherapeutic doxorubicin.

In this application, SNPs serve as oligonucleotides carriers to facilitate their intracellular delivery. If the SNPs are formed within the range of 1-100 nm in diameter, they have excellent cellular delivery capabilities because particles of that size are not generally removed by the reticuloendothelial system (reviewed by (Bawarski, Chidlowsky et al. 2008)). In general, the

number of applications utilizing nanoparticles has increased greatly due to improvements in ease of their synthesis and bioconjugation (reviewed by (Biju, Itoh et al. 2008)). Noble metal nanoparticles have distinctive electronic and photonic properties (reviewed by (Hutter and Fendler 2004),) which can be utilized for this application. These properties include high scattering efficiency, large extinction coefficients, and localized surface plasmon resonance (LSPR) (Yguerabide and Yguerabide 1998, Hutter and Fendler 2004). Colloidal silver nanoparticles possess the additive benefit of surface enhanced spectroscopy, which enables qualitative and quantitative analysis of low levels of target analytes (Munro, Smith et al. 1995, Munro, Smith et al. 1995) . These properties ultimately assist in driving the reactions for drug delivery since the electric field will cause strain to the bonds of the nanoparticle, allowing for easier release of functionalized oligonucleotides(Chen and Goodman 2004, Eustis and El-Sayed 2006).

DNAzyme oligonucleotides conjugated to the surface of SNP via thiol-metal linkages are thought to pack densely(Qureshi, Monroe et al. 2013), thus protecting them from enzymatic degradation . Johnson *et al.* reported 11-mercaptoundecanoic acid aided the homogeneous dispersal of silver nanoparticles (Johnson Jr, Kang et al. 2008) addressing an important need for reduced aggregation to aid in a greater packing density. TEM imaging showed packing density was enhanced by "backfilling" the oligonucleotide-functionalized particle via subsequent addition of the alkane thiol 11-mercaptoundecanoic acid. In addition, the DNA construct includes a photocleavable nitrobenzyl group to permit oligonucleotide release from the SNP with UV light exposure. The SNP-DNAzyme construct was designed to be evaluated in a system requiring targeted gene silencing, whereby precise light exposure offers spatiotermporal control.

This project has significance because it addresses the need to develop effective means of delivering therapeutic oligonucleotides to targeted cells with high efficiency and precision.

2.2 MATERIALS AND METHODS

2.2.1 Materials

DNAzyme and RNA materials

Silver nanoparticles were functionalized with thiol-modified miRNA 125b DNAzyme ordered from Integrated DNA Technologies (DA: 5'- TCA CAA GTT AGG GGG CTA GCT ACA ACG ACT CAG GGA -3' and DC: 5'- A GTT AGG I GG CTA GCT ACA ACG A U T CAG GGA -3', IDT, Coralville, IA) or EXIQON (LA: 5'- TCACAAGT+**T**AG+**G**/ideoxyI/ GGCTAGCTACAA CGA/ideoxyU/T+**C**A+**G**GGA-3', Bold letters have modification locked nucleic acid, Woburn, MA) based on miRNA125b reported by Zhou *et al.*(Zhou, Liu et al. 2010). Silver nanoparticles were functionalized with thiol-modified KRAS DNAzymes ordered from Integrated DNA Technologies (5'- CTA CGC CAA GGC TAG CTA CAA CGA AGC TCC AAC T /3ThioMC3-D/ -3', IDT, Coralville, IA) or Trilink Biotechnologies (5' (TAMRA) (C6-NH) CTA CGC CAA GGC TAG CTA CAA CGA AGC TCC AAC T (PC Spacer) T (C3-S-S-C3) 3', San Diego, CA) based on DNAzyme reported by Yu et al.(Yu, Wang et al. 2009). miRNA 125 mRNA were ordered from Integrated DNA Technologies (5'- rUrCrC rCrUrG rArGrA rCrCrC rUrArA rCrUrU rGrUrG rA/36-FAM/ -3' or 5'- /TYE665/-TTTTTTTTTT-rUrCrC rCrUrG rArGrA rCrCrC rUrArA rCrUrU rGrUrG rA-3', IDT, Coralville, IA) based on complementary sequence to DNAzyme. KRAS mRNA were ordered from Integrated DNA Technologies (5'- rArGrU rUrGrG rArGrC rUrGrU rUrGrG rCrGrU rArG -3' or 5'- /5TYE665/rArGrU rUrGrG rArGrC rUrGrU rUrGrG rCrGrU rArG -3', IDT, Coralville, IA)) based on complementary sequence to DNAzyme.

Gel Electrophoresis Materials

Mini-PROTEAN® Tetra cell, Mini-PROTEAN® TBE precast gels (15% polyacrylamide, 12-well comb, 20µl/well), Mini-PROTEAN TBE-Urea precast gels (15% precast polyacrylamide gel, 12-well comb, 20µl/well), 10X TBE buffer, and PowerPac™ Basic Power Supply were purchased from Bio-Rad (Hercules, CA). Low Molecular Weight Marker 10-100 nt was purchased from Affymetrix (Santa Clara, CA). Fragment Sizes: 10 nt; 15 nt; 20 nt; 25 nt; 30 nt; 35 nt; 40 nt; 45 nt; 50 nt; 60 nt; 70 nt;80 nt; 90 nt; 100 nt. 2X Formamide Loading Buffer was supplied with the marker. Syber Gold™ stain 10,000X was purchased from Molecular Probes via Thermo Fisher Scientific (Rochester, NY).

Reaction and Stopping Buffer Materials

Magnesium chloride, Trizma® hydrochloride, and sodium chloride were purchased from Sigma Aldrich (St. Louis, MO). Potassium chloride was purchased from Fischer Scientific (Pittsburgh, PA). EDTA was purchased from Amresco (Solon, OH). All solvents purchased were for molecular biology.

Citrate and HPC Silver Nanoparticle Oligonucleotide Materials

Silver nitrate (Sigma Ultra >99%) and sodium citrate were purchased from Sigma Aldrich (St. Louis, MO). PTFE resin-coated magnetic stirring bars were purchased from VWR (West Chester, PA). 100 mL Glass syringes used to dispense sodium citrate dropwise to reduce silver nitrate in solution were purchased from KD scientific (Holliston, MA). All other glassware was purchased through Fisher Scientific (Pittsburgh, PA). Hydroxypropyl cellulose SNPs, SmartSilver^{TM}AS, was purchased from NanoHorizons Inc (Bellefonte, PA). Silver nanoparticles were functionalized with thiol-modified miRNA 125b or KRAS DNAzymes ordered from Integrated DNA Technologies (IDT, Coralville, IA) or Trilink Biotechnologies (San Diego, CA).

2M Tris-NaCl buffer (pH 8.0) was made up from Biotechnology grade Tris (Amresco Inc, Solon, OH) and sodium chloride (Fischer Scientific, Pittsburgh, PA). 11-Mercaptoundecanoic acid was ordered from Sigma Aldrich (St. Louis, MO).

SNP Characterization Materials

Transmission Electron Microscopy (TEM) grids were obtained from Electron Microscopy Sciences (Hatfield, PA). Malvern ZEN0040 disposable cuvettes were purchased from Malvern (Worcestershire, United Kingdom). DL-Dithiothreitol, 1M aqueous solution was purchased from Sigma Aldrich (St. Louis, MO)

2.2.2 Methods

***In vitro* Photocleavage of DNAzyme Oligonucleotide or SNP-DNAzyme**

miRNA125b DNAzyme and miRNA125b RNA were pooled together (1:1) for 0, 30, and 60 minutes. KRAS DNAzyme and KRAS RNA were pooled together 0, 30, and 60 minutes. KRAS SNP-DNAzyme and KRAS RNA were pooled together 0, 30, and 60 minutes. 50mM EDTA pH 7.5 stopping buffer was applied to stop the reactions. Samples were hit with ultraviolet light using the High Performance Ultraviolet Transilluminator (UVP, Upland, CA) purchased via Fisher Scientific (Pittsburgh, PA). 10µl of sample, Loading Buffer, and DEPC water were run in individual wells in the Mini-PROTEAN® TBE precast gels (15% polyacrylamide, 12-well comb, 20µl/well) or Mini-PROTEAN TBE-Urea precast gels (15% precast polyacrylamide gel, 12-well comb, 20µl/well), in the Mini-PROTEAN® Tetra cell (100V native/180V denaturing) with 1X TBE buffer. Low Molecular Weight Marker 10-100 nt was loaded in individual wells. Gels were stained in 1X SYBR Gold (30 µl 1XSYBR Gold in 300mL 1X TBE buffer) for 30 minutes. Samples were visualized on a Typhoon 9410 Variable Mode Imager (normal sensitivity, 400 PMT Volts, prescan at 1000 microns pixel size, imaging at 100

microns pixel size) (GE Healthcare, Piscataway, NJ). 488nm laser line was used to image gels stained with SYBR Gold (540bp30 filter). 633 nm laser line was used to image gels with RNA containing TYE665 (648/666) present (670bp30 filter).

WCIF Image J Image Processing

Images were processed and analyzed using WCIF Image J. The mean pixel intensity of one line was taken on the left, middle, and right side of each sample. The mean pixel intensities of the samples hit with UV divided by the mean pixel intensities of the samples not hit with UV is plotted on a bar graph.

SNP Synthesis

Citrate-reduced silver nanoparticles were prepared according to the method written by Brown *et al*.(Brown, Qureshi et al. 2013) Hydroxypropyl cellulose SNPs, SmartSilver^{TM}AS, was purchased from NanoHorizons Inc (Bellefonte, PA).

SNP Functionalization

Silver nanoparticles were functionalized by a revised 'salt-aging' technique. Thiol-modified TAMRA(NHSester)-labeled oligonucleotides (543/571, Trilink Biotechnologies) were mixed with silver nanoparticles (128ppm) at an oligo-to-particle stoichiometry of 700:1. The mixtures incubate at 37°C under rocking conditions for 24 hours to support the beginning of oligonucleotide adsorption to the silver nanoparticle by their end thiol bond. Following the 24hr incubation period, the SNP-DNAzyme oligonucleotide conjugate solution was first adjusted to 1% SDS and 25mM phosphate buffer. Then the SNP-DNAzyme oligonucleotide conjugate solution went through a 48hr Tris-buffer based salt-aging process ending in a 80mM NaCl and 80mM Tris buffer (10ul aliquot additions 7X of a 2M Tris-NaCl buffer pH 8.0 per 48hrs, 10µl addition every 3-4 hours) concentration. Functionalized nanoparticles were purified by

centrifugation (3 20 minute spins at 7000 RPM) and pellets were resuspended in a modified buffer (1% SDS, 50mM Tris-NaCl) prior to experimental analysis. Purified particles were backfilled with 0.169 μM 11-Mercaptoundecanoic acid (1/10 DNAzyme concentration).

SNP Characterization and Oligonucleotide Surface coverage Methods

Ultraviolet-Visible Spectroscopy was performed using a Genesys6 UV–Visible Spectrophotometer (Thermo Scientific, Madison, WI). 100 μl of various SNP samples were pipetted into disposable cuvettes, and the absorbance spectrum of 200-700 nm wavelengths was collected. The peak absorbance of the SNP, at approximately 420 nm(Yguerabide and Yguerabide 1998), undergoes a red-shift when functionalized with DNAzyme oligonucleotides.

Transmission Electron Microscopy (TEM) images were imaged on a JOEL 2011 TM (Tokyo, Japan). 5 μL of diluted sample was added to a carbon film 400 square mesh copper grid (Electron Microscopy Sciences), and was air dried for 10 minutes. Images were taken at various magnifications. TEM images were analyzed using ImageJ. The diameters of nanoparticles of each type were measured using digital calipers.

Dynamic Light Scattering (DLS) was performed using a Malvern Zetasizer nano series (Worcestershire, UK). Hydrodynamic diameters of samples were measured in Malvern ZEN0040 disposable cuvettes at 25˚ C. SNP samples were measured in 1% SDS, 50mM Tris-NaCl.

Zeta potential was performed using a Malvern Zetasizer nano series (Worcestershire, UK). Charges of samples were measured in Zetasizer nano series folded capillary cells at 25˚ C. SNP samples were measured in deionized water.

Inductively Coupled Plasma Optical Emission Spectrometry (ICP-OES) was performed using a Varian Vista MPX (Palo Alto, CA). The masses of a 10mL glass test tube, 100μL of

treated SNP samples, 1mL nitric acid, and 10mL of DI water were recorded in an Excel file after each additional item was pipetted in. The silver concentrations of triplicate treated samples were measured by the Vista MPX. The component densities and the collected silver data were used to calculate the concentrations of the treated samples.

Oligonucleotide surface coverage was quantified using fluorescence calibrations of known concentrations of TAMRA DNAzyme (546/576) in 100 µl volumes. The fluorescence was recorded using a Wallac 1420 VICTOR2™ plate reader (Perkin Elmer, Shelton, CT). A standard curve was established with results. The concentration of oligonucleotide in the experimental samples that were photocleaved or DL-Dithiothreitol (DTT)-treated could then be determined. Surface coverage was determined based on a method using ICP-OES results and oligonucleotide concentration reported by Qureshi *et al*.(Qureshi, Monroe et al. 2013).

Statistical analysis

All results were expressed as mean ± % standard error.

2.3 RESULTS AND DISCUSSION

This project is focused on designing a nanoparticle drug delivery system based on the gene silencing effects of a 10-23 deoxyribozyme(Santoro and Joyce 1998). The drug delivery vehicle, silver nanoparticle(SNP), is functionalized with a thiol-modified deoxyribozyme with internal photocleavable linkers(Brown, Qureshi et al. 2013). The internal photocleavable linkers are essential to the spatiotemporal control of the release of the gene silencing deoxyribozymes(reviewed by(Pelliccioli and Wirz 2002)).

The original proposed plan in this project targeted the disruption of miRNA 125b (Zhou, Liu et al. 2010) as strategy of treatment for cancer. It was hypothesized that the cleavage of miRNA 125b via DNAzyme action, followed by the administration of naturally-formulated

rubusoside-Paclitaxel, would offer a means to sensitize targeted cancer cells. miRNA 125b is an important signal pathway regulator, which in breast cancer cells, cleaves Bak1 mRNA, which is responsible for apoptosis(Zhou, Liu et al. 2010). As shown in Figure 2.1, three DNAzymes were synthesized to cut miRNA125b:1) same core as the 10-23 DNAzyme and the recognition arms with complimentary bases, 2) modified core to the DNAzyme with wobble base pairs and shorter complementary recognition arms, 3) modified core to the DNAzyme with wobble base pairs and longer complementary recognition arms. None of these DNAzymes were successful in cleaving the substrate RNA despite evaluation in varying buffer, time, and concentration conditions. Breast cancer cell lines, MDA-MB-231 and MDA-MB-435, were proposed to be treated with increasing doses of naturally-formulated rubusoside-Paclitaxel to form sensitive and resistant cell lines. The cell lines used started at high passage numbers and did not survive after two weeks of splitting.

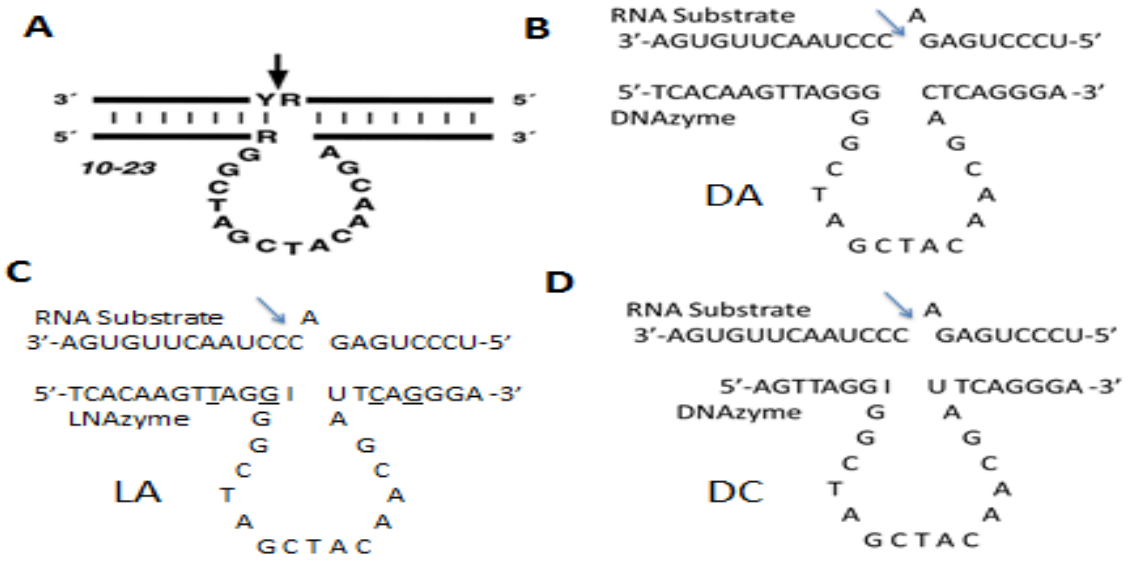

Figure 2.1. Hybridization of the mi125b DNAzyme to the miRNA125 mRNA. DNAzymes synthesized to cut miRNA 125b mRNA: A) 10-23 DNAzyme core, B) same core as the 10-23 DNAzyme and the recognition arms with complimentary bases, C) modified core to the DNAzyme with wobble base pairs and longer complementary recognition arms with locked nucleic acid modifications, and D) modified core to the DNAzyme with wobble base pairs and shorter complementary recognition arms.

Figure 2.2 shows that anti-miRNA125b linked with the fluorescent molecule 6-FAM (lane 2) was the same size as DNAzyme A (lane 5) and LNAzyme A (lane 7), thus the RNA could not be used for determination of cutting cleavage effectiveness. Anti-miRNA125b linked with TYE665 (lane 3) showed a significant difference in size compared to the other DNAzyme controls.

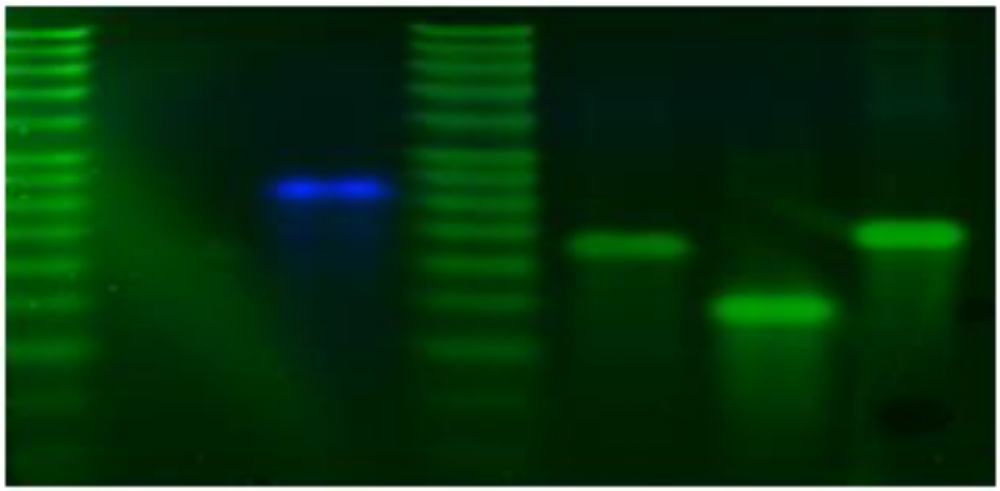

Lane	1	2	3	4	5	6	7
Ladder	+			+			
RNA		FAM-6 22nt	TYE665 22nt				
DNAzyme					DA 36nt	DC 31nt	LA 36nt

Figure 2.2. Overlay of 2 images (SYBR Gold stained and 6FAM-488nm laser & 520bp40 filter and TYE665-633nm laser & 670bp30): miRNA125b RNA and DNAzyme controls. Lanes 1 and 4) Low Molecular Weight Ladder 10-100 nt; Lane 2) 6FAM miRNA125b (520bp40); Lane 3) TYE665 miRNA125b (670bp30); Lane 5) DA; Lane 6) DC; and Lane 7)LA.

Figure 2.3 shows the ineffectiveness of LNAzyme A cutting TYE665 anti-miRNA125b. LNAzyme A was even concentrated 50:1 compared to the TYE^^% anti-miRNA 125b. The gel also shows the timed reaction of 60 minutes, including the samples placed in several reaction buffers.

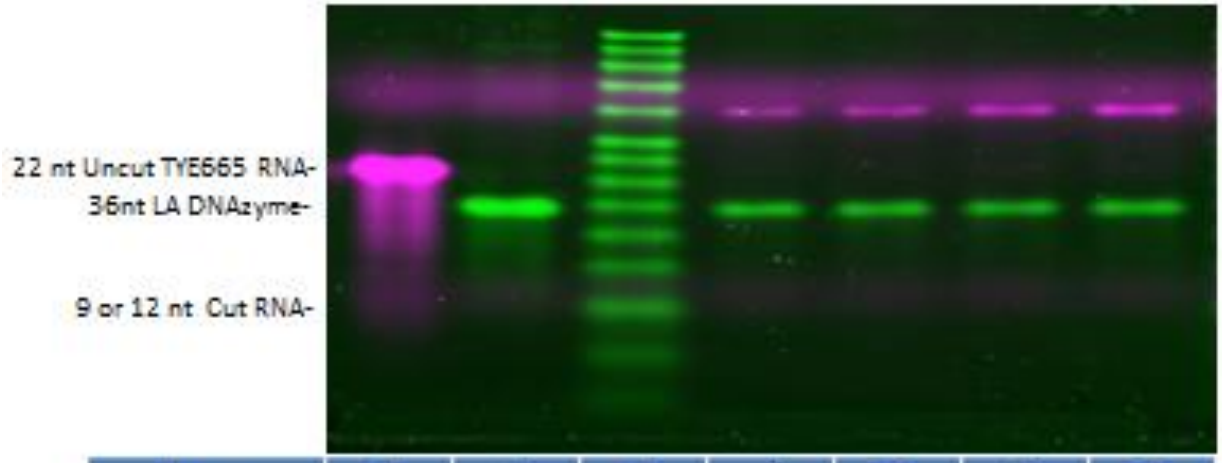

Lane	1	2	3	4	5	6	7
Ladder			+				
TYE665 RNA	+			+	+	+	+
LA DNAzyme		+		+	+	+	+
Buffer				B2	B3	B4	B5

Figure 2.3. Overlay of 2 images (SYBR Gold stained -488nm laser & 520bp40 filter and TYE665-633nm laser & 670bp30): 50:1 LA DNAzyme:TYE665 miRNA125b RNA cleavage reaction for 60 minutes. Lanes 1) TYE665 miRNA125b (670bp30); Lane 2) LA DNAzyme; Lane 3) Low Molecular Weight Ladder 10-100 nt; Lane 4) 50:1 LA DNAzyme; RNA in B2; Lane 5) 50:1 LA DNAzyme; RNA in B3; Lane 6) 50:1 LA DNAzyme; RNA in B4; and Lane 7) 50:1 LA DNAzyme; RNA in B5. Buffers: B2-150mM NaCl & 2 mM $MgCl_2$; B3-150mM KCl & 2 mM $MgCl_2$; B4-60mM NaCl & 2 mM $MgCl_2$; and B5-60mM KCl & 2 mM $MgCl_2$).

An alternate approach was explored, a DNAzyme known to target the mutant K-Ras gene as shown in Figure 2.4, which is a critical signal transduction pathway that when mutated leads to pancreatic, colorectal, endometrial, biliary tract, lung, and cervical cancers(Yu, Wang et al. 2009). The 10-23 DNAzyme was shown to be effective in the studies conducted by Yu *et al.* The basis of this hypothesis is that the pyrimidine-purine pair to be cut by the K-Ras 10-23 DNAzyme is a 'G-U' pair, unlike the 'A-C' pair to be cut by the miRNA 125b DNAzyme shown in Figure 2.1 (Yu, Wang et al. 2009, Zhou, Liu et al. 2010). In comparison to the original Ras gene, the mutant K-Ras gene has a point mutation with a U substituted for a G. This mutation

allows a 10-23 deoxyribozyme to hybridize to the pyrimidine-purine site and cleave the mutant K-Ras mRNA(Yu, Wang et al. 2009). Modification of these nucleotide pairs has been explored by Cairns et al., demosnstrating that AU = GU > GC >> AC in the effectiveness of cleavage (Cairns, King et al. 2003). The K-Ras 10-23 DNAzyme will be used in this project to sensitize mutant K-RAS colon and breast cancer cells to the chemotherapeutic doxorubicin. The additional light will increase uncaging the DNAzyme from silver nanoparticles, thus allowing for an effective therapy treatment. Paclitaxel will not be an appropriate option for treatment since taxol works through the microtubule network and so does the expression of the K-Ras proteins(Thissen, Gross et al. 1997, Chen, Otto et al. 2000).

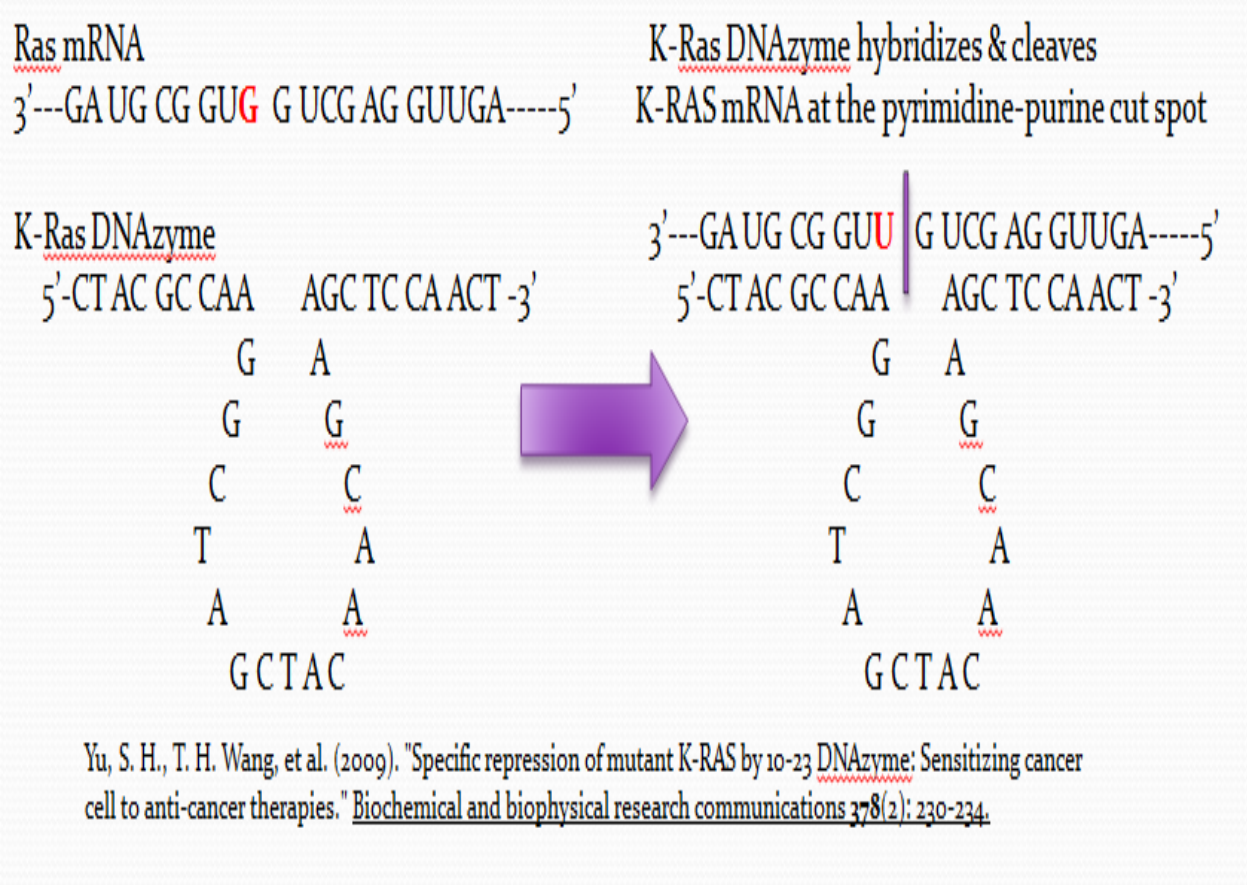

Yu, S. H., T. H. Wang, et al. (2009). "Specific repression of mutant K-RAS by 10-23 DNAzyme: Sensitizing cancer cell to anti-cancer therapies." Biochemical and biophysical research communications 378(2): 230-234.

Figure 2.4. Hybridization of the K-Ras DNAzyme to the Mutant K-Ras Gene.

The design of the KRAS DNAzyme (KRAS DZ) construct evaluated several elements: effective cleavage ability, thiol modification (thiolDZ), incorporation of the photocleavable linker (PC DZ), and TAMRA fluorophore conjugation (TAMRA DZ), effective removal of the thiolDZ from SNP using DTT, optimization of the coverage of DNAzyme oligonucleotide surrounding the citrate or HPC SNP surface; photolysis of the nitrophenylethyl internal photocleavable linker, and protection of the oligonucleotide from enzymatic degradation.

Effective cleavage ability of the KRAS DNAzyme is shown in Figure 2.5. Figure 2.5 displays the electrophoresis gel of the combination of 10-23 DNAzyme and its target K-Ras mRNA substrate in 3 different buffers. The first two lanes to the left of the ladder are control wells of pure DNAzyme and RNA, respectively. A 1:1 DNAzyme: mRNA reaction was carried out in Buffer 2 (150 mM NaCl, 2 mM $MgCl_2$, 50 mM Tris-HCl), Buffer 4 (60 mM NaCl, 2 mM $MgCl_2$, 50 mM Tris-HCl), and Buffer 6 (60 mM NaCl, 20 mM $MgCl_2$, 15 mM Tris-HCl) to compare DNAzyme efficacy in various salts. Oligonucleotides were stained by SYBR gold. Lanes 5, 7, and 9 show the presence of cleavage products of the mutant K-Ras mRNA produced after incubation for 60 minutes at 37°C in Buffers 2, 4, and 6.

Effective cleavage ability of the thiolDZ is shown in Figure 2.6. The thiol bond is vital for the oligonucleotide to covalently bond to the SNP. Figure 2.6 displays the denaturing electrophoresis gel of the combination of 10-23 DNAzyme and its target K-Ras mRNA substrate reacted at three different times. The first two lanes are using the K-Ras DNAzyme to react with a TYE665 labeled K-RAS mRNA. Lanes 3-5 are using the thiol conjugated DNAzyme to react with a TYE665 labeled K-RAS mRNA. A 1:1 DNAzyme: mRNA reaction was carried out in Buffer 4 (60 mM NaCl, 2 mM $MgCl_2$, 50 mM Tris-HCl), chosen from Figure 2.2 as the best buffer to work with. Oligonucleotides were stained by SYBR gold. Images were taken of the

TYE665 labeled RNA and overlayed with the SYBRgold images in ImageJ. Lanes 2 and 5 show the presence of cleavage products of the mutant K-Ras mRNA produced after incubation for 60 minutes at 37°C. Lane 4 shows the presence of cleavage products of the mutant K-Ras mRNA produced after incubation for 30 minutes at 37°C with a 2:1 ratio amount of DNAzyme:RNA

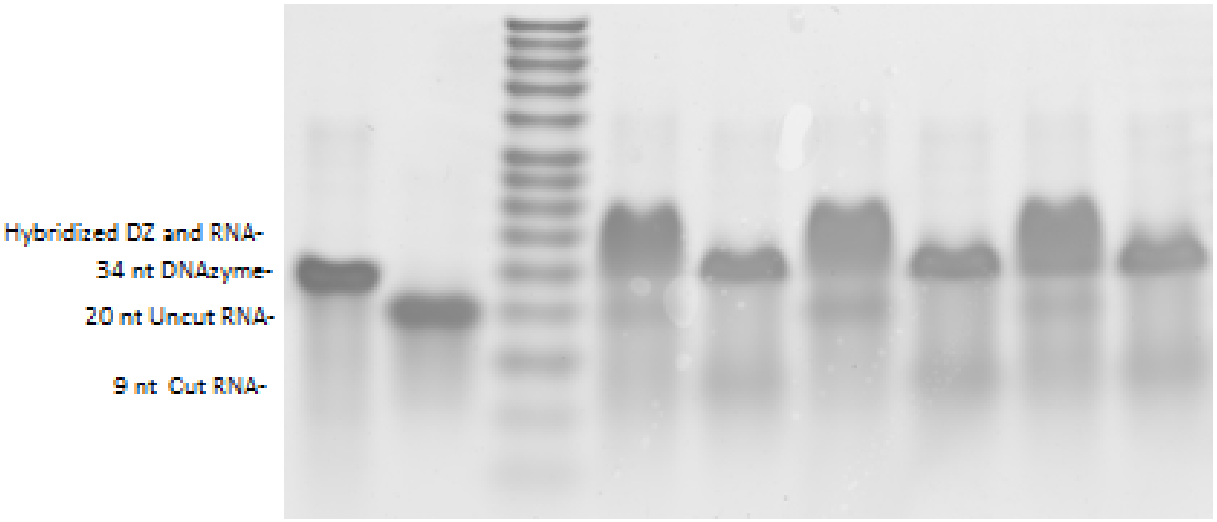

Lane	1	2	3	4	5	6	7	8	9
Ladder			+						
KRAS RNA		+		+	+	+	+	+	+
KRAS DZ	+			+	+	+	+	+	+
Buffer				B2	B2	B4	B4	B6	B6
Time of Reaction				0 min	60 min	0 min	60 min	0 min	60 min

Figure 2.5. Cleavage of mutant K-Ras DZ using a 1:1 ratio of DNAzyme: mRNA in 3 separate buffers at 37°C for 60 minutes (SYBR Gold stained -488nm laser & 520bp40 filter). Lane 1) KRAS RNA; Lane 2)KRAS DZ; Lane 3) Low Molecular Weight Ladder 10-100 nt; Lane 4) 1:1 KRAS DZ; KRAS RNA in B2 for 0min; Lane 5) 1:1 KRAS DZ; KRAS RNA in B2 for 60min; Lane 6) 1:1 KRAS DZ; KRAS RNA in B4 for 0min; Lane 7) 1:1 KRAS DZ; KRAS RNA in B4 for 60min; Lane 8) 1:1 KRAS DZ; KRAS RNA in B6 for 0min; and Lane 9) 1:1 KRAS DZ; KRAS RNA in B6 for 60min. Buffers: B2-150mM NaCl & 2 mM $MgCl_2$;; B4-60mM NaCl & 2 mM $MgCl_2$; and B6-60mM NaCl & 20 mM $MgCl_2$).

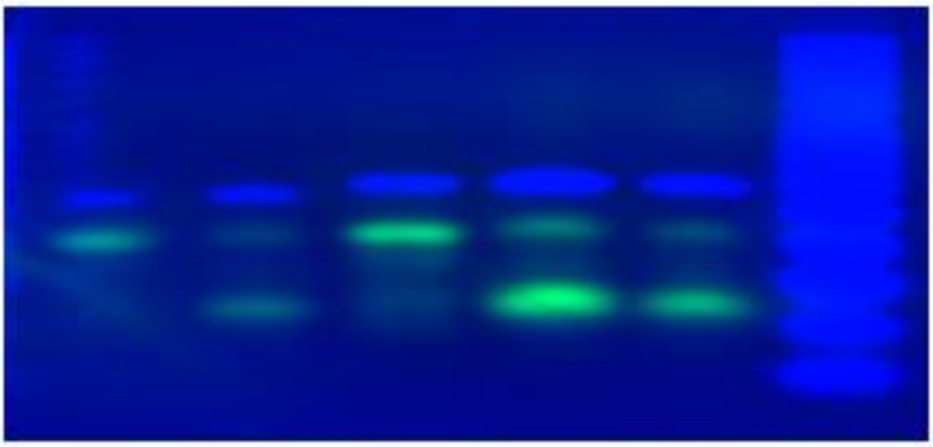

Lane	1	2	3	4	5	6
Ladder						+
TYE665RNA	+	+	+	+	+	
ThiolKRASDz	+	+	+	(2X)	+	
1% DTT added			+	+	+	
Time of Reaction	0min	60min	0min	30min	60min	

Figure 2.6. Cleavage of mutant ThiolK-RasDZ using a 1:1 ratio of DNAzyme: mRNA in 60mM NaCl & 2 mM $MgCl_2$ at 37°C for 0, 30, and 60 minutes. Denaturing gel was used. 1% DTT was added to break any formation of disulfide bonds.

Components of the KRAS DNAzyme construct were characterized to help the main goals of the whole project. Figure 2.7A shows the SNP-TAMRA DZ construct fully. ThiolDZ and PC DZ would take the place of the TAMRA DZ in the Figure 2.7A construct. UV-Vis spectroscopy was used to characterize the presence of silver and any oligonucleotide additions to silver. Figure 2.7B shows the presence of HPC SNPs with and without the DNAzyme added to it. There was no red shift seen at the normal absorbance of silver, which is approximately 420nm. Figure 2.7C and 2.7D did show a red shift when the citrate SNP was compared to the functionalized SNP with TAMRA DZ.

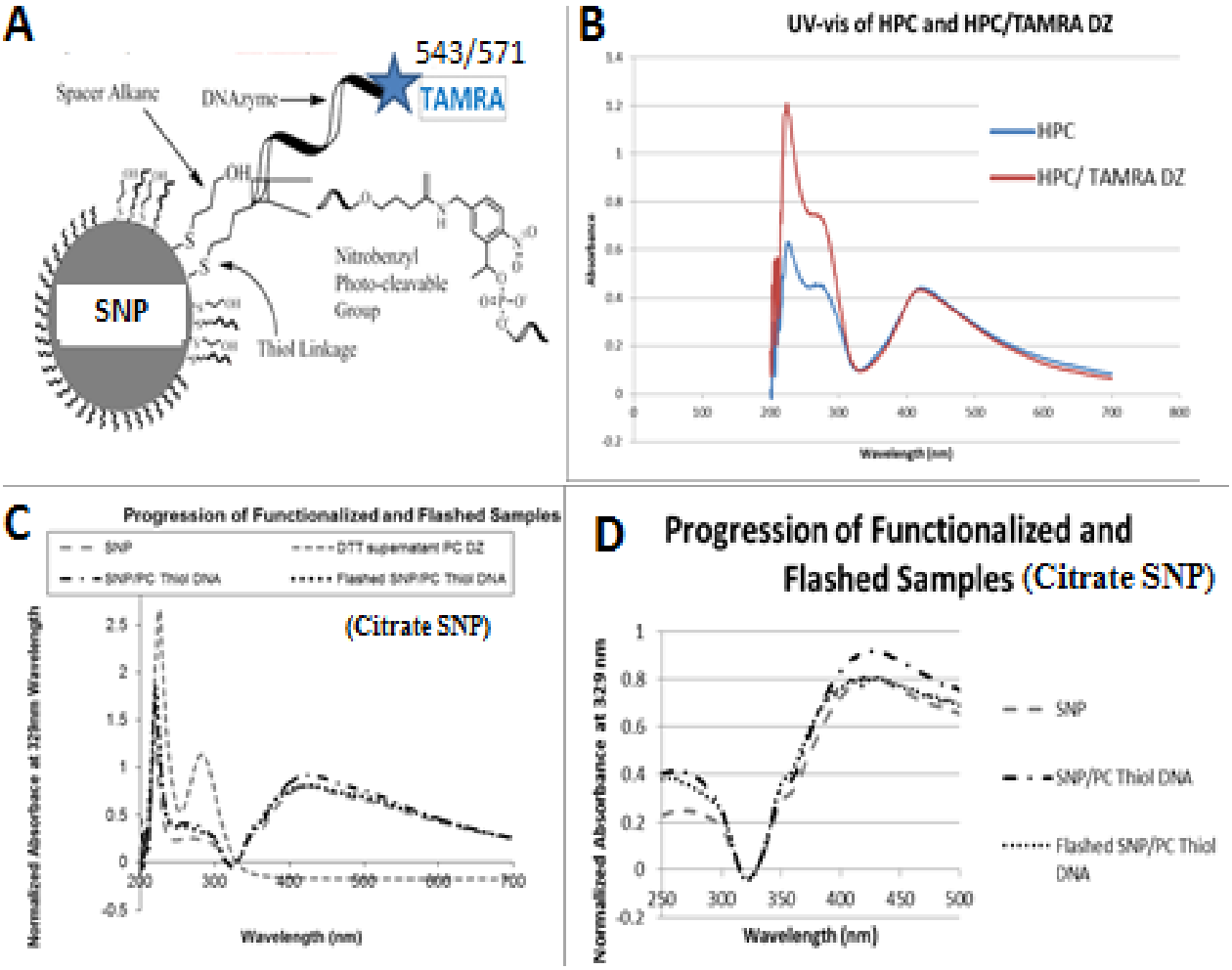

Figure 2.7. Design of TAMRA DZ construct and UV-Vis spectroscopy for HPC and Citrate SNPs. A) SNP functionalized with TAMRA DZ (including thiol bond, photocleavable linker, and KRAS DNAzyme oligonucleotide), B) 200-700nm UV-Vis spectroscopy of HPC SNP, C) 200-700nm UV-Vis spectroscopy of Citrate SNP, and D) Zoomed in view of 250-500nm UV-Vis spectroscopy of Citrate SNP in C.

Since the size of nanoparticles used for drug delivery entering the body is critically important, the SNPs were characterized using TEM. Figure 2.8A shows the unfunctionalized citrate SNPs. Figure 2.8B shows the functionalized citrate SNP. Figure 2.8C shows the unfunctionalized HPC SNP. Figure 2.8D shows the functionalized HPC SNP.

Determination of oligonucleotide concentration is essential in characterizing the DNAzyme surface coverage around the SNPs. Figure 2.9 shows the standard curve established

for the TAMRA DZ oligonucleotide. The best fit line was used for all Tamra Oligonucleotide samples following after this.

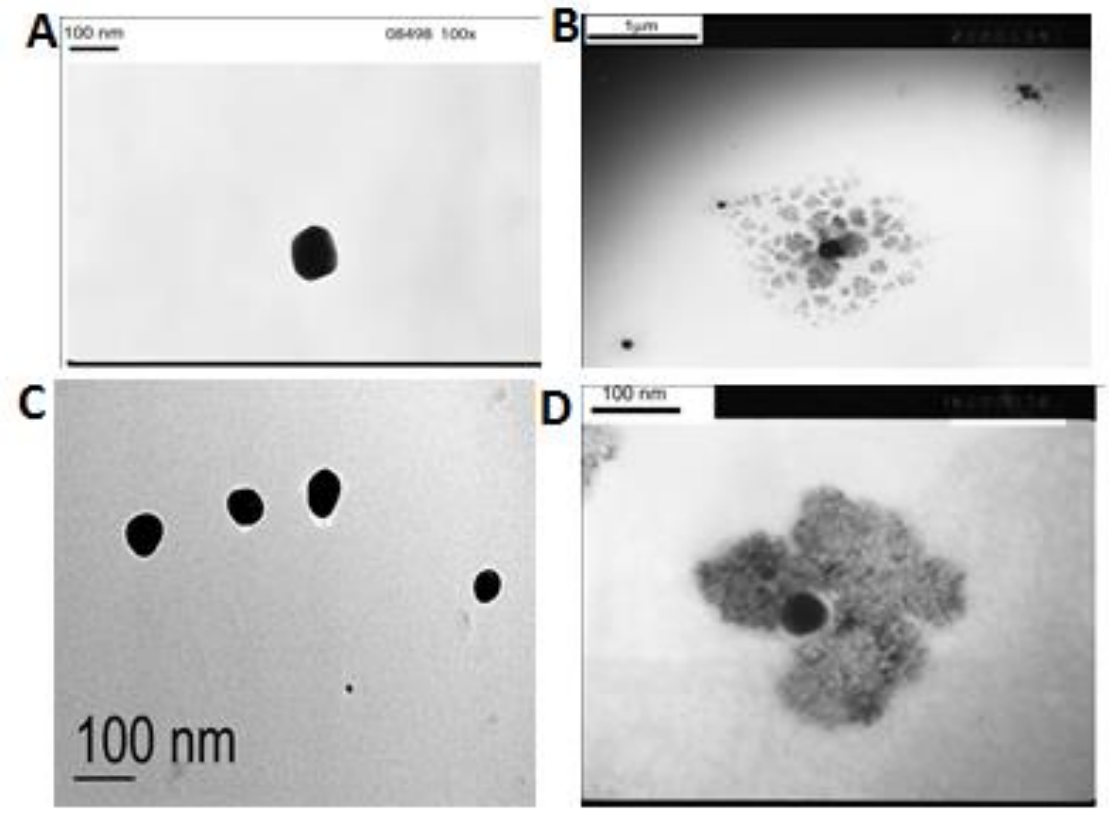

Figure 2.8. TEM images of particles. A) Citrate SNP, B) Citrate SNP functionalized with TAMRA DZ, C) HPC SNP, and D) HPC SNP functionalized with TAMRA DZ.

Table 2.1 shows the characterization of unfunctionalized and functionalized citrate and HPC SNPs using TEM, DLS, Zeta potential, ICP-OES, TAMRA DZ concentration determination, and surface coverage. Table 2.1 shows an increase in diameter size based on TEM results when comparing the unfunctionalized SNPs versus the functionalized SNPs, which includes the TAMRA DZ oligonucleotide. Table 2.1 DLS results show an increase from unfunctionalized citrate SNPs versus functionalized citrate SNPs including TAMRA DZ. Unfunctionalized HPC SNPs DLS results are shown to be larger than functionalized HPC SNPs

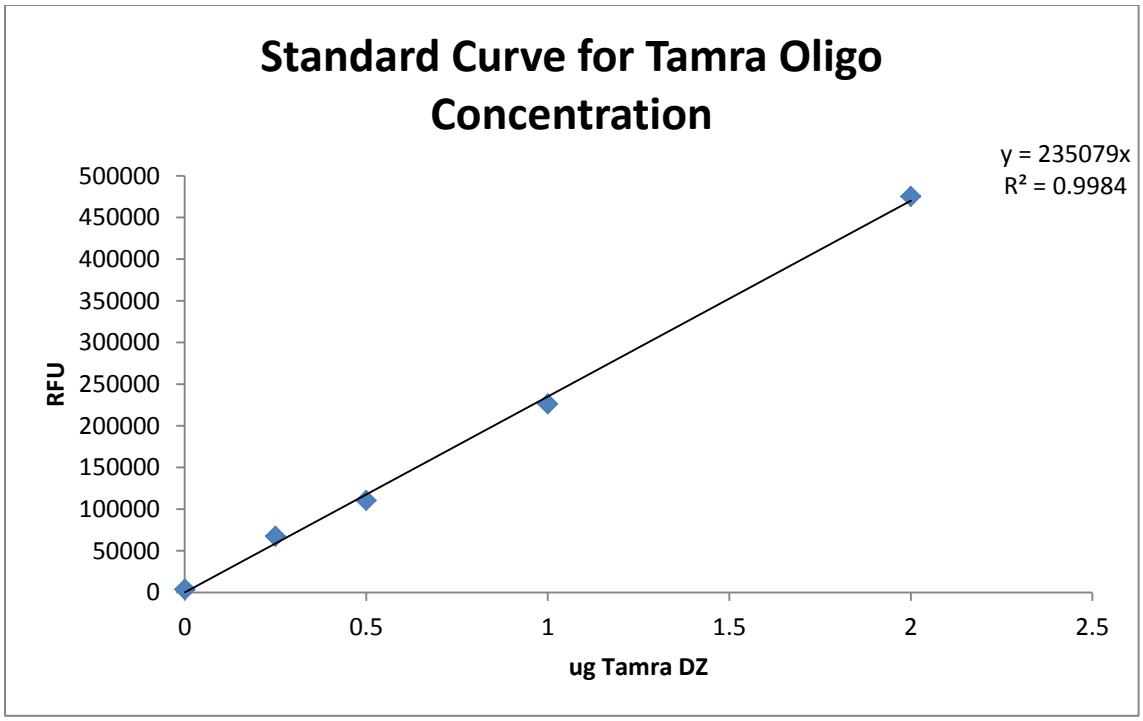

Figure 2.9.Standard curve for TAMRA DZ to quantify surface coverage.

and backfilled HPC SNPs. 1%vol Dithiothreitol (DTT) was added to the functionalized SNPs to remove the oligos from the outer silver surface. Following oligonucleotide removal, the silver quickly agglomerated as displayed in an even higher increase detected by dynamic light scattering (DLS). Table 2.1 zeta potential results show negative numbers correlating to the negative charge on the oligonucleotides. The backfilled functionalized HPC SNPs are even more negative in charge compared to the unfunctionalized HPC SNPs. TAMRA DZ oligonucleotide concentrations were taken after being cleaved from citrate and HPC SNPs by DTT or UV. DTT always removes more oligonucleotide. Surface coverage of citrate and HPC SNPs were determined using previous methods reported by Qureshi *et al(Qureshi, Monroe et al. 2013).* Table 2.1 results show an increase in number of oligonucleotides present on the surface of citrate and HPC SNPs per 100µl of treated sample.

Table 2.1. Characterization of SNPs, functionalized SNPs, and oligonucleotide surface coverage

Table 1. Characterization of SNPs and Oligonucleotide Surface Coverage Quantification					
	Citrate SNP	**Citrate SNP/ TAMRA DZ**	**HPC SNP**	**HPC SNP/ TAMRA DZ**	**HPC SNP/ TAMRA DZ/ 11-MUA**
TEM	91.5+/-7.1nm	220.9+/-50.1nm	59.0+/-7.2nm	120.6+/-7.3nm	277.7+/-5.3nm
DLS	76.3+/-1.1nm	103.8+/-1.1nm	239.6+/-14.1nm	99.8+/-5.0nm	120.0+/-10.1nm
Zeta	-27.7+/-0.7mV	Undetermined	-22.6+/-1.2mV	Undetermined	-33.1+/-1.0mV
ICP-OES	88.4+/-1.1ppm	42.8+/-6.8ppm	127.3+/-8.7ppm	117.40+/-13.44 ppm	11.7+/-1.3ppm
TAMRA DZ Oligo	NA	DTT:1.34 µg UV: 0.27 µg	NA	DTT: 0.24 µg UV: 0.10 µg	DTT:0.41 µg UV:0.13 µg
Surface Coverage	NA	DTT: 3503 oligos: 1 SNP UV: 706 oligos: 1 SNP	NA	DTT: 1360 oligos: 1 SNP UV: 567 oligos: 1 SNP	DTT: 23266 oligos: 1 SNP UV: 7377 oligos: 1 SNP

Effective cleavage ability of the ThiolDZ and effective removal of the thiolDZ from SNP using DTT is shown in Figure 2.10. The electrophoresis gel was used as an activity assay. Average pixel intensity normalized by background pixel intensity was measured using Image J. The average pixel intensity of the cut KRAS mRNA was divided by the average pixel intensity of the uncut KRAS mRNA. Figure 2.10 lane 8 shows the bands produced after SNP-ThiolDZ was reacted with TYE665 KRAS mRNA for 60 minutes. ThiolDZ was removed from citrate SNPs using DTT. The quotient of average pixel intensity for the cut and uncut mRNA bands was 0.68. Since the number was less than one, it was confirmed that there was more uncut mRNA than cut mRNA. Figure 2.10 lane 10 shows the bands produced after ThiolDZ was removed from citrate SNPs using DTT. ThiolDZ was reacted with TYE665 KRAS mRNA for 60 minutes. The quotient of average pixel intensity for the cut and uncut mRNA bands was 1.97. Since the

number was greater than one, it was confirmed that there was more cut mRNA than uncut mRNA.

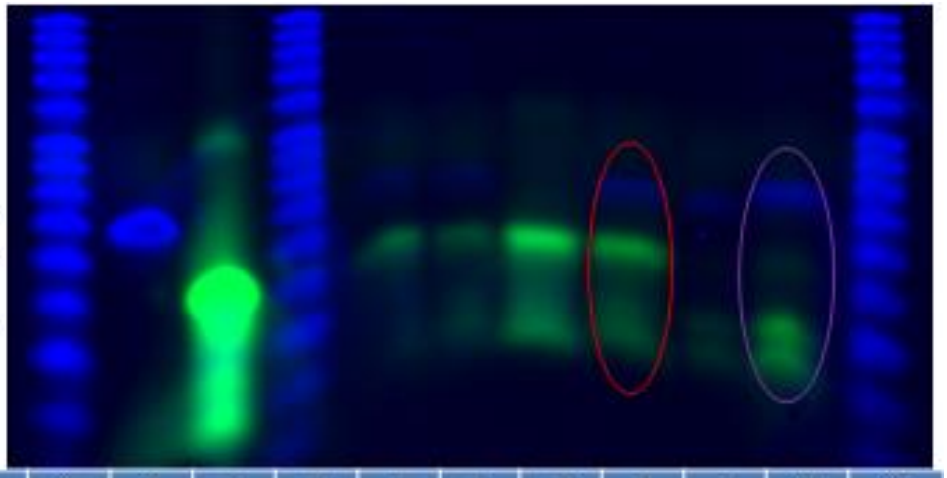

Lane	1	2	3	4	5	6	7	8	9	10	11
Ladder	+			+							+
TYE665 RNA			+		+	+	+	+	+	+	
ThiolDZ		+			+	+					
SNP/Thiol DZ							+	+	+	+	
RNA; DTT							+	+			
DTT;RNA									+	+	
Time					0 min	60 min	0 min	60 min	0 min	60 min	

Figure 2.10. A) Overlay of 2 images (SYBR Gold stained -488nm laser & 520bp40 filter and TYE665-633nm laser & 670bp30). Cleavage of mutant ThiolK-RasDZ using a 1:1 ratio of DNAzyme: mRNA in 60mM NaCl & 2 mM $MgCl_2$ at 37°C for 0 and 60 minutes. Functionalized citrate SNP samples had DTT and then RNA added or RNA and then DTT added. Denaturing gel was used. 1% DTT was added to the Citrate SNP for 2hrs and rocked at 37°C. Sample was centrifuged (3x, 7000RPM, 20min each) to remove SNPs. B) Ratio of Uncut and Cut RNA compared to DNAzyme present.

Effective cleavage ability of the PC DZ and photolysis of the nitrophenylethyl internal photocleavable linker are shown in Figure 2.11. The focus of Figure 2.11 is lanes 3-6. Lane 3 and 5 were photolysed, and lanes 4 and 6 were not photolysed. SNP-PC DZ and PC DZ were

reacted with TYE665 KRAS mRNA for 5 and 30 minutes. The quotient of average pixel intensity for the cut and uncut mRNA bands for lanes 3 and 4 were 0.76 and 0.75. Since the number was less than one, it was confirmed that there was more uncut mRNA than cut mRNA. The quotient of average pixel intensity for the cut and uncut mRNA bands for lanes 5and 6 were 1.25 and 1.22. Since the number was greater than one, it was confirmed that there was more cut mRNA than uncut mRNA. During a time when several experiments were run in parallel, analysis of the results suggested that the HPC SNPs would need to be backfilled for better cleavage activity in the assay. Too much of the DNAzyme is cleaving KRAS mRNA, even when the oligonucleotide is not released from the SNP.

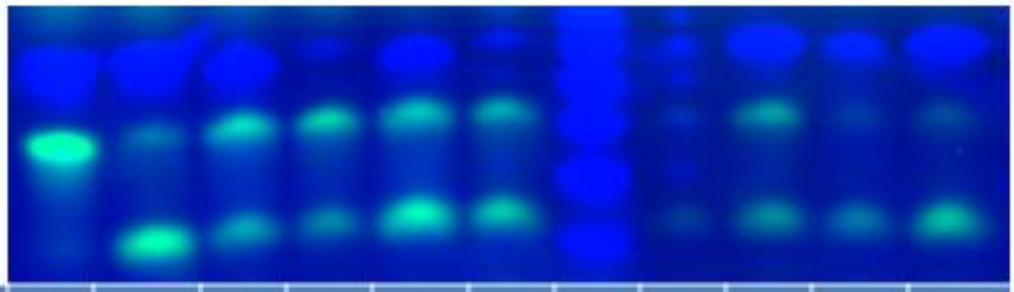

Lane	1	2	3	4	5	6	7	8	9	10	11
Ladder							+				
TYE665 RNA	+	+	+	+	+	+		+	+	+	+
PC DZ	+	+									
SNP/PC DZ			+	+	+	+		+	+	+	+
UV			+		+			+		+	
DTT								+	+	+	+
Time(min)	0	30	5	5	30	30		5	5	30	30
Cut /Uncut (RNA)	0.16	2.18	0.76	0.75	1.25	1.22		1.33	0.97	1.79	2.33

Figure 2.11. Flashed and Unflashed samples. Cleavage of mutant ThiolK-RasDZ using a 1:1 ratio of DNAzyme: mRNA in 60mM NaCl & 2 mM $MgCl_2$ at 37°C for 0 , 30, and 60 minutes on and off Citrate SNPs. Denaturing gel was used. 1% DTT was added to the Citrate SNP for 2hrs and rocked at 37°C. Sample was centrifuged (3x, 7000RPM, 20min each) to remove SNPs.

Effective cleavage ability of the TAMRA DZ, photolysis of the nitrophenylethyl internal photocleavable linker, and enzymatic protection of the oligonucleotide are shown in Figure 2.12. The focus of Figure 2.12 is lanes 8-10. SNP-PC DZ was reacted with DNase I for 0,5, and 15 minutes. Several bands are visualized at all three time periods. Again, analysis of the results suggested that the HPC SNPs would need to be backfilled for better protection from enzymatic cleavage.

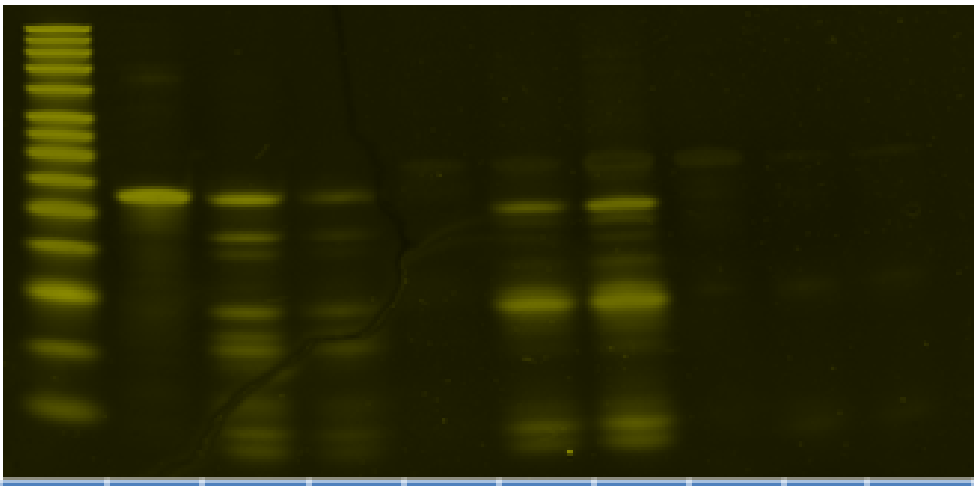

Lane	1	2	3	4	5	6	7	8	9	10
Ladder	+									
KRAS DZ		+	+	+						
PC DZ					+	+	+			
SNP/PC DZ (DTT-removed)								+	+	+
Time of Reaction		0 min	5 min	15 min	0 min	5 min	15 min	0 min	5 min	15 min

Figure 2.12. DNase I cleavage of unprotected mutant K-Ras DZ and protected HPC SNP/PC DZ for reactions of 0,5, and 15 minutes in buffers rocking at 37°C (SYBR Gold stained -488nm laser & 520bp40 filter). Lane 1) Low Molecular Weight Ladder 10-100 nt; Lane 2, 3, and 4) KRAS DZ reacting with DNase I for 0,5, and 15 minutes; Lanes 5,6,and 7) PC KRAS DZ reacting with DNase I for 0,5, and 15 minutes; Lanes 8,9, and 10) SNP/ PC KRAS DZ reacting with DNase I for 0, 5, and 15 minutes. 1% DTT was added to the SNP for 2hrs and rocked at 37°C. Supernatant was collected after sample was centrifuged (3x, 7000RPM, 20min each) to remove SNPs.

Overall, the DNAzyme on the HPC SNPs required less cleavage of the KRAS mRNA and offered better protection from enzymatic cleavage in the tethered form. This finding prompted the backfilling of HPC SNPs with one tenth the concentration of DNAzyme using 11-Mercaptoundecanoic acid. Increased optimization of the coverage of DNAzyme oligonucleotide surrounding the SNP surface is shown in Figure 2.13. Table 2.1 results show that an increase in oligonucleotide surface coverage took place with the backfilled particles.

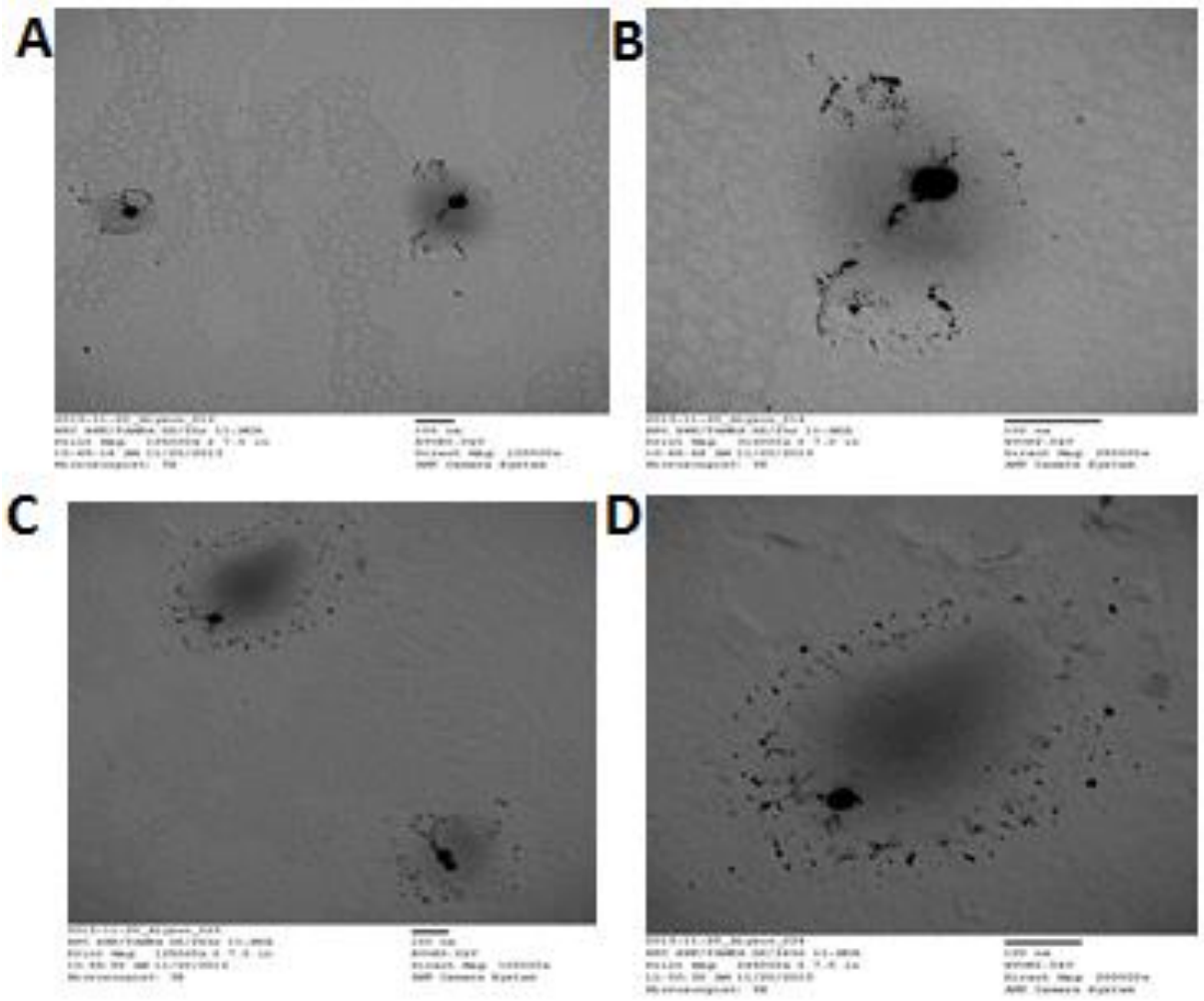

Figure 2.13. TEM images of particles. A) HPC SNP functionalized with TAMRA DZ and backfilled with 11-Mercaptoundecanoic acid for 2 hrs, B) HPC SNP functionalized with TAMRA DZ DZ and backfilled with 11-Mercaptoundecanoic acid for 2 hrs, C) HPC SNP functionalized with TAMRA DZ DZ and backfilled with 11-Mercaptoundecanoic acid for 24 hrs, and D) HPC SNP functionalized with TAMRA DZ DZ and backfilled with 11-Mercaptoundecanoic acid for 24 hrs. Scale bar is 100nm.

2.4 CONCLUSIONS

The construction of a SNP-10-23 DNAzyme oligonucleotide conjugate is significant in several regards to current developments in photoactivated gene regulation. An inducible DNAzyme oligonucleotide that could be delivered to cells via SNP transport by stable and consistent particles is the critical point made by this project's goals. While citrate-stabilized SNP were first utilized in the project, hydroxypropylcellulose (HPC)-stabilized particles were chosen for future cell studies since they were highly biocompatible, aggregated less than the citrate SNPs, and were more shelf-stable. Gel electrophoresis was used to demonstrate effective cleavage activity in the various forms of the KRAS DNAzyme, which included thiol, photocleavable linker, and TAMRA modified forms, all showing similar degradation of RNA similar to the original unmodified DNAzyme. Similarly, gel electrophoresis was used to show that DNAzyme tethered to the SNP showed less activity than when photoreleased from the conjugate. DNAse did not digest SNP-tethered DNAzymes as quickly as DNAzymes free in solution, indicating protection of the nucleic acids in the conjugated form.

The next directions of the project involved evaluation the photoactivation of the construct in cells, hypothesized to sensitize mutant KRAS positive cells to chemotherapeutic, yet not affecting non-mutant containing KRAS cells. An aim motivating the use of this SNP construct is to cause less collateral damage due to off-target effects of medicines in unintended tissues. This gene-regulated approach could improve current chemotherapy efficacy, allowing use of lower concentrations of drug and thereby improving patient tolerance as well as targeted cancer cell necrosis.

2.5 REFERENCES

Akkina, R., A. Banerjea, J. Bai, J. Anderson, M. Li and J. Rossi "siRNAs, ribozymes and RNA decoys in modeling stem cell-based gene therapy for HIV/AIDS." Anticancer research 23(3A): 1997.

Bawarski, W., E. Chidlowsky, D. Bharali and S. Mousa (2008). "Emerging nanopharmaceuticals." Nanomedicine: Nanotechnology, Biology and Medicine 4(4): 273-282.

Bianco, P. and P. Robey (2001). "Stem cells in tissue engineering." NATURE-LONDON-: 118-121.

Biju, V., T. Itoh, A. Anas, A. Sujith and M. Ishikawa (2008). "Semiconductor quantum dots and metal nanoparticles: syntheses, optical properties, and biological applications." Analytical and Bioanalytical Chemistry 391(7): 2469-2495.

Brown, P. K., A. T. Qureshi, A. N. Moll, D. J. Hayes and W. T. Monroe (2013). "Silver Nanoscale Antisense Drug Delivery System for Photoactivated Gene Silencing." ACS nano.

Cairns, M. J., A. King and L. Q. Sun (2003). "Optimisation of the 10–23 DNAzyme–substrate pairing interactions enhanced RNA cleavage activity at purine–cytosine target sites." Nucleic acids research 31(11): 2883.

Chen, M. and D. Goodman (2004). "The structure of catalytically active gold on titania." Science 306(5694): 252-255.

Chen, Z., J. C. Otto, M. O. Bergo, S. G. Young and P. J. Casey (2000). "The C-terminal polylysine region and methylation of K-Ras are critical for the interaction between K-Ras and microtubules." Journal of Biological Chemistry 275(52): 41251.

Eustis, S. and M. El-Sayed (2006). "Why gold nanoparticles are more precious than pretty gold: Noble metal surface plasmon resonance and its enhancement of the radiative and nonradiative properties of nanocrystals of different shapes." Chemical Society Reviews 35(3): 209-217.

Hutter, E. and J. Fendler (2004). "Exploitation of localized surface plasmon resonance." Advanced Materials 16(19): 1685-1706.

Johnson Jr, D. D., B. Kang, J. L. Vigorita, A. Amram and E. M. Spain (2008). "Marangoni Flow of Ag Nanoparticles from the Fluid− Fluid Interface†." The Journal of Physical Chemistry A 112(39): 9318-9323.

Kurreck, J. (2003). "Antisense technologies." Eur. J. Biochem 270: 1628-1644.

Munro, C., W. Smith, D. Armstrong and P. White (1995). "Assignments and mechanism of SERRS of the hydrazone form for the azo dye solvent yellow 14." The Journal of Physical Chemistry 99(3): 879-885.

Munro, C., W. Smith, M. Garner, J. Clarkson and P. White (1995). "Characterization of the surface of a citrate-reduced colloid optimized for use as a substrate for surface-enhanced resonance Raman scattering." Langmuir 11(10): 3712-3720.

Pelliccioli, A. and J. Wirz (2002). "Photoremovable protecting groups: reaction mechanisms and applications." Photochemical & Photobiological Sciences 1(7): 441-458.

Qureshi, A. T., W. T. Monroe, V. Dasa, J. M. Gimble and D. J. Hayes (2013). "miR-148b–Nanoparticle conjugates for light mediated osteogenesis of human adipose stromal/stem cells." Biomaterials 34(31): 7799-7810.

Santoro, S. and G. Joyce (1998). "Mechanism and Utility of an RNA-Cleaving DNA Enzyme†." Biochemistry 37(38): 13330-13342.

Thissen, J. A., J. M. Gross, K. Subramanian, T. Meyer and P. J. Casey (1997). "Prenylation-dependent association of Ki-Ras with microtubules." Journal of Biological Chemistry 272(48): 30362.

Yguerabide, J. and E. Yguerabide (1998). "Light-Scattering Submicroscopic Particles as Highly Fluorescent Analogs and Their Use as Tracer Labels in Clinical and Biological Applications:: I. Theory." Analytical Biochemistry 262(2): 137-156.

Yu, S. H., T. H. Wang and L. C. Au (2009). "Specific repression of mutant K-RAS by 10-23 DNAzyme: Sensitizing cancer cell to anti-cancer therapies." Biochemical and biophysical research communications 378(2): 230-234.

Zhou, M., Z. Liu, Y. Zhao, Y. Ding, H. Liu, Y. Xi, W. Xiong, G. Li, J. Lu and O. Fodstad (2010). "MicroRNA-125b confers the resistance of breast cancer cells to paclitaxel through suppression of pro-apoptotic Bcl-2 antagonist killer 1 (Bak1) expression." Journal of Biological Chemistry 285(28): 21496.

Zhou, M., Z. Liu, Y. Zhao, Y. Ding, H. Liu, Y. Xi, W. Xiong, G. Li, J. Lu and O. Fodstad (2010). "MicroRNA-125b confers the resistance of breast cancer cells to paclitaxel through suppression of pro-apoptotic Bcl-2 antagonist killer 1 (Bak1) expression." Journal of Biological Chemistry 285(28): 21496-21507.

CHAPTER 3. CHARACTERIZATION OF CELLULAR RESPONSES TO SNP-DNAZYME AND DOXORUBICIN

3.1 INTRODUCTION

In this portion of the project, the silver nanoparticle (SNP) conjugated with DNAzyme was evaluated in cells as a potential cancer treatment. To increase cancer cell sensitivity to the chemotherapeutic doxorubicin, cells are treated with the SNP-DNAzyme construct, which when combined with photoactivation, permits mutant KRAS mRNA cleavage and induction of apoptosis in cancer cells. The photocleavable construct permits spatiotemporal targeting, offering another level of control in increasing cell death only in those cells exposed to light. Paclitaxel was the initially chosen as the chemotherapeutic drug choice for this project, but was decided against given that it targets the same microtubule network pathway as does the K-Ras regulatory system (Thissen, Gross et al. 1997, Chen, Otto et al. 2000). Doxorubicin is an excellent alternative chemotherapeutic agent since it functions by intercalating DNA. The drug is used in the treatment of several cancers including breast and colon cancer (Reviewed by (Khasraw, Bell et al. 2012)). Doxorubicin is an anthracycline antibiotic derived from the bacterial species *Streptomyces* and further modified using a chemical semisynthesis (Guilfoile and Hutchinson 1991) (Reviewed by (Aubel-Sadron and Londos-Gagliardi 1984)). As a chemotherapeutic, it is delivered intraveneously liposome-encapsulated or as a hydrochloride salt (Reviewed by(Gabizon, Shmeeda et al. 2003) (Travis, Curtis et al. 1991, Khasraw, Bell et al. 2012)).

K-RAS is an oncogene which is essential for regulating cell division (Reviewed by(Dahabreh, Terasawa et al. 2011)). According to oncologists, the most common KRAS mutation occurs on codons 12 and 13, while the more rare forms of KRAS mutations affect codons 61 and 146 (Reviewed by (Allegra, Jessup et al. 2009)). Wild type cell lines have normal conversions between on and off in normal KRAS genes. On the other hand, mutant cell lines are

continuously dividing due to the inactivation of this essential cellular division toggle switch. These mutant signal transduction pathway proteins are major causes for pancreatic, colorectal, endometrial, biliary tract, lung, and cervical cancers (Reviewed by (Yu, Wang et al. 2009)). Another issue with the KRAS mutation is that not all therapies are recommended to fix this mutation. Specifically, Allegra *et al.* did not recommend the use of anti-EGFR monoclonal antibody therapy (Reviewed by (Allegra, Jessup et al. 2009, Dahabreh, Terasawa et al. 2011)). Yu *et al.* suggest a treatment of DNAzyme and doxorubicin as alternative method of treatment(Yu, Wang et al. 2009). Our project suggests a step further with the addition of a silver nanoparticle carrier for intracellular delivery and spatial control of cleavage of mutant KRAS mRNA. The cell lines evaluated in this project include control lines, HT29 and HEK293, and the mutant K-RAS-positive cancer lines SW480 and SW620. The breast cancer cell lines include a control line, MCF-7, and the mutant KRAS-positive line, MDA-MB-231.

In this portion of this project, the delivery of SNP-DNAzyme and doxorubicin-HCl was staggered, allowing the DNAzyme to degrade KRAS mRNA, thus sensitizing the cell to doxorubicin before its application. SNP-DNAzyme is delivered and photoactivated in the corresponding colon and breast cancer cell lines 24 hours prior to treatment with doxorubicin. Photoreleasing the DNAzyme from the SNP and initiating gene-regulating of KRAS mRNA is thought to enhance the sensitivity of the colon and breast cancer cells to doxorubicin, and demonstrate the potential of this therapy.

3.2 MATERIALS AND METHODS

3.2.1 Materials

DNAzyme and RNA materials

Silver nanoparticles were functionalized with thiol-modified KRAS DNAzymes ordered from Integrated DNA Technologies (5'- CTA CGC CAA GGC TAG CTA CAA CGA AGC TCC AAC T /3ThioMC3-D/ -3', IDT, Coralville, IA) or Trilink Biotechnologies (5' (TAMRA) (C6-NH) CTA CGC CAA GGC TAG CTA CAA CGA AGC TCC AAC T (PC Spacer) T (C3-S-S-C3) 3', San Diego, CA) based on DNAzyme reported by Yu et al.(Yu, Wang et al. 2009). KRAS mRNA were ordered from Integrated DNA Technologies (5'- rArGrU rUrGrG rArGrC rUrGrU rUrGrG rCrGrU rArG -3' or 5'-/5TYE665/rArGrU rUrGrG rArGrC rUrGrU rUrGrG rCrGrU rArG -3', IDT, Coralville, IA) based on complementary sequence to DNAzyme. Turbofect transfection reagent was purchased from Thermo Fisher Scientific (Rochester, NY).

Citrate and HPC Silver Nanoparticle Oligonucleotide Materials

Silver nitrate (Sigma Ultra >99%) and sodium citrate were purchased from Sigma Aldrich (St. Louis, MO). PTFE resin-coated magnetic stirring bars were purchased from VWR (West Chester, PA). 100 mL Glass syringes used to dispense sodium citrate dropwise to reduce silver nitrate in solution were purchased from KD scientific (Holliston, MA). All other glassware was purchased through Fisher Scientific (Pittsburgh, PA). Hydroxypropyl cellulose SNP, SmartSilver^{TM}AS, was purchased from NanoHorizons Inc (Bellefonte, PA). Silver nanoparticles were functionalized with thiol-modified miRNA 125b or KRAS DNAzymes ordered from Integrated DNA Technologies (IDT, Coralville, IA) or Trilink Biotechnologies (San Diego, CA). 2M Tris-NaCl buffer (pH 8.0) was made up from Biotechnology grade Tris (Amresco Inc, Solon, OH) and sodium chloride (Fischer Scientific, Pittsburgh, PA). 11-Mercaptoundecanoic acid was

obtained from Sigma Aldrich (St. Louis, MO). 16% paraformaldehyde was obtained from Electron Microscopy Sciences (Hatfield, PA).

Cell Materials

Cell studies have been performed on 3T3 (Mouse fibroblast cells, American Type Culture Collection), HT29 (Human colon adenocarcinoma grade II cells, American Type Culture Collection), SW620 (Human colon adenocarcinoma grade II cells, American Type Culture Collection), NIH/3T3 (Mouse fibroblast cells, American Type Culture Collection), HEK293 (Human kidney epithelial cells, American Type Culture Collection), SW480 (Human colon adenocarcinoma grade II cells, American Type Culture Collection), MCF-7 (Human mammary gland/breast cancer cells, American Type Culture Collection), and MDA-MB-231 cells (Human mammary gland/breast cancer cells, American Type Culture Collection). All cells are maintained in 25 cm^2 flasks (BD Falcon, Franklin Lakes, NJ) and incubated at 37°C in a humidified 5% CO_2 environment. Dulbecco's Modified Eagle's Medium (DMEM); Dulbecco's Phosphate-Buffered Saline (DPBS); Fetal Bovine Serum (FBS); Calf serum; GlutaMAX™; Sodium Pyruvate (NaPyr); Non-Essential Amino Acids (NEAA); HEPES buffer; Supplement of Insulin, Transferrin and Selenium (ITS); and 0.25% Trypsin were purchased from Fischer Scientific (Pittsburgh,PA). Dulbecco's Modified Eagle's Medium-High glucose (DMEMHG) and Minimum Essential Medium (MEM) were purchased from GIBCO™ via Thermo Fisher Scientific (Rochester, NY).

3T3, HT29, SW620, HEK293, and SW480 cells were originally grown in 5 mL of Dulbecco's Modified Eagle's medium-reduced serum (DMEM-RS, Fischer Scientific, Pittsburgh, PA) supplemented with 10% fetal bovine serum (FBS, Fischer Scientific, Pittsburgh, PA). NIH/3T3 cells are grown in 5 mL of DMEMHG (Thermo Fischer Scientific, Rochester,

NY) supplemented with 10% calf serum, 2mM glutaMAX™, 1mM NaPyr, 1X NEAA, and 10mM HEPES buffer (Fischer Scientific, Pittsburgh, PA). HEK293 and SW480 cells are grown in 5 mL of MEM (Thermo Fischer Scientific, Rochester, NY) supplemented with 10% FBS, 2mM glutaMAX™, 1mM NaPyr, and 1X NEAA (Fischer Scientific, Pittsburgh, PA). MCF-7 cells are grown in 5 mL of DMEMHG (Thermo Fischer Scientific, Rochester, NY) supplemented with 10% FBS, 2mM glutaMAX™, 1mM NaPyr, 1X NEAA, 10mM HEPES buffer, and 1X ITS (Fischer Scientific, Pittsburgh, PA).

MTS, Alamar Blue, and Flow Cytometry Assays

CellTiter 96® AQueous Non-Radioactive Cell Proliferation Assay (MTS) was purchased from Promega (Madison, WI). Alamar Blue® Cell Viability Reagent was purchased from Invitrogen^{TM} by Thermo Fisher Scientific (Rochester, NY). Sytox® Red dead cell stain was purchased from Molecular Probes^{TM} by Thermo Fisher Scientific (Rochester, NY). Pure ethanol was purchased from PHARMCO-AAPER (CT), and 3% hydrogen peroxide was purchased from Humco (Texarkana,TX). Doxorubicin hydrochloride was purchased from MP Biomedicals. All solvents purchased were of analytical grade.

3.2.2 Methods

***Ex vivo* Photocleavage of SNP-DNAzyme Oligonucleotide**

Cells were seeded in 96, 48, 24, or 12 well plates (2,500cells/0.32cm^2) and allowed to incubate for 24 hours in appropriate media at 37°C prior to SNP, SNP-DNAzyme oligonucleotide conjugate, or DNAzyme treatment in a cell media volume (100 µl /96 wells, 600 µl/12 wells). DNAzyme was added with Turbofect transfection reagent; various amounts of SNP-DNAzyme oligonucleotide conjugates (54pM silver, ~700 oligos:1 SNP) were added to the wells. Treated cells were incubated at 37°C in a CO_2 incubator for 16 hours followed by flashing

for 21 seconds at 365nm (12 J/cm^2) using a GreenSpot system (American Ultraviolet, Lebanon, IN). The system has a 100–watt, pressurized mercury lamp with a 5mm x 1000mm light guide, which has a peak spectral output of 365nm. The lamp has a fluence of 186.4 mW/cm2 when used with the short bandpass filter (1.5mm thick, 2.4mm diameter SWP–2502U–400, Lambda Research Optics, CA) and the long bandpass filter (Newport Corporation, Irvine, CA). Together these filters pass only 320-400nm light, which is appropriate for photocleavage of the nitrobenzyul which has peak absorption at 365nm. Several controls were performed, including cells not exposed to UV light yet injected with 5µl of SNP-DNAzyme oligonucleotide conjugates, as well as the addition of doxorubicin with or without ultraviolet light and with or without SNP-DNAzyme conjugates.

Flow Cytometry Assay: Cytotoxicity of Treatment on Designated Cells

3T3, HT29, and SW620 cells were maintained in 25 cm^2 flasks (BD Falcon, Franklin Lakes, NJ) with 5 ml of Dulbecco's Modified Eagle's medium-reduced serum (DMEM-RS) supplemented with 10% FBS and incubated at 37ºC in 5% CO_2. NIH/3T3 cells are grown in 5 mL of DMEMHG supplemented with 10% calf serum, 2mM glutaMAX™, 1mM NaPyr, 1X NEAA, and 10mM HEPES buffer and incubated at 37ºC in 5% CO_2. HEK293 and SW480 cells are grown in 5 mL of MEM supplemented with 10% FBS, 2mM glutaMAX™, 1mM NaPyr, and 1X NEAA and incubated at 37ºC in 5% CO_2. MCF-7 cells are grown in 5 mL of DMEMHG supplemented with 10% FBS, 2mM glutaMAX™, 1mM NaPyr, 1X NEAA, 10mM HEPES buffer, and 1X ITS and incubated at 37ºC in 5% CO_2. The cells were plated at a density of 3x10^4 cells/well in 12-well culture plates (BD Falcon, Franklin Lakes, NJ) and were allowed to adhere and grow for 24 hours prior to treatment. Samples treated with silver or SNP-conjugated oligonucleotides were incubated at 37ºC in 5% CO_2 for 16 hours or 6 days; samples treated with

12 J/cm^2 ultraviolet light (UV) were incubated at 37ºC in 5% CO_2 for 24 hours or 6 days; samples treated with varying amounts of doxorubicin (DOX) were incubated at 37ºC in 5% CO_2 for 48 hours or 6 days; samples treated with silver or SNP-conjugated oligonucleotides, UV, and DOX were incubated at 37ºC in 5% CO_2 for 6 days. 6 day experiments followed the method reported by Yu *et al* (Yu, Wang et al. 2009). For a necrotic control, cells were incubated for 24 hours with 4µl of 3% hydrogen peroxide. After treatment, non-adhered cells were washed with 1 ml D-PBS and collected while adhered cells were harvested by trypsinization (0.25% Trypsin). The cells were pooled together and centrifuged at 1800 rpm to obtain cell pellet. Cells were re-suspended in 1 ml D-PBS and stained with ending concentration of 5nM Sytox Red for 15 minutes in the dark, then centrifuged and fixed in 250 ul of 1% paraformaldehyde (PFA) solution in D-PBS for flow cytometric analysis of viability with a BD FACS Calibur cytometer (Franklin Lakes, NJ). For each sample, scatter and fluorescent data was collected for 1,000-30,000 cell events using Cellquest pro (BD Biosciences, San Jose, CA) and former analyzed using WinMDI 2.8 software (by Dr M Dietrich, LSUHSC Veterinary School, Baton Rouge, LA).

MTS Assay: Cytotoxicity of Treatment on Designated Cells

3T3, HEK293, and SW480 cells were maintained in 25 cm^2 flasks (BD Falcon, Franklin Lakes, NJ) with 5 ml of Dulbecco's Modified Eagle's medium-reduced serum (DMEM-RS) supplemented with 10% fetal bovine serum (FBS) and incubated at 37ºC in 5% CO_2. The cells were plated at a density of $2.5x10^{-3}$ cells/well in 96-well culture plates (BD Falcon, Franklin Lakes, NJ) and were allowed to adhere and grow for 24 hours before being injected with various treatments for appropriate corresponding times. Samples treated with silver or SNP-conjugated oligonucleotides were incubated at 37ºC in 5% CO_2 for 16 hours; samples treated with 12 J/cm^2 ultraviolet light (UV) were incubated at 37ºC in 5% CO_2 for 24 hours; samples treated with

varying amounts of doxorubicin (DOX) were incubated at 37ºC in 5% CO^2 for 48 hours; and samples treated with silver or SNP-conjugated oligonucleotides, UV, and DOX were incubated at 37ºC in 5% CO_2 for 6 days. 6 day experiments followed the method reported by Yu *et al* (Yu, Wang et al. 2009). For a necrotic control, cells were incubated for 4 hours with 4µl of hydrogen peroxide or 100µl 70% ethanol. After appropriate treatment time, 20µl of pooled 20:1 MTS/PMS solution were added to each treated well. After 4 hours of incubation at 37ºC in 5% CO_2, the absorbance at 490nm was recorded using a Wallac 1420 VICTOR2™ plate reader (Perkin Elmer, Shelton, CT).

Alamar Blue Assay: Cytotoxicity of Treatment on Designated Cells

3T3cells were maintained in 25 cm^2 flasks (BD Falcon, Franklin Lakes, NJ) with 5 ml of DMEM supplemented with 10% FBS and incubated at 37ºC in 5% CO_2. NIH/3T3 cells are grown in 5 mL of DMEMHG supplemented with 10% calf serum, 2mM glutaMAX™, 1mM NaPyr, 1X NEAA, and 10mM HEPES buffer and incubated at 37ºC in 5% CO_2. HEK293 and SW480 cells are grown in 5 mL of MEM supplemented with 10% FBS, 2mM glutaMAX™, 1mM NaPyr, and 1X NEAA and incubated at 37ºC in 5% CO_2. The cells were plated at a density of $2.5x10^{-3}$ cells/well in 96-well culture plates (BD Falcon, Franklin Lakes, NJ) and were allowed to adhere and grow for 24 h prior to injecting with various treatments for appropriate corresponding times. Samples treated with silver or SNP-conjugated oligonucleotides were incubated at 37ºC in 5% CO_2 for 16 hours or 6 days; samples treated with 12 J/cm^2 ultraviolet light (UV) were incubated at 37ºC in 5% CO_2 for 24 hours or 6 days; samples treated with varying amounts of doxorubicin (DOX) were incubated at 37ºC in 5% CO_2 for 48 hours or 6 days; samples treated with silver or SNP-conjugated oligonucleotides, UV, and DOX were incubated at 37ºC in 5% CO_2 for 6 days. 6 day experiments followed the method reported by Yu

et al (Yu, Wang et al. 2009). For a necrotic control, cells were incubated for 24 hours with 4µl 3% hydrogen peroxide, 100µl 70% ethanol, or 100µl 100% ethanol. After appropriate treatment time, 100µl of pooled 10:1 corresponding media/ alamarBlue® dye solution were added to each treated well. After 4 hours of incubation at 37ºC in 5% CO_2, the fluorescence with excitation and emission 531nm/ 595nm nm was recorded using a Wallac 1420 VICTOR2™ plate reader (Perkin Elmer, Shelton, CT).

3.3 RESULTS AND DISCUSSION

The goals of this portion of the project include the determination of cellular thresholds to photoactivating doses of UV light, doxorubicin dose-response thresholds, cellular responses to treatment with DNAzyme alone and with synergistic doses of DNAzyme, UV, and doxorubicin. The system of cells used for proof of concept is crucial to show the actual effect of the treatment in comparison to the negative control. Three sets of cells were analyzed using either a flow cytometry viability assay, a spectrophotometric MTS assay, a fluorescence-based alamar blue assay, or a combination of these assays. In each group, three cell lines were used: a cell line containing the wild type KRAS gene, a cell line containing the mutant KRAS gene, and one cell line not containing either wild type or mutant KRAS gene.

3.3.1 KRAS DNAzyme Experiments

KRAS DZ Cytotoxicity Assay

Because colon cancer was shown in the literature to respond to KRAS-targeted therapies, the first two sets of wild type and mutant cell lines in this project included colon cancer cell lines. Set 1 included the negative control wild type KRAS line (HT29), the mutant KRAS line (SW620), and the negative control line (3T3). Figure 3.1 shows the ineffectiveness of 5 µg (8.3 mM) of KRAS DNAzyme on the SW620 colon cancer cells or 3T3 control fibroblast cells after

16 hours. Analysis of the HT29 cells treated with the same degrees of DNAzyme concentration was not reliable since positive control live cells were not effectively living (HT29 cells flow cytometry data was not shown). Yu *et al.* found an effective dose in their study at approximately 8.0mM DNAzyme using mutant KRAS gene SW480 and wild type KRAS gene HEK293 cell lines. Thus, the SW620 and HT29 cells were replaced with a new set of SW480 and HEK293 cell lines to appropriately compare the treatment of SNP-TAMRA DZ conjugates to that of DNAzyme alone.

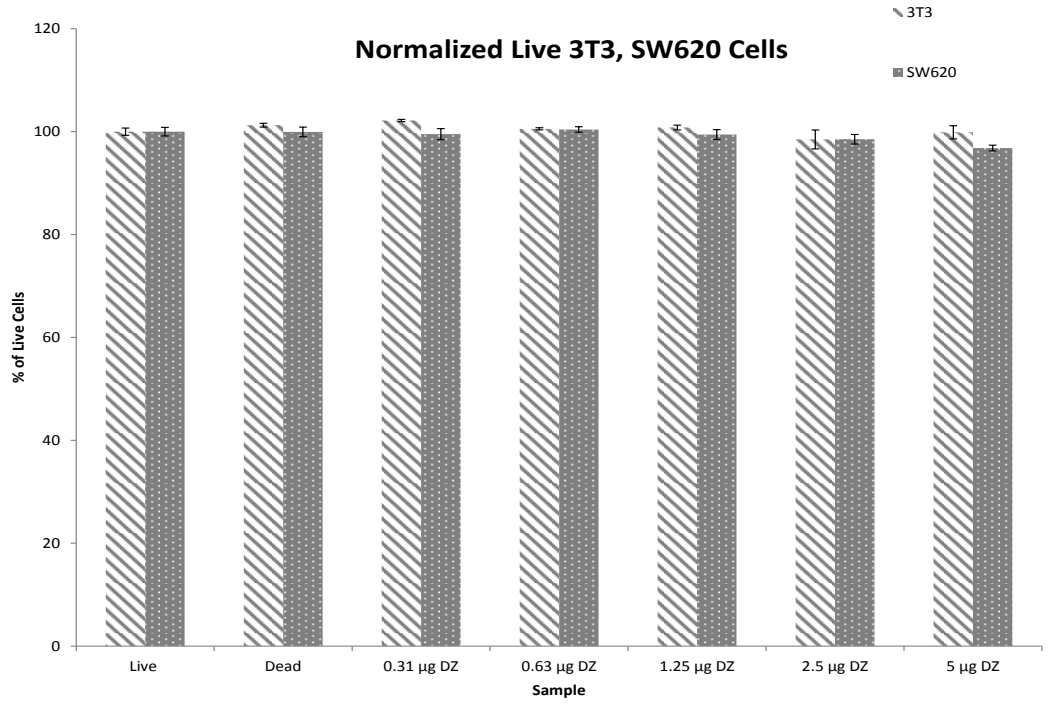

Figure 3.1. KRAS DZ Cytotoxicity Assay using Flow Cytometry.

Treatment Plan Protocol

Set 2 included the negative control wild type KRAS line (HEK293), the mutant KRAS line (SW480), and the negative control line (3T3). Figure 3.2 shows the 5 day process used for the following results shown. There were several experiments testing the effective dosage of DNAzyme given to cells after 16 hours, the effective dosage of UV given to cells after 24 hours,

and the effective dosage of Doxorubicin given to cells after 48 hours. However, the full synergistic effect of all components could not be compared until all cells and their controls went through the 5 day process. Cells are seeded on Day 0. A treatment of SNP, DNAzyme, or SNP-DNAzyme conjugate is delivered on Day 1 (16 hours later). A dosage of UV light is delivered to untreated or treated cells on Day 2 (24 hours later). A dosage of doxorubicin is delivered to untreated or treated cells on Day 3 (48 hours later). The treatment time for oligonucleotide construct delivery and UV dosage was determined from the method reported by Brown *et al*.. The treatment time for doxorubicin delivery was determined from the method reported by Yu *et al*. After the 5 day process, positive results would show the death of SW480 cells, tolerable amount of mortality of HEK293 cells, and viable negative control 3T3 cells.

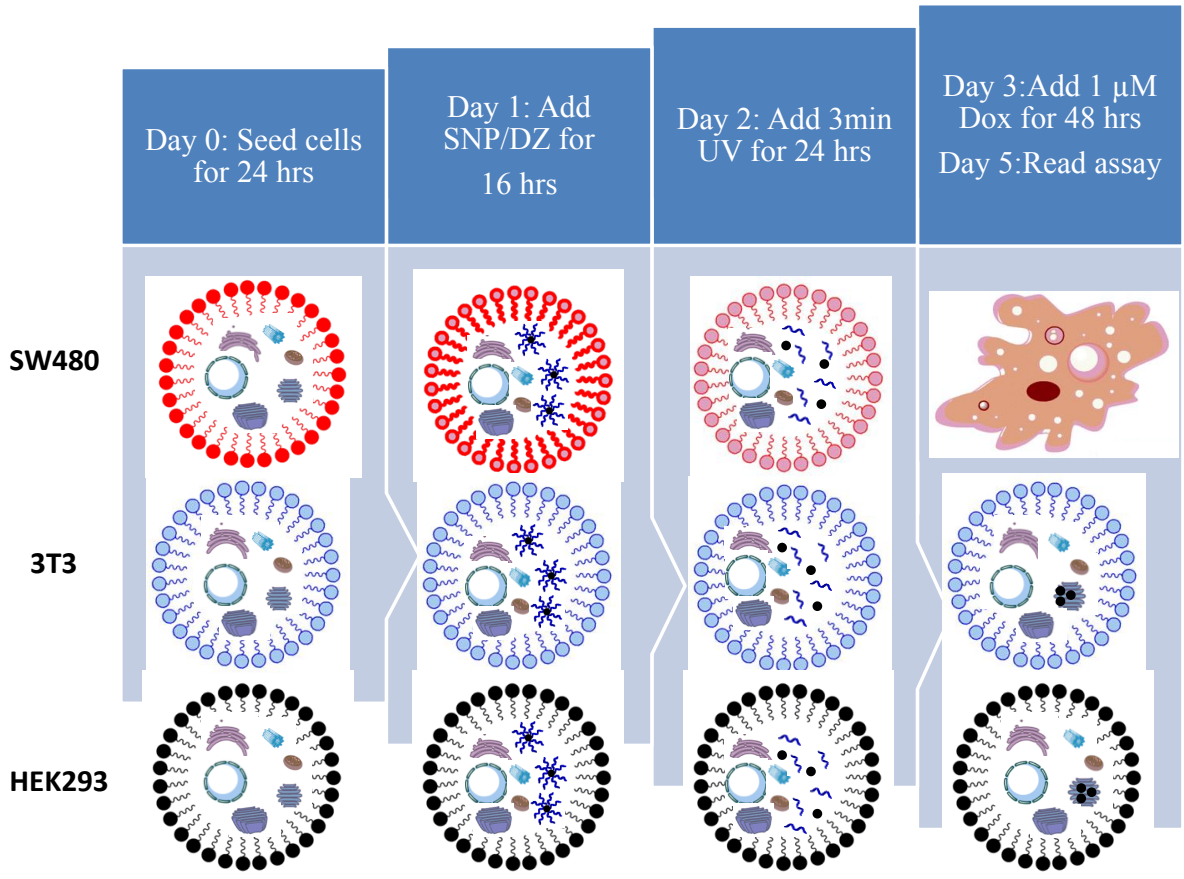

Figure 3.2. 5 day plan of seeding cells, treated with SNP conjugate samples, UV, and Doxorubicin.

UV and Doxorubicin Cytotoxicity Assay

Doses of UV light, SNP-DNAzyme, and doxorubicin were chosen based on results from individual experiments testing the effective dosage of DNAzyme given to cells after 16 hours, the effective dosage of UV given to cells after 24 hours, and the effective dosage of Doxorubicin given to cells after 48 hours. The effective dose of UV given to cells after 24 hours was 12 J/cm^2 (optimized dosage data not shown). The effective dosage of Doxorubicin given to cells after 48 hours was 1 μM Doxorubicin (optimized dosage data not shown). Figure 3.3 shows the 5 day treatment response of cells to controls of 12 J/cm^2 UV, 1 μM Doxorubicin, combined 12 J/cm^2 UV and 1 μM Doxorubicin, and 8.0 mM dosage of 2'omethyl KRAS DNAzyme conjugated with Turbofect. Figure 3.3 lane 3 shows the SW480 colon cancer cells were less viable than the 3T3 control fibroblast cells with the 12 J/cm^2 UV. Figure 3.3 lane 4 shows the SW480 colon cancer cells and the 3T3 control fibroblast cells had high viability with the 1 μM Doxorubicin dosage. Figure 3.3 lane 5 shows the SW480 colon cancer cells and the 3T3 control fibroblast cells had high viability with the 12 J/cm^2 UV and 1 μM Doxorubicin dosage. Figure 3.3 lane 6 shows the SW480 colon cancer cells and the 3T3 control fibroblast cells had high viability with the SNP dosage (1x, same amount of silver given in SNP-DNAzyme construct dosage). Figure 3.3 lane 8 shows the SW480 colon cancer cells and the 3T3 control fibroblast cells were less viable with the 8.0 mM 2'omethyl DNAzyme conjugated to turbofect dosage. Analysis of the HEK293 cells treated with the same treatments was not reliable since positive control live cells were not effectively surviving (HEK293 cells MTS and Alamar Blue assays data was not shown). Analysis of the results showed positive feedback from the synergistic treatment of UV and Doxorubicin dosages, thus the full treatment of SNP-DNAzyme constructs were attempted.

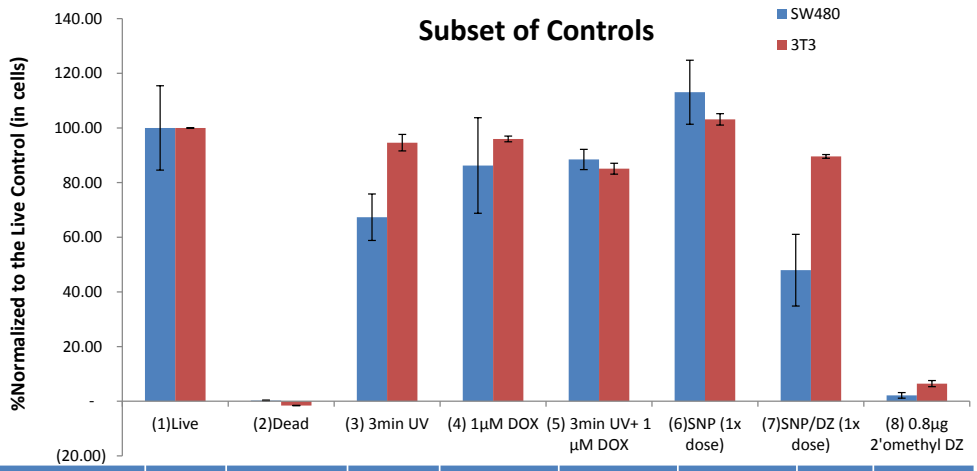

	1	2	3	4	5	6	7	8
UV	-	-	+	-	+	-	-	-
Dox	-	-	-	+	+	-	-	-
SNP	-	-	-	-	-	+	+	-
DZ	-	-	-	-	-	-	+	2’

Figure 3.3. Results from control treatments of SW480 and 3T3 cells for 5 days using an alamar blue assay. Lane 1: positive control live cells; Lane 2: negative control dead cells; Lane 3:12 J/cm^2 UV dosage; Lane 4: 1 µM Doxorubicin dosage; Lane 5: 12 J/cm^2 UV and 1 µM Doxorubicin dosage; Lane 6:SNP dosage (1x, corresponding to silver present in 1x dosage of SNP-TAMRA DNAzyme construct); Lane 7: SNP-TAMRA DNAzyme construct dosage (1x); and Lane 8: 8.0 mM 2’omethyl DNAzyme conjugated with Turbofect.

SNP-DNAzyme Construct Cytotoxicity Assay

For the 5 experimental protocol, 12 J/cm^2 UV and 1µM doxorubicin dosages were given to SW480 colon cancer cells. A comparison of samples that were and were not photoexposed was the focus of Figure 3.4. Figure 3.4 lanes 7-10 show the SW480 cells treated with SNP-DNAzyme construct, photoexposed, and doxorubicin treated were less viable than the SW480 colon cancer cells treated with SNP-DNAzyme construct and doxorubicin but not photoexposed. These results were encouraging; however, the cells treated only with 12 J/cm^2 UV were not highly viable (Figure 3.4 lane 4). This varies significantly from results previously shown. Since one of the negative controls showed inconclusive results, further evaluation was deemed necessary.

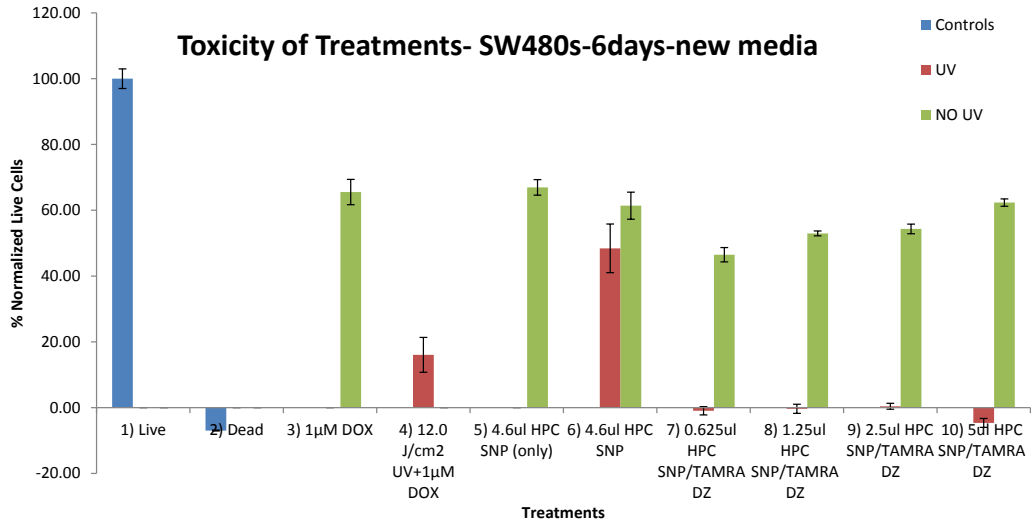

	1	2	3	4	5	6	7	8	9	10
Dox	-	-	+	+	-	+	+	+	+	+
SNP	-	-	-	-	+	+	+	+	+	+
DZ	-	-	-	-	-	-	+	+	+	+

Figure 3.4. Results from control treatments of SW480 for 5 days using an alamar blue assay. Lane 1: positive control live cells; Lane 2: negative control dead cells; Lane 3: 1 µM Doxorubicin dosage; Lane 4: 12 J/cm^2 UV and 1 µM Doxorubicin dosage; Lane 5:SNP dosage (1x, corresponding to silver present in 1x dosage of SNP-TAMRA DNAzyme construct); Lane 6:SNP dosage (1x, corresponding to silver present in 1x dosage of SNP-TAMRA DNAzyme construct) and 1 µM Doxorubicin; Lane 7: SNP-TAMRA DNAzyme construct dosage (0.13x); Lane 8: SNP-TAMRA DNAzyme construct dosage (0.25x); Lane 9: SNP-TAMRA DNAzyme construct dosage (0.5x); and Lane 10: SNP-TAMRA DNAzyme construct dosage (1x). Concentration of sample was 0.10µg/100µl.

SNP-DNAzyme Backfilled with 11-Mercaptoundecanic Acid Construct Cytotoxicity Assay

Since one of the objectives of this project was to have greater protection of the DNAzymes from endonucleases, the SNP-DNAzyme constructs were backfilled with 11-Mercaptoundecanoic acid. Backfilled SNP-DNAzyme constructs were also tried as treatments in SW480 cells. Since several experiments ran concurrently, some of the data results shown in Figure 3.5 were also shown in Figure 3.4. For this 5 day experimental protocol in Figure 3.5, 12 J/cm^2 UV and 1µM Doxorubicin dosages were used for the following experiment using SW480 cells. A comparison of backfilled and not backfilled samples that were and were not

photoexposed was the focus of Figure 3.5. Figure 3.5 lanes 5-8 show the SW480 colon cancer cells treated with SNP-DNAzyme construct, photoexposed, and doxorubicin treated were less viable than the SW480 colon cancer cells treated with SNP-DNAzyme construct and doxorubicin but not photoexposed. Figure 3.5 lanes 9-12 show the SW480 colon cancer cells treated with backfilled SNP-DNAzyme construct, photoexposed, and doxorubicin treated were less viable than the SW480 colon cancer cells treated with SNP-DNAzyme construct and doxorubicin but not photoexposed. Again, these results are promising since the treatment quantitatively has a significant difference to the non-photoexposed samples in both the backfilled and non-backfilled samples. However, Figure 3.5 lane 4 shows the SW480 colon cancer cells photoexposed with 12 J/cm^2 UV were not largely viable. This varies significantly from results previously shown. Since one of the negative controls in this experiment also showed inconclusive results, it was concluded that further evaluation was necessary.

SW480 Positive and Negative Control Cytotoxicity Assay

Since one of the objectives of this project was to establish an appropriate cell system to show the proof of concept of this drug-targeted gene therapy, it became crucial to check the viability of the control treatments using flow cytometry rather than bulk cell well measurements as done previously which showed unreliable control results (Figures 3.4 and 3.5). Another experiment was run on live and dead controls alone that showed similar problems with cell counts being entirely too low; samples were unsuccessfully treated to different processing techniques to improve cell counts (data not shown). Figure 3.6 shows the number of cell events collected at the top of the bars. Clearly, the data is questionable when the dead control shows 100% viability with a 4,000 cell events count, as after 5 days in this experimental protocol, the number of cells should be greater than 50,000. Also concerning was the difficulty in

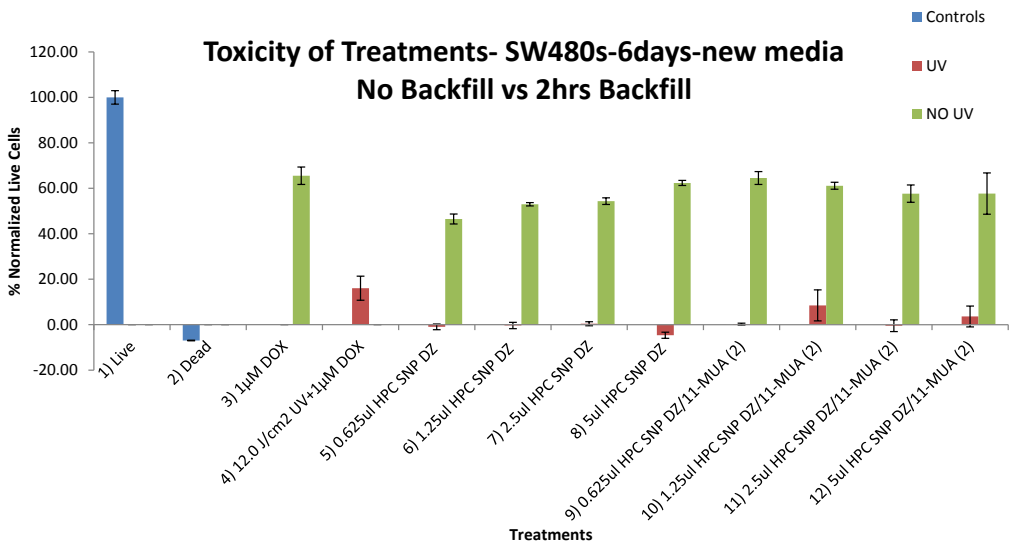

	1	2	3	4	5	6	7	8	9	10	11	12
SNP	-	-	-	-	+	+	+	+	+	+	+	+
DZ	-	-	-	-	+	+	+	+	+	+	+	+
11-MUA	-	-	-	-	-	-	-	-	+	+	+	+
DOX	-	-	+	+	+	+	+	+	+	+	+	+

Figure 3.5. Results from control treatments of SW480 for 5 days using an alamar blue assay. Lane 1: positive control live cells; Lane 2: negative control dead cells; Lane 3: 1 µM Doxorubicin dosage; Lane 4: 12 J/cm^2 UV and 1 µM Doxorubicin dosage; Lane 5: SNP-TAMRA DNAzyme construct dosage (0.13x); Lane 6: SNP-TAMRA DNAzyme construct dosage (0.25x); Lane 7: SNP-TAMRA DNAzyme construct dosage (0.5x); Lane 8: SNP-TAMRA DNAzyme construct dosage (1x). DNAzyme concentration of sample from Lanes 5-8 was 0.10µg/100µl. Lane 9: Dosage of SNP-TAMRA DNAzyme construct backfilled with 11-mercaptoundecanoic acid (0.13x); Lane 10: Dosage of SNP-TAMRA DNAzyme construct backfilled with 11-mercaptoundecanoic acid (0.25x); Lane 11: Dosage of SNP-TAMRA DNAzyme construct backfilled with 11-mercaptoundecanoic acid (0.5x); Lane 12: Dosage of SNP-TAMRA DNAzyme construct backfilled with 11-mercaptoundecanoic acid (1x). DNAzyme concentration of sample from Lanes 9-12 was 0.13µg/100µl.

inducing death in dead-control cells. Treatments such as 70% ethanol, 100% ethanol, and hydrogen peroxide were used at different times to treat these dead control samples. In addition to having a difficult time collecting cells for these dead control samples, data collected for the treated samples was also problematic. Numbers of cell events collected varied significantly and could not be reliably trusted for accurate interpretations of the SNP-DNAzyme effects of cancer cell viability.

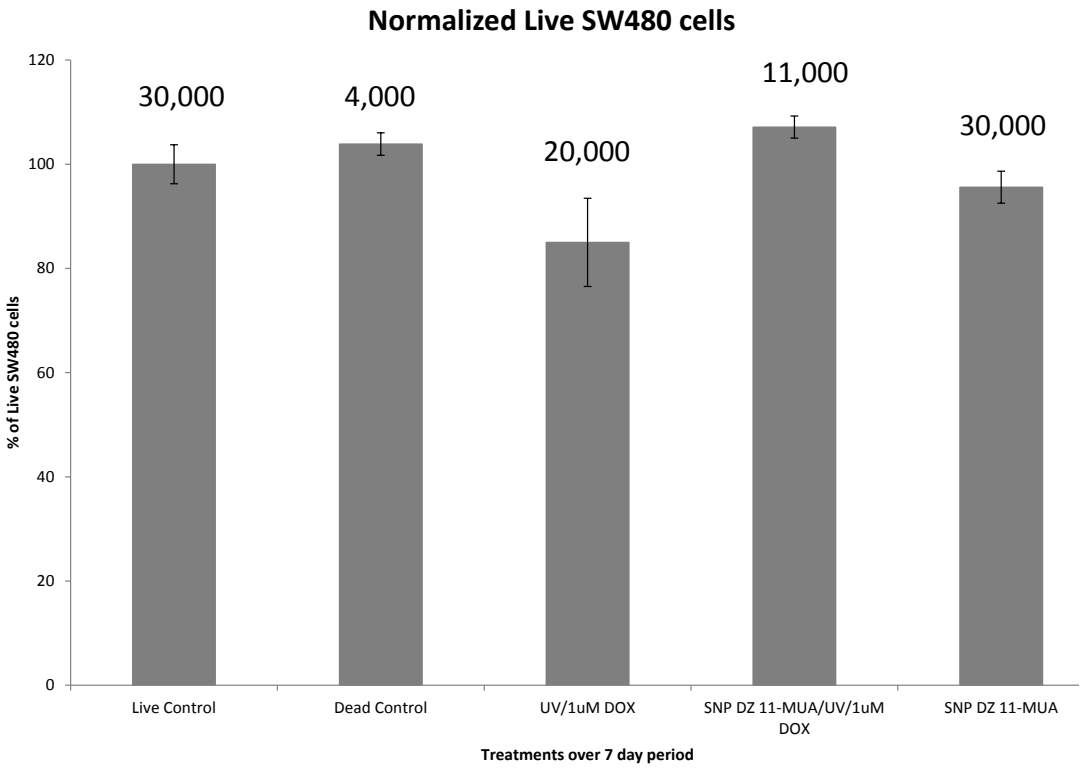

Figure 3.6. Results from treatments of SW480 for 5 days using a flow cytometry assay. Lane 1: positive control live cells; Lane 2: negative control dead cells; Lane 3: 12 J/cm^2 UV and 1 μM Doxorubicin dosage; Lane 4: Backfilled SNP-TAMRA DNAzyme construct 12 J/cm^2 UV and 1 μM Doxorubicin dosage, (1x); and Lane 5: Backfilled SNP-TAMRA DNAzyme construct dosage.

Evaluation of SNP-DNAzyme in MCF-7 and MDA-MB-231 Cells

Since the colon cancer cells were not appropriate systems for proof of concept, MCF-7 and MDA-MB-231 breast cancer cells were evaluated for treatment with the SNP-DNAzyme therapy. These experiments, grouped as "Set 3", included the negative control wild type RAS line (MCF-7) and the mutant KRAS line (MDA-MB-231)(Ikediobi, Davies et al. 2006, Adams, Deremer et al. 2010). This set of cells was used because it contains a KRAS mutation. However, in the late stages of the project it was noted that MDA-MB-231 cells actually contain the KRAS mutant gene on the 13th codon instead of on the 12th codon similar to the mutation in the SW480 and SW620 cells (ATCC® CRM-HTB-26™, www.atcc.org, (Ikediobi, Davies et al. 2006)). This

different location of the KRAS mutation on the MDA-MB-231 indicates that the DNAzyme designed to cleave the KRAS mRNA would not be effective. This result was confirmed in the results shown in Figure 3.7, where all samples had showed viability, even those treated with KRAS-DNAzyme and UV light.

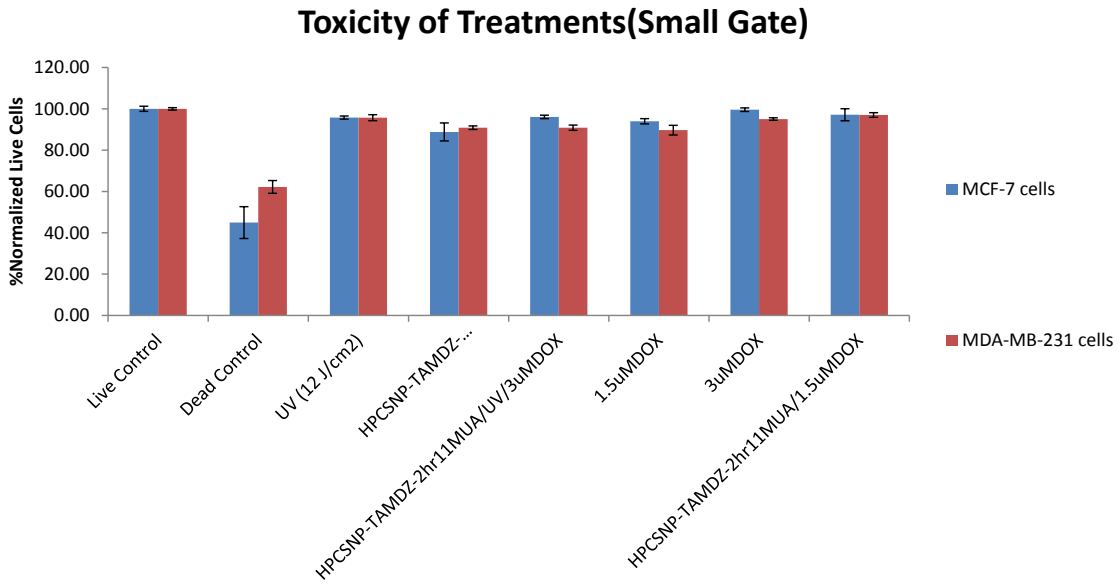

Lane	1	2	3	4	5	6	7	8
Live Control	+							
Dead Control		+						
SNP				+	+			+
TAMRA DZ				+	+			+
11-MUA				+	+			+
UV (12 J/cm^2)			+	+	+			
DOX				1.5µM	3µM	1.5µM	3µM	1.5µM

Figure 3.7. Results from control treatments of MCF-7 and MDA-MB-231 cells for 5 days using a flow cytometry assay. Lane 1: positive control live cells; Lane 2: negative control dead cells; Lane 3: 12 J/cm^2 UV dosage; Lane 4: SNP-TAMRA DNAzyme construct dosage (1x, 5µl), 12 J/cm^2 UV, and 1.5µM Doxorubicin dosage; Lane 5: SNP-TAMRA DNAzyme construct dosage (1x, 5µl),12 J/cm^2 UV, and 3µM Doxorubicin dosage; Lane 6: 1.5 µM Doxorubicin dosage; Lane 7: 3 µM Doxorubicin dosage; Lane 8: SNP-TAMRA DNAzyme construct dosage (1x, 5µl) and 1.5µM Doxorubicin dosage. DNAzyme concentration of sample from Lanes 4, 5, and 8 was 0.13µg/100µl.

3.4 CONCLUSIONS

The goals of this portion of the project include the determination of cellular thresholds to photoactivating doses of UV light, doxorubicin dose-response thresholds, cellular responses to treatment with DNAzyme alone and with synergistic doses of DNAzyme, UV, and doxorubicin. The system of cells used for proof of concept was crucial to show the actual effect of the treatment in comparison to the negative control. Three sets of cells were analyzed using either the flow cytometry assay, MTS assay, Alamar Blue assay, or a combination of these methods. In each group, three cell lines were used. The group included one cell line containing the wild type KRAS gene, one cell line containing the mutant KRAS gene, and one cell line not containing either wild type or mutant KRAS gene.

Cell "Set 1" included the negative control wild type KRAS line (HT29), the mutant KRAS line (SW620), and the negative control line (3T3). A large dose (5 μg, 8.3 mM) of KRAS DNAzyme showed no response in the SW620 colon cancer cells or 3T3 control fibroblast cells after 16 hours. Results from HT29 cells treated with the these DNAzyme concentration were not deemed reliable since the positive control live cells showed low viability. Thus the decision was made to evaluate the constructs in different cells, termed "Set 2", which included the negative control wild type KRAS line (HEK293), the mutant KRAS line (SW480), and the negative control line (3T3).

There were several experiments testing the effective dosage of DNAzyme given to cells after 16 hours, the effective dosage of UV given to cells after 24 hours, and the effective dosage of Doxorubicin given to cells after 48 hours. However, the full synergistic effect of all components could not be compared until all cells and their controls went through the 5 day experimental protocol. Cells were seeded on Day 0. A treatment of SNP, DNAzyme, or SNP-

DNAzyme conjugate is delivered on Day 1 (after 16 hours). Cells were treated with UV light on Day 2 (after 24 hours). Doxorubicin was delivered on Day 3 (after 48 hours). The treatment time for oligonucleotide construct delivery and UV dosage was determined from the method reported by Brown *et al*.(Brown, Qureshi et al. 2013). The treatment time for Doxorubicin delivery was determined from the method reported by Yu *et al*.(Yu, Wang et al. 2009). After the 5 day process, positive results would show the death of SW480 cells, tolerable amount of mortality of HEK293 cells, and viable negative control 3T3 cells.

The effective dosage of UV given to cells after 24 hours was 12 J/cm^2 (optimized dosage data not shown). The effective dosage of Doxorubicin given to cells after 48 hours was 1 μM Doxorubicin (optimized dosage data not shown). Figure 3.4 lanes 7-10 show the SW480 colon cancer cells treated with SNP-DNAzyme construct, photoexposed, and doxorubicin treated were less viable than the SW480 colon cancer cells treated with SNP-DNAzyme construct and doxorubicin but not photoexposed. These results were encouraging; however, Figure 3.4 lane 4 shows the SW480 colon cancer cells photoexposed with 12 J/cm2 UV were not highly viable, which varies significantly from results previously shown. Since one of the negative controls showed inconclusive results, definitive conclusions were not able to be made.

Since one of the objectives of this project was to confer greater protection of the SNP-tethered oligonucleotides from endonucleases, the SNP-DNAzyme constructs were backfilled with 11-Mercaptoundecanoic acid. A comparison of backfilled and not backfilled samples that were and were not photoexposed was the focus of Figure 3.5. Again, these results are promising since the treatment quantitatively has a significant difference to the non-photoexposed samples in both the backfilled and non-backfilled samples. However, Figure 3.5 lane 4 shows the SW480 colon cancer cells photoexposed with 12 J/cm2 UV were not highly viable. This varies

significantly from results previously shown. Since one of the negative controls is showing inconclusive results, it is hard to accept the reliability of the results.

Since one of the objectives of this project was to establish an appropriate cell system to show the proof of concept of this drug-targeted gene therapy, it became crucial to check the viability of the controls using flow cytometry. This experiment was an attempt to verify or to disqualify this system entirely. Figure 3.6 shows the data is unreliable when the dead control shows 100% viability with a 4,000 cell events count. After 5 days, the number of cells should be much larger than 50,000 cells. However, the cells were tough to kill and then collect to show a proper dead control. 70% ethanol, 100% ethanol, and hydrogen peroxide were used at different times to treat the dead control. In addition to having a difficult time collecting cells for the dead controls, data collected for the treated samples was also troublesome. Numbers of cell events collected varied significantly and could not be reliably trusted for accurate interpretations of treated samples' effects.

Cell set 3 included the negative control wild type RAS line (MCF-7) and the mutant KRAS line (MDA-MB-231)(Ikediobi, Davies et al. 2006, Adams, Deremer et al. 2010). This set of cells was used because it contains a KRAS mutation. However, MDA-MB-231 cells contain the KRAS mutant gene on the 13^{th} codon instead of on the 12^{th} codon similar to the mutation in the SW480 and SW620 cells (ATCC® CRM-HTB-26™, www.atcc.org, (Ikediobi, Davies et al. 2006). This means the DNAzyme designed to cleave the KRAS mRNA will not be effective. Figure 3.7 is proof since all treated samples had high viability. In Chapter 3, the construction of a SNP-10-23 DNAzyme oligonucleotide conjugate is significant in several regards to current developments in photoactivated gene regulation. Thus, a photoactivated DNAzyme

oligonucleotide that could be easily delivered to cells via SNP transport, and then activated spatiotemporally has not been demonstrated in an appropriate cell system.

The construction of the SNP-10-23 DNAzyme oligonucleotide conjugate is significant in several regards to current developments in photoactivated gene regulation. A photoactivated DNAzyme oligonucleotide that could be easily delivered to cells via SNP transport, and then activated spatiotemporally has not been demonstrated in an appropriate cell system. The two objectives shown in this paper include increased protection of the SNP-DNAzyme construct, and establishment of a proper model showing the accurate effects of the treatment on cells. The backfilled SNP-DNAzyme constructs were shown through characterization in Chapter 2 to be more packed together and DNAzymes were better protected from endonucleases, however their major impact in treatment could not be established since an appropriate model of cells could not be chosen.

3.5 REFERENCES

Adams, V. R., D. L. Deremer, B. Stevich, C. A. Mattingly, B. Gallt, T. Subramanian, J. M. Troutman and H. P. Spielmann (2010). "Anticancer activity of novel unnatural synthetic isoprenoids." Anticancer research **30**(7): 2505-2512.

Allegra, C. J., J. M. Jessup, M. R. Somerfield, S. R. Hamilton, E. H. Hammond, D. F. Hayes, P. K. McAllister, R. F. Morton and R. L. Schilsky (2009). "American Society of Clinical Oncology provisional clinical opinion: testing for KRAS gene mutations in patients with metastatic colorectal carcinoma to predict response to anti–epidermal growth factor receptor monoclonal antibody therapy." Journal of Clinical Oncology **27**(12): 2091-2096.

Aubel-Sadron, G. and D. Londos-Gagliardi (1984). "Daunorubicin and doxorubicin, anthracycline antibiotics, a physicochemical and biological review." Biochimie **66**(5): 333-352.

Brown, P. K., A. T. Qureshi, A. N. Moll, D. J. Hayes and W. T. Monroe (2013). "Silver Nanoscale Antisense Drug Delivery System for Photoactivated Gene Silencing." ACS nano.

Chen, Z., J. C. Otto, M. O. Bergo, S. G. Young and P. J. Casey (2000). "The C-terminal polylysine region and methylation of K-Ras are critical for the interaction between K-Ras and microtubules." Journal of Biological Chemistry **275**(52): 41251.

Dahabreh, I. J., T. Terasawa, P. J. Castaldi and T. A. Trikalinos (2011). "Systematic review: Anti–epidermal growth factor receptor treatment effect modification by KRAS mutations in advanced colorectal cancer." Annals of internal medicine **154**(1): 37-49.

Gabizon, A., H. Shmeeda and Y. Barenholz (2003). "Pharmacokinetics of pegylated liposomal doxorubicin." Clinical pharmacokinetics **42**(5): 419-436.

Guilfoile, P. G. and C. R. Hutchinson (1991). "A bacterial analog of the mdr gene of mammalian tumor cells is present in Streptomyces peucetius, the producer of daunorubicin and doxorubicin." Proceedings of the National Academy of Sciences **88**(19): 8553-8557.

Ikediobi, O. N., H. Davies, G. Bignell, S. Edkins, C. Stevens, S. O'Meara, T. Santarius, T. Avis, S. Barthorpe and L. Brackenbury (2006). "Mutation analysis of 24 known cancer genes in the NCI-60 cell line set." Molecular cancer therapeutics **5**(11): 2606-2612.

Khasraw, M., R. Bell and C. Dang (2012). "Epirubicin: Is it like doxorubicin in breast cancer? A clinical review." The Breast **21**(2): 142-149.

Thissen, J. A., J. M. Gross, K. Subramanian, T. Meyer and P. J. Casey (1997). "Prenylation-dependent association of Ki-Ras with microtubules." Journal of Biological Chemistry **272**(48): 30362.

Travis, L. B., R. E. Curtis, J. D. Boice, B. F. Hankey and J. F. Fraumeni (1991). "Second cancers following non-Hodgkin's lymphoma." Cancer **67**(7): 2002-2009.

Yu, S.-H., T.-H. Wang and L.-C. Au (2009). "Specific repression of mutant K-RAS by 10–23 DNAzyme: Sensitizing cancer cell to anti-cancer therapies." Biochemical and biophysical research communications **378**(2): 230-234.

Yu, S. H., T. H. Wang and L. C. Au (2009). "Specific repression of mutant K-RAS by 10-23 DNAzyme: Sensitizing cancer cell to anti-cancer therapies." Biochemical and biophysical research communications **378**(2): 230-234.

CHAPTER 4. CONCLUSION AND FUTURE WORK

4.1 CONCLUSION

This project explored a gene-regulated chemotherapy using a silver nanoparticle (SNP) conjugated with DNAzyme oligonucleotides that target the mutant K-RAS gene to sensitize cancer cells to doxorubicin treatment. UV light exposure to the conjugates disengages the oligonucleotides and permits DNAzyme-mediated cleavage of K-RAS mRNA. As such these conjugates offer a targeted chemotherapeutic which could offer spatiotemporal specificity in killing only those cells with a mutant gene and in the intended therapeutic region of a patient. The goals of this project were to propose a nanoscale oligonucleotide delivery system that is designed to overcome known hurdles of nuclease protection and cellular delivery in chemotherapeutic applications.

In the first portion of the project, detailed in Chapter 2, characterization of the stability and activity of citrate and HPC silver nanoparticle drug delivery systems constructed for the release of a photolabile DNA oligonucleotide were tested to show the improvement of temporal and spatial control efficiency of the designed construct. The drug delivery vehicle, a ~60nm silver nanoparticle, is functionalized with a thiol-modified 10-23 DNAzyme oligonucleotide with an internal nitrobenzyl photocleavable linker. The intended target for hybridization and gene silencing control is K-RAS mRNA. The internal photocleavable linker permits spatiotemporal control release of the gene silencing K-RAS 10-23 DNAzyme oligonucleotides.

The construction of a SNP-10-23 DNAzyme oligonucleotide conjugate is significant in several regards to current developments in photoactivated gene regulation. An inducible DNAzyme oligonucleotide that could be delivered to cells via SNP transport by stable and consistent particles is the critical point made by this project's goals. While citrate-stabilized SNP

were first utilized in the project, hydroxypropylcellulose (HPC)-stabilized particles were chosen for future cell studies since they were highly biocompatible, aggregated less than the citrate SNPs, and were more shelf-stable. Gel electrophoresis was used to demonstrate effective cleavage activity in the various forms of the KRAS DNAzyme, which included thiol, photocleavable linker, and TAMRA modified forms, all showing similar degradation of RNA similar to the original unmodified DNAzyme. Similarly, gel electrophoresis was used to show that DNAzyme tethered to the SNP showed less activity than when photoreleased from the conjugate. DNAse did not digest SNP-tethered DNAzymes as quickly as DNAzymes free in solution, indicating protection of the nucleic acids in the conjugated form.

The next directions of the project involved photoactivation evaluation of the construct in cells, hypothesized to sensitize mutant KRAS positive cells to chemotherapeutic, yet not affecting non-mutant containing KRAS cells. An aim motivating the use of this SNP construct is to cause less collateral damage due to off-target effects of medicines in unintended tissues. This gene-regulated approach could improve current chemotherapy efficacy, allowing use of lower concentrations of drug and thereby improving patient tolerance as well as targeted cancer cell necrosis.

In the second portion of the project, detailed in Chapter 3, the goals of this portion of the project include the determination of cellular thresholds to photoactivating doses of UV light, doxorubicin dose-response thresholds, cellular responses to treatment with DNAzyme alone and with synergistic doses of DNAzyme, UV, and doxorubicin. The system of cells used for proof of concept was crucial to show the actual effect of the treatment in comparison to the negative control. Three sets of cells were analyzed using either the flow cytometry assay, MTS assay, Alamar Blue assay, or a combination of these methods. In each group, three cell lines were used.

The group included one cell line containing the wild type KRAS gene, one cell line containing the mutant KRAS gene, and one cell line not containing either wild type or mutant KRAS gene.

A large dose (5 μg, 8.3 mM) of KRAS DNAzyme showed no response in Cell "Set 1", thus the decision was made to evaluate the constructs in different cells, termed "Set 2", which included the negative control wild type KRAS line (HEK293), the mutant KRAS line (SW480), and the negative control line (3T3). Several experiments testing the effective dosage of DNAzyme given to cells after 16 hours, the effective dosage of UV given to cells after 24 hours, and the effective dosage of Doxorubicin given to cells after 48 hours were performed.

The full synergistic effect of all components could not be compared until all cells and their controls went through the 5 day experimental protocol. Cells were seeded on Day 0. A treatment of SNP, DNAzyme, or SNP-DNAzyme conjugate is delivered on Day 1 (after 16 hours). Cells were treated with UV light on Day 2 (after 24 hours). Doxorubicin was delivered on Day 3 (after 48 hours). The treatment time for oligonucleotide construct delivery and UV dosage was determined from the method reported by Brown *et al*.(Brown, Qureshi et al. 2013). The treatment time for Doxorubicin delivery was determined from the method reported by Yu *et al*.(Yu, Wang et al. 2009). After the 5 day process, positive results would show the death of SW480 cells, tolerable amount of mortality of HEK293 cells, and viable negative control 3T3 cells.

The effective dosage of UV given to cells after 24 hours was 12 J/cm^2 (optimized dosage data not shown). The effective dosage of Doxorubicin given to cells after 48 hours was 1 μM Doxorubicin (optimized dosage data not shown). SW480 colon cancer cells treated with SNP-DNAzyme construct, photoexposed, and doxorubicin treated were less viable than the SW480 colon cancer cells treated with SNP-DNAzyme construct and doxorubicin but not photoexposed.

However, in a later experiment, SW480 colon cancer cells photoexposed with 12 J/cm2 UV were not highly viable. The SNP-DNAzyme constructs were backfilled with 11-Mercaptoundecanoic acid was to confer greater protection of the SNP-tethered oligonucleotides from endonucleases. The treatment showed a quantitative difference to the non-photoexposed samples in both the backfilled and non-backfilled samples. However, SW480 colon cancer cells photoexposed with 12 J/cm2 UV were not highly viable. Since one of the negative controls is showing inconclusive results, it is hard to accept the reliability of the results.

An appropriate cell system was needed to show the proof of concept of this drug-targeted gene therapy. Flow cytometry was used to check the viability of the controls. This experiment was an attempt to verify or to disqualify this system entirely. Flow data was unreliable since the dead control showed 100% viability with a 4,000 cell events count. After 5 days, the number of cells should be much larger than 50,000 cells. However, the cells were tough to kill and then collect to show a proper dead control. 70% ethanol, 100% ethanol, and hydrogen peroxide were used at different times to treat the dead control. In addition to having a difficult time collecting cells for the dead controls, data collected for the treated samples was also troublesome. Numbers of cell events collected varied significantly and could not be reliably trusted for accurate interpretations of treated samples' effects.

Cell "set 3" included the negative control wild type RAS line (MCF-7) and the mutant KRAS line (MDA-MB-231)(Ikediobi, Davies et al. 2006, Adams, Deremer et al. 2010). However, MDA-MB-231 cells contain the KRAS mutant gene on the 13^{th} codon instead of on the 12^{th} codon similar to the mutation in the SW480 and SW620 cells (ATCC® CRM-HTB-26™, www.atcc.org, (Ikediobi, Davies et al. 2006). This means the DNAzyme designed to cleave the KRAS mRNA will not be effective.

The construction of the SNP-10-23 DNAzyme oligonucleotide conjugate is significant in several regards to current developments in photoactivated gene regulation. A photoactivated DNAzyme oligonucleotide that could be easily delivered to cells via SNP transport, and then activated spatiotemporally has not been demonstrated in an appropriate cell system. The two objectives shown in this project include increased protection of the SNP-DNAzyme construct, and establishment of a proper model showing the accurate effects of the treatment on cells. The backfilled SNP-DNAzyme constructs were shown through characterization in Chapter 2 to be more densely packed, with DNAzymes better protected from endonucleases, however their major impact in treatment could not be established since an appropriate model of cells could not be chosen.

4.2 FUTURE WORK

This project has demonstrated a promising proof of concept of cleavage of a targeted mRNA using complementary DNAzyme, cell delivery using the HPC SNPs, and packing of DNAzyme on the HPC SNPs backfilling with 11-mercaptoundecanoic acid. DNAzyme oligonucleotides conjugated to the surface of SNP via thiol-metal linkages are thought to pack densely(Qureshi, Monroe et al. 2013), thus protecting them from enzymatic degradation. Johnson *et al.* reported 11-mercaptoundecanoic acid aided the homogeneous dispersal of silver nanoparticles (Johnson Jr, Kang et al. 2008) addressing an important need for reduced aggregation to aid in a greater packing density for this project. By using this more successful packing method, future work will specifically focus on finding cell lines to test the enhanced DNAzyme construct and to find a more sensitive assay to test for cell viability.

The DNA construct includes a photocleavable nitrobenzyl group to permit oligonucleotide release from the SNP with UV light exposure. The SNP-DNAzyme construct

was designed to be evaluated in a system requiring targeted gene silencing, whereby precise light exposure offers spatiotemporal control. However, there is a great need for an appropriate cell line to prove the synergistic effect of the spatialtemporal control of the released DNAzyme and Doxorubicin *in vitro*. Thus, new cell lines were sought after that included the KRAS mutant gene. Haraguchi *et al.* reported the identification and characterization of side populations of cancer cells that act similarly to stem cells(Haraguchi, Utsunomiya et al. 2006). Specifically, the cells have regenerative properties. However, the SW480s can generate side populations of cancer cells and non-side populations of cancer cells. For future use, the project could be moved forward using the side population of SW480 cancer cells since they are a hardier cell line preconditioned through generations of side passages in culture. The hardier cell line which would ideally be robust enough for the 5 day experiment protocol, remain through sample processing, and show better dynamic range between positive and negative control responses in the viability assays may be worth evaluation. Haraguchi *et al.* also were successful in dosing HuH7 side population and non-side population cells with doxorubicin; thus these lines may also warrant exploration.

Instead of using an alamar blue assay or MTT assay, Haraguchi *et al.* used the CellTiter-Glo luminescent cell viability assay from Promega (Hannah, Beck et al. 2001, Haraguchi, Utsunomiya et al. 2006) to evaluate doxorubicin-induced cell death. Petty *et al.* report that ATP-based assays have greater sensitivity distinguishing viability with lower numbers of cells than MTT (Petty, Sutherland et al. 1995). These sensitive ATP-based assays are an excellent future option for viability since they do not require trypsination as do the flow cytometry assays; thus cells will be counted and they will not deteriorate during processing.

This project has significance because it addresses the need to develop effective means of delivering therapeutic oligonucleotides to targeted cells with high efficiency and precision. Another suggestion for the future directions of this project is to address that high efficiency and precision targeting by using tumors from metastatic colorectal cancer patients with the KRAS mutant gene in the 12th codon to test. Lièvre *et al.* reported the effectiveness of Cetuximab therapy in 30 tumors from metastatic colorectal cancer patients(Lievre, Bachet et al. 2006). *Ex vivo* tumor tissue samples from patients could be tested as an alternative to the immortalized cell lines.

Future directions also include comparison of DNAzyme activity between direct-caged DNAzyme oligonucleotides and the SNP-DNAzyme constructs used in this project. The packaging of the delivery method could be redesigned and characterized for most effective delivery within cells since one of the main goals has been to produce less collateral damage due to off-target effects of medicines released in unintended tissues.

Overall, several changes can be tried to change this proof of concept idea into an effective gene-regulated therapy. Truly, the ultimate end point is to improve current patient therapy. With possibly the use of one of these new suggestions, the project can begin the start of a new therapy regimen which allows patients one more option in their medical choices.

4.3 REFERENCES

Adams, V. R., D. L. Deremer, B. Stevich, C. A. Mattingly, B. Gallt, T. Subramanian, J. M. Troutman and H. P. Spielmann (2010). "Anticancer activity of novel unnatural synthetic isoprenoids." Anticancer research **30**(7): 2505-2512.

Brown, P. K., A. T. Qureshi, A. N. Moll, D. J. Hayes and W. T. Monroe (2013). "Silver Nanoscale Antisense Drug Delivery System for Photoactivated Gene Silencing." ACS nano.

Hannah, R., M. Beck, R. Moravec and T. Riss (2001). "CellTiter-Glo™ luminescent cell viability assay: a sensitive and rapid method for determining cell viability." Promega Cell Notes **2**: 11-13.

Haraguchi, N., T. Utsunomiya, H. Inoue, F. Tanaka, K. Mimori, G. F. Barnard and M. Mori (2006). "Characterization of a side population of cancer cells from human gastrointestinal system." Stem cells **24**(3): 506-513.

Ikediobi, O. N., H. Davies, G. Bignell, S. Edkins, C. Stevens, S. O'Meara, T. Santarius, T. Avis, S. Barthorpe and L. Brackenbury (2006). "Mutation analysis of 24 known cancer genes in the NCI-60 cell line set." Molecular cancer therapeutics **5**(11): 2606-2612.

Johnson Jr, D. D., B. Kang, J. L. Vigorita, A. Amram and E. M. Spain (2008). "Marangoni Flow of Ag Nanoparticles from the Fluid− Fluid Interface†." The Journal of Physical Chemistry A **112**(39): 9318-9323.

Lievre, A., J.-B. Bachet, D. Le Corre, V. Boige, B. Landi, J.-F. Emile, J.-F. Côté, G. Tomasic, C. Penna and M. Ducreux (2006). "KRAS mutation status is predictive of response to cetuximab therapy in colorectal cancer." Cancer research **66**(8): 3992-3995.

Petty, R. D., L. A. Sutherland, E. M. Hunter and I. A. Cree (1995). "Comparison of MTT and ATP-based assays for the measurement of viable cell number." Journal of bioluminescence and chemiluminescence **10**(1): 29-34.

Qureshi, A. T., W. T. Monroe, V. Dasa, J. M. Gimble and D. J. Hayes (2013). "miR-148b–Nanoparticle conjugates for light mediated osteogenesis of human adipose stromal/stem cells." Biomaterials **34**(31): 7799-7810.

Yu, S. H., T. H. Wang and L. C. Au (2009). "Specific repression of mutant K-RAS by 10-23 DNAzyme: Sensitizing cancer cell to anti-cancer therapies." Biochemical and biophysical research communications **378**(2): 230-234.

APPENDIX A. PROTOCOLS

Note: The protocols listed in this section are proposed methods used in the Monroe lab including ones passed down from previous graduate students and student undergraduate workers. They represent the most updated versions at the time of the distribution of this thesis. All procedures can be changed for successful completion of an individual project.

A1. Cell Culture: Cell Splitting and Seeding Procedure

A. Feeding
   1. Aspirate Media
   2. Add 5 ml of fresh media per T-25 flask (doubling time = 24 hours)
   3. Feed once a week for T-25 flask

B. Splitting Cells
   1. Aspirate media from flask to waste
   2. Rinse w/ 5 ml D-PBS (Ca+ & Mg+ free) and swivel in flask
   3. Aspirate off D-PBS to waste
   4. Add 5ml of Trypsin solution
      a. Wait ~10 min for cells to come off dish at room temperature. Gently rock flask periodically and observe under microscope to make sure the cells are detaching
   5. Add 5 ml of media to inactivate trypsin
   6. Transfer suspension to a 50 ml centrifuge tube
   7. Spin down the cells at 1800rpm for 5 min on the centrifuge (Eppendorf 5702)
   8. Decant supernatant
   9. Resuspend in 5ml of media
      a. For passaging:
         i. Add 5ml fresh media to a new T-25 flask
         ii. Add 3-5 drops of the cell suspension in the new T-25 flask for the flask passaging
      b. For experiment:
      c. Dilute cell media (1 ml into 9 ml fresh media) and seed 500 ul diluted cell solution into 8-well chambered wells (LabTek Chambered Slides, NUNC)

A2. Transfection

A. Transfection Protocol
   1. Add TrojanPorter to 100ul of SFM (serum-free media) and incubate for 5 min at RT
   2. Complex DNA & TrojanPorter for ~15 min at RT
   3. Add polyplexes directly to 500 ul of cell media in 8-well chambers, transfect for 16-24 hrs

B. Transfection of SNP-oligo complexes:
   1. Concentrate final purified SNP-oligo sample (10x)

2. Add 5-10ul of 5x SNP-oligo concentrate (50pM concentration) per well in 8-well confocal microscopy chambered slide (500 ul total volume cell media – 0.8 cm^2/well of culture area)
3. Final amount of oligo added is approximated at 2ug for 5ul of 5x SNP-oligo concentrate (1000:1 oligo to particle ratio)

A3. Nuclease Digestion Assay

A) Nuclease Assay for SNP-oligo conjugates
   1. Purify SNP-oligo conjugates and resuspend in DNase I NEB Buffer
   2. Prepare TYE-oligo solution in DNase I buffer (3 samples)
   3. Add DNase I to sample solutions – incubate at 37°C for digestion intervals
   4. Add STOP buffer (EDTA) to inactive DNase I
   5. Purify digested SNP-oligo conjugates (1x)
   6. DTT-remove oligo dorm SNP-oligo conjugates
   7. Amicon filter TYE-oligo samples to remove salt and reduce volume for gel

A4. SNP Synthesis

A) Citrate SNP Synthesis
   1. Thorough cleaning of all glassware with ethanol
   2. Add .09g silver nitrate to 500ml DI water in large beaker
   3. Add .3g sodium citrate (1%) ro 30ml DI water in small beaker
   4. Bring silver nitrate to a boil while stirring (95°C)
   5. Add 10ml of 1% citrate at a rate of 0.5ml/min (drop wise)
   6. Color will change eat 2ml of added citrate (pale yellow)
   7. Color will change at 5ml of added citrate (dark green)
   8. Let solution boil 10 min after addition of 10ml citrate
   9. Cool solution to RT and quickly transfer to fridge in airtight, dark conditions

A5. SNP Functionalization

A) 4500: 1 oligo to nanoparticles ratio; 1ml 72 pM colloid=$7.2x10^{14}$mol nanoparticles; 0.324 uM Oligo per 1ml silver colloid
B) Protocol
   1. Add Thiol-modified or cyclic-disulfide-modified oligonucleotides to citrate-stabilized silver nanoparticles (~ .324 nmoles oligonucleotide per 1ml of 72 pM colloid)
   2. After 3hrs, add 10ul of 10% SDS, 25ul phosphate buffer (0.1 M; pH=7.4) to bring the mixture to 0.0025 M phosphate
   3. After 12 hrs begin salt aging process: in 4 hr intervals add 10ul aliquots of Tris-NaCl buffer (2M in DI water, pH=8-8.5) to a final concentration of 160-200 mM Tris-NaCl (8-10 additions of 10ul aliquots) or until conjugate colloid is fading due to functionalization (to lighter golden color)

4. Rock resulting mixture gently (lowest speed) over course of 48 hrs
5. Purification via centrifugation (3x 7000RPM)
6. Pull supernatant off SNP pellet and resuspend in dilute (100mM) Tris-NaCl Buffer + 10% SDS
7. Purify particles with centrifugation 3X 20min @ 7,000rpm
8. Backfill SNPs with 1/10 DNAzyme concentration of 11-Mercaptoundecanoic acid for 2 hrs
9. Purify particles with centrifugation 3X 20min @ 7,000rpm. Samples are ready.

A6. Flash Photolysis Using Gel Box

1. Warm up UV lamp for thirty minutes prior to flashing
2. Transfer ½ of each reaction solution to a 0.2ml PCR tube
3. Place samples under the UV lamp for 30mins (caged solutions should turn yellow)
4. Samples can be analyzed, purified, or placed in an assay at this point.

A7. Gel Electrophoresis

Materials
Mini-PROTEAN 3 System (Bio-Rad)
Precast 5% and 15% polyacrylamide (Bio-Rad)
10X TBE buffer (Bio-Rad)
Syber Gold™ stain 10,000X (Molecular Probes)
Procedure
1. Prepare samples and markers with appropriate dyes.
2. Remove gel from sleeve and record all pertinent information.
3. Using a razor blade, cut the plastic coating along the line at the bottom of the gel.
4. Peel the released strip of plastic exposing the gel.
5. Mount the gel cassette into the Mini-PROTEAN 3 System.
• Position the wells to face the inner chamber.
• Hold the cassette down firmly and close both clamps simultaneously.
6. Load the inner chamber above the wells with 1X TBE buffer.
7. Remove the well comb.
8. Wait 5 minutes to ensure a proper seal has been formed.
9. Flush each well several times with excess TBE buffer.
10. Load the outer chamber above the expose gel with 1X TBE buffer.
11. Load each sample into its specified well.
12. Connect the lid ensuring proper electrode connections (color coded).
13. Set the voltage and the timer settings as desired (do not exceed 75 Volts).
14. Press run.
15. Periodically inspect that the system is running properly.
16. When completed, remove the gel from the plastic casing.
17. Stain with Syber Gold™ at 1X (gently rock for 20 minutes).
18. Rinse the gel with distilled water.
19. Perform a UV visualization of the gel under several exposure times
20. Clean all surfaces and dispose of the gel and all consumables.

21. Treat all potentially Syber Gold™ contaminated materials as hazardous waste.

A8. Typhoon 9410 Variable Mode Imager

1. Samples were visualized on a Typhoon 9410 Variable Mode Imager (normal sensitivity, 400 PMT Volts, prescan at 1000 microns pixel size, imaging at 100 microns pixel size) (GE Healthcare, Piscataway, NJ).
2. 488nm laser line was used to image gels stained with SYBR Gold using the 540bp30 filter.
3. 633 nm laser line was used to image gels with RNA containing TYE665 (648/666) using the 670bp30 filter.

A9. Flash Photolysis Using GreenSpot

1. Warm up GreenSpot UV lamp for thirty minutes prior to flashing
2. Transfer appropriate amount of each reaction solution to a 96, 48, or 12 well plate
3. Place samples under the GreenSpot UV lamp assembly with 3cm from fiber to bottom of plate allowing for a 12 J/cm^2 dosage
4. Samples can be analyzed, purified, further treated, or placed in an assay at this point.

A10. MTS Assay

A. MTS Cell Proliferation Assay Protocol for Cells in 96-well plates
Required Materials: CellTiter 96® AQueous Non-Radioactive Cell Proliferation Assay (MTS) was purchased from Promega (Madison, WI).

1. Seed cells into 96-well plate at desired density. (See cell count optimization sheet for instructions on counting cells and optimizing plate-reader signal. Aim for a plate reader readout of 0.75-1.25.) Remember to leave wells blank (but filled with DMEM) for control groups.
2. If you wish to have a dead control group.
    a. Empty DMEM from wells, pipette 30uL of 2% H_2O_2 or paraformaldahyde (PFA). Incubate for 20 minutes.
    b. Empty PFA from wells. H_2O_2 removes cells from the plate surface while PFA adheres them. Therefore removing H_2O_2 will remove dead cells as well. Small amount of remnant H_2O_2 will not interfere with the assay.
    c. Add 100uL DMEM to emptied wells. This is necessary because the MTS assay reacts with DMEM to produce color change effect. If you are imaging cells in PBS or the buffer, remove them and replace with DMEM before conducting MTS assay.
3. Retrieve cells from incubator, and add 20uL 20:1 MTS/PMS solution to all wells (including blank control wells) under sterile hood.
4. Incubate the cells for 4 hours.
5. Retrieve cells from incubator and check for a purple precipitate that should form inside cells.
6. Measure the absorbance of each well at 490 nm on the plate reader in room 112. Remember to bring a flash drive.

a. Turn on plate reader, then computer. Password to the computer is molly02.
b. Make sure that you are using a 490nm filter.
c. Click on the "Wallac" plate reader icon on the desktop. For first users, a new test must be created.
    i. To create new test.
        1. Go to "tools" menu, click on explorer.
        2. Create a new folder by right clicking.
        3. Create a new test inside your folder by right clicking.
    ii. To run test:
        1. Go to "tools" menu, click on start wizard. Follow the instructions and choose the test you wish to use.
d. Export data:
    i. In "Tools" menu, click "explorer." This will take you to a database of all your recorded results.
    ii. Click on the one you wish to export. When the file opens, go to the left most menu, and click "export."
e. Turn off the computer, then the plate reader.

A11. Alamar Blue Assay

A. Alamar Blue® Cell Viability Assay Protocol for Cells in 96-well plates
Required Materials: Alamar Blue® Cell Viability Reagent was purchased from Invitrogen™ by Thermo Fisher Scientific (Rochester, NY).

1. Seed cells into 96-well plate at desired density. (See cell count optimization sheet for instructions on counting cells and optimizing plate-reader signal. Aim for a plate reader readout of 0.75-1.25.) Remember to leave wells blank (but filled with DMEM) for control groups.
2. If you wish to have a dead control group.
    a. Empty DMEM from wells, pipette 30uL of 2% H_2O_2 or paraformaldahyde (PFA). Incubate for 20 minutes.
    b. Empty PFA from wells. H_2O_2 removes cells from the plate surface while PFA adheres them. Therefore removing H_2O_2 will remove dead cells as well. Small amount of remnant H_2O_2 will not interfere with the assay.
    c. Add 100uL DMEM to emptied wells. This is necessary because the MTS assay reacts with DMEM to produce color change effect. If you are imaging cells in PBS or the buffer, remove them and replace with DMEM before conducting Alamar Blue assay.
3. Retrieve cells from incubator, and add 100µl of pooled 10:1 corresponding media/ alamarBlue® dye solution to all wells (including blank control wells) under sterile hood.
4. Incubate the cells for 4 hours.
5. Retrieve cells from incubator and check for a color change.

6. Measure the fluorescence of each well at excitation and emission 531nm/ 595nm on the plate reader in room 112. Remember to bring a flash drive.
    a. Turn on plate reader, then computer. Password to the computer is molly02.
    b. Make sure that you are using an appropriate filter.
    c. Click on the "Wallac" plate reader icon on the desktop. For first users, a new test must be created.
        i. To create new test.
            1. Go to "tools" menu, click on explorer.
            2. Create a new folder by right clicking.
            3. Create a new test inside your folder by right clicking.
        ii. To run test:
            1. Go to "tools" menu, click on start wizard. Follow the instructions and choose the test you wish to use.
    d. Export data:
        i. In "Tools" menu, click "explorer." This will take you to a database of all your recorded results.
        ii. Click on the one you wish to export. When the file opens, go to the left most menu, and click "export."
    e. Turn off the computer, then the plate reader.

A12. Flow Cytometry Assay

A. Flow Cytometry Assay Protocol for Cells in 12-well plates
Required Materials: Sytox® Red dead cell stain was purchased from Molecular Probes™ by Thermo Fisher Scientific (Rochester, NY).

1. Seed cells into 12-well plate at desired density.
2. If you wish to have a dead control group.
    a. Empty DMEM from wells, pipette 30uL of 2% H_2O_2 or paraformaldahyde (PFA). Incubate for 20 minutes.
    b. Empty PFA from wells. H_2O_2 removes cells from the plate surface while PFA adheres them. Therefore removing H_2O_2 will remove dead cells as well. Small amount of remnant H_2O_2 will not interfere with the assay.
3. After treatment, wash non-adhered cells with 1 ml D-PBS and collect.
4. Harvest adhered cells by trypsinization (0.25% Trypsin) for 10 minutes.
5. Pool cells together and centrifuge at 1800 rpm for 5 minutes to obtain cell pellet.
6. Re-suspend cells in 1 ml D-PBS and stain with ending concentration of 5nM Sytox Red for 15 minutes in the dark.
7. Centrifuge and fix pellet in 250 ul of 1% paraformaldehyde (PFA) solution in D-PBS
8. Bring samples to Ms. Marilyn for flow cytometric analysis of viability with a BD FACS Calibur cytometer (Franklin Lakes, NJ).

9. For each sample, scatter and fluorescent data are collected for 30,000 cell events using Cellquest pro (BD Biosciences, San Jose, CA) and further analyzed using WinMDI 2.8 software (by Dr M Dietrich, LSUHSC Veterinary School, Baton Rouge, LA).

VITA

Alyson Moll grew up in Metairie, Louisiana. She earned a Bachelor's of Science in Biochemistry in 2007 at Louisiana State University in Baton Rouge. After working as a biology high school teacher and research associate at Clear Lake High school and LSU Health Science Center New Orleans respectively, Alyson entered graduate school to pursue her interests in gene targeted drug delivery. She earned a Master's of Science in Engineering Science in 2014. She attends the LSU Health Sciences Center Shreveport Physician Assistant Program.